

Dissertation

zum Thema

Charge transfer at phthalocyanine interfaces

der Fakultät Mathematik und Naturwissenschaften
der Technischen Universität Dresden
vorgelegt von

Dipl. Nat. Susi Lindner

geboren am 30.04.1987

in Riesa

zur Erlangung des akademischen Grades
Doctor rerum naturalium
(Dr. rer. nat.)
begutachtet durch

Prof. Dr. Bernd Büchner
Prof. Dr. Georgeta Salvan



Leibniz-Institut
für Festkörper- und
Werkstoffforschung
Dresden



**TECHNISCHE
UNIVERSITÄT
DRESDEN**

Eingereicht am 31.03.2014

Verteidigt am 05.06.2014

CONTENTS

List of Figures	5
Preface	9
1. Transition metal phthalocyanines	13
1.1. Molecular structure	13
1.2. Symmetry and electronic structure	13
1.3. Morphology and crystal structure	15
2. Electronic properties of organic/metal and organic/organic interfaces	17
2.1. Electronic structure of metals	17
2.2. Electronic structure of organic semiconductors	19
2.3. Organic/metal interfaces	21
2.4. Origin of the interface dipole	22
2.4.1. Reduce metal work function (Pillow effect)	22
2.4.2. Interface charge transfer	23
2.4.3. Induced density of states model (IDIS)	24
2.5. Organic/organic interfaces	26
3. Photoelectron spectroscopy	27
3.1. Basic principles	28
3.1.1. Photoelectric effect	28
3.1.2. Three-step model	29
3.1.3. Surface sensitivity and UHV-condition	31
3.1.4. Definition of the binding energy	32
3.1.5. Light sources	34
3.1.6. Electron energy analyzer	35

Contents

3.2. Experimental details	36
3.2.1. The spectrometer system	36
3.2.2. Sample preparation	37
3.3. Analysis of the electronic and chemical properties	39
3.3.1. Analysis of UPS data	39
3.3.2. Analysis of XPS	41
4. Results and discussion	45
4.1. Charge transfer at phthalocyanine interfaces to noble metals	46
4.1.1. F ₁₆ CoPc and CoPc on Au(100)	47
4.1.2. FePc on Ag(111)	51
4.1.3. The complex nature of phthalocyanine/gold interfaces	54
4.2. Charge transfer at phthalocyanine hetero-interfaces	58
4.2.1. Heterojunction: MnPc/F ₁₆ CoPc	59
4.2.2. A phthalocyanine blend: MnPc/F ₁₆ CoPc	71
4.2.3. Other phthalocyanine heterojunctions	76
4.3. Outlook	81
A. Appendix	83
A.1. Computational aspects for the phthalocaynine heterojunction	83
A.2. XAS: Experimental details	84
A.3. EELS: Experimental details	84
A.4. Computational aspects for the phthalocaynine dimer	85
Bibliography	87
List of Publications	97
Danksagung	99
Selbstständigkeitserklärung	101

LIST OF FIGURES

0.1. Schematic energy level alignment for an organic semiconductor heterojunction with charge transfer	10
1.1. Chemical structure of a transition metal phthalocyanine molecule	14
1.2. Sketch of the energy splitting for transition metal phthalocyanine molecules	15
1.3. The crystal structures of α - and β - transition metal phthalocyanines	16
2.1. Jellium model	18
2.2. Scheme of the orbitals and bonds for 2 sp^2 -hybridized carbon atoms and for a benzene ring with delocalized π system	19
2.3. Electronic structure represented with potential wells for an organic solid	20
2.4. Energy level alignment of an organic solid	21
2.5. Energy level alignment of an organic/metal interface	22
2.6. Models for the interface dipole layer formation (part I)	23
2.7. Experimental work function change for monolayer xenon adsorption on metal surfaces	24
2.8. Models for the interface dipole layer formation (part II)	25
2.9. Scheme of the calculated molecular-orbital energies for the isolated and the Lorentzian-broadened DOS	25
2.10. IDIS model: Evolution of the energy-level alignment when two π -conjugated organic semiconductors are brought into contact	26
3.1. Scheme of the photoemission process	28
3.2. Three-step model	29
3.3. Mean-free path of the electrons in solids	31
3.4. Relation between the energy levels in a solid and the electron distribution	33
3.5. Energy scheme of a sample in contact with the spectrometer	34
3.6. Scheme of the spectrometer	36

List of Figures

3.7. Single crystal and evaporator	37
3.8. Scheme of the interface parameter	40
3.9. Scheme of the chemical shift	41
3.10. Chemical shifts of C 1s core level in ethyl trifluoroacetate	42
4.1. Valence band photoemission spectra of the thick films of CoPc and F ₁₆ CoPc	48
4.2. Valence band photoemission spectra of the monolayers of CoPc and F ₁₆ CoPc	49
4.3. Co 2p core level spectra of a monolayer and a thick film of a) CoPc and b) F ₁₆ CoPc	50
4.4. Fe 2p core level spectra of a monolayer and a thick film of FePc on Ag(111)	52
4.5. Valence band photoemission spectrum of the thick film of FePc and the corresponding monolayer	53
4.6. High binding energy cutoff for 3nm CoPc, a monolayer (ML) of CoPc and Au(100).	54
4.7. Schematic energy level alignment for the phtahlocyanine gold interfaces as obtained from the photoemission measurements	55
4.8. Co 2p core level spectra of a monolayer and a thick film of CoPc and F ₁₆ CoPc on Au(100) to illustrate the close similarity.	57
4.9. Scheme of the two types of charge transfer at the CoPc/Au interface	58
4.10. Evolution of the C 1s core level photoemission profile upon deposition of F ₁₆ CoPc on a 3 nm thick layer of MnPc	59
4.11. Evolution of the N 1s core level photoemission profile	60
4.12. Co 2p _{3/2} core level photoemission spectra of a thin and thick F ₁₆ CoPc layer on top of MnPc	61
4.13. a) Co 2p _{3/2} and b) Mn 2p _{3/2} core level photoemission spectra for a MnPc/F ₁₆ CoPc heterojunction when MnPc is deposited on a 3 nm thick F ₁₆ CoPc layer . . .	62
4.14. Comparison of the energy levels of MnPc, F ₁₆ CoPc, CoPc	63
4.15. Interaction of the MnPc and F ₁₆ CoPc states in the MnPc-F ₁₆ CoPc dimer close to the Fermi-level	64
4.16. N 1s excitation spectra for a) 2.0 nm MnPc on Au(100) b) 0.6 nm F ₁₆ CoPc on MnPc c) 1.1 nm F ₁₆ CoPc on MnPc d) 3.0 nm F ₁₆ CoPc on MnPc and e) 2.0 nm F ₁₆ CoPc on Au(100)	66
4.17. Co L ₃ edge absorption spectra for a) 0.6 nm F ₁₆ CoPc on MnPc b) 1.1 nm F ₁₆ CoPc on MnPc c) 3.0 nm F ₁₆ CoPc on MnPc and d) 2.0 nm F ₁₆ CoPc on Au(100)	67
4.18. Co 2p _{2/3} x-ray absorption edges of K _x CoPc films	68

4.19. Mn $L_{2,3}$ edge absorption spectra for a) 2.0 nm MnPc on Au(100) b) 0.6 nm F_{16} CoPc on MnPc c) 3 nm F_{16} CoPc on MnPc	69
4.20. C $1s$ core level photoemission profile for a coevaporated blend of MnPc and F_{16} CoPc	71
4.21. a) Co $2p_{3/2}$ and b) Mn $2p_{3/2}$ core level photoemission spectra for a coevaporated blend of MnPc and F_{16} CoPc	72
4.22. Electronic excitation spectra of the phthalocyanine blend in comparison to the pure materials measured with EELS	73
4.23. Electronic excitation spectrum of the phthalocyanine blend in comparison to the theoretical calculation	74
4.24. Transitions in the spectral region below 1.5 eV	75
4.25. Evolution of the a) C $1s$ and the b) N $1s$ core level photoemission profile . .	77
4.26. Co $2p_{3/2}$ core level photoemission spectra for a CoPc/MnPc heterojunction when CoPc is deposited on a 3 nm thick MnPc layer	78
4.27. Fe $2p$ core level photoemission spectra for a FePc/MnPc heterojunction when FePc is deposited on a 3 nm thick MnPc layer	79

PREFACE

Surface and interface studies help to understand the fundamental processes at the corresponding interfaces. In the field of organic molecular materials, many fascinating phenomena can occur at hetero-interfaces, and their importance bridges the entire range from fundamental aspects to application in organic devices. Recently, we have studied a number of organic hetero-interfaces within the family of phthalocyanines. Intriguingly, at a particular phthalocyanine interface we discovered an interaction that is characterized by charge and spin transfer between the molecules at the interface, which leads to new physical properties. This might even be an initial representative of a fascinating novel material class.

The addition or the removal of charge as a successful tool to modify physical properties plays an important role in fundamental and applied science. In the field of molecular solids, charge transfer has a long-standing and successful history and prominent examples can be found in, e.g., the classes of organic conductors, as well as superconductors [1–4]. So-called charge transfer salts have been manufactured and demonstrated interesting and often unexpected physical properties ranging from metallicity and superconductivity over complex phase diagrams including charge density and spin density wave phases to highly correlated materials (Mott insulators) [2, 4]. Intriguingly, even the formation of a two-dimensional metallic layer has been reported as a consequence of charge transfer between the two insulating organic molecular crystals (TTF and TCNQ) [5, 6]. Most recently, superconductivity was reported for some alkali intercalated molecular solids built from hydrocarbons such as picene, which renewed interest in the study of charge transfer materials and variations of their physical properties upon charging [7, 8].

In view of more applied aspects, charge transfer has also been investigated and exploited in order to improve or engineer the performance of organic electronic devices. For instance, it has been shown that the inclusion of organic dopants in organic semiconductors can significantly enhance charge carrier injection from electrodes and the modification

Preface

of electrode surfaces with particular organic layers accompanied by charge transfer allows tuning of hole injection barriers at such junctions [9, 10].

Within the huge family of π -conjugated molecular materials which are also considered in organic (opto-)electronic devices, transition metal phthalocyanines offer an additional degree of freedom via the incorporation of the transition metal in the center of the molecule. The transition metals provide a magnetic moment, which results in an interesting combination of organic semiconductors plus magnetism. This has intriguing aspects in view of the development of a spin electronic based on organics [11, 12].

In general, metal phthalocyanines are rather stable against e.g. heat, light, moisture or oxygen, and they have been applied already in organic light-emitting diodes (OLEDs) [13], organic photovoltaic cells [13–15], organic field-effect transistors (OFETs) [16, 17] and even first organic spintronic devices [18, 19]. Within the research activities on organic heterojunctions, we have recently combined selected phthalocyanines that should allow for charge transfer at the respective interface. An important criterion to be considered in order to render charge transfer feasible is the relative size of the ionisation energies and the electron affinities of the involved molecules. This is outlined in Fig. 0.1.

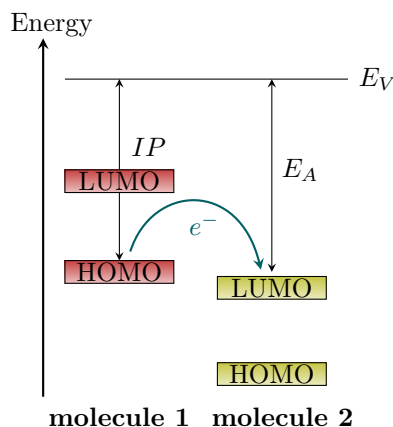


Figure 0.1.: Schematic energy level alignment for an organic semiconductor heterojunction with charge transfer. An important condition for charge transfer is fulfilled when the ionisation energy (IP) of molecule 1 approaches the electron affinity (E_A) of molecule 2. HOMO means highest occupied molecular orbital, whereas lowest occupied molecular orbital is abbreviated LUMO.

In detail, charge transfer becomes likely when the ionisation energy of the donor (molecule 1) approaches the electron affinity of the acceptor (molecule 2). Following this conjecture the two phthalocyanines MnPc and F₁₆CoPc were chosen.

Using photoelectron spectroscopy studies and calculations based on density functional theory (DFT) it could be unambiguously demonstrated that the interface between MnPc and F₁₆CoPc is characterized by a sizable charge transfer between the two molecular

species. This transfer of charge is also accompanied by a transfer of spin. The obtained results are of importance for the application of such interfaces in organic electronic devices since charge transfer considerably affects the energy level alignment and the transport behavior of the respective heterojunction.

1

TRANSITION METAL PHTHALOCYANINES

1.1 Molecular structure

Transition metal phthalocyanines are carbon-based molecules and they are formed by a very stable π -conjugated macrocycle ring. The phthalocyanato ion $C_{32}H_{16}N_8^{2-}$ is abbreviated Pc. The structure of such a transition metal phthalocyanine molecule is shown in Fig. 1.1. The molecule is characterized by the presence of a transition metal ion in the center. They are surrounded by 4 pyrrole nitrogen (N_1), 4 bridging aza nitrogen (N_2), 8 pyrrole carbon (C_1) as well as 24 benzene ring carbon atoms (C_2, C_3 and C_4). In this thesis we focused on manganese (Mn), iron (Fe) and cobalt (Co) as central ion. The formal oxidation state of the transition metal ion is 2+ in the center of the molecule. Thereby the phthalocyanato ion acts as ligand to the central metal one whereas the bonding between the ligand and the transition metal is significantly covalent [21].

1.2 Symmetry and electronic structure

Transition metal phthalocyanines have a planar structure with a D_{4h} point symmetry [22, 23]. When a transition metal is placed in a phthalocyanine molecule the degeneracy of the $3d$ transition metal orbitals are lifted, which results in a splitting of these transition metal orbitals. Depending on the symmetry of the surrounding molecule, in the case of the D_{4h} symmetry, the 5 transition metal $3d$ orbitals transform as b_{1g} ($d_{x^2-y^2}$), a_{1g} (d_{z^2}),

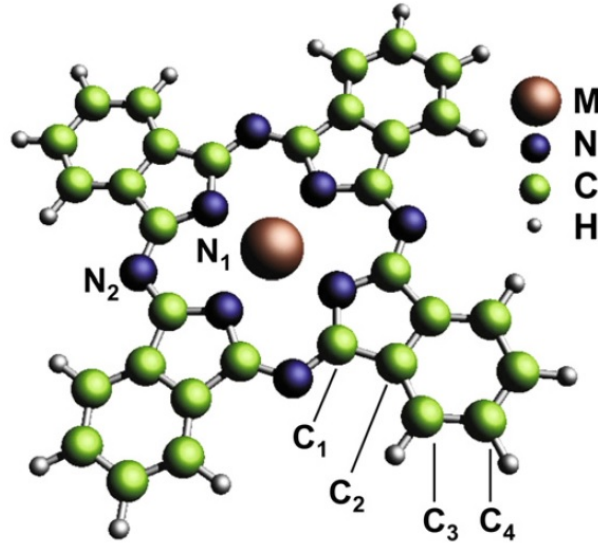


Figure 1.1.: Schematic illustration of the chemical structure of a transition metal phthalocyanine molecule. With M the central transition metal ion is denoted, which is surrounded by 4 pyrrole nitrogen (N_1) and 4 bridging aza nitrogen (N_2) atoms. The 24 carbon atoms in the outer benzene rings are labeled with C_2 , C_3 , and C_4 , respectively. With the label C_1 the 8 pyrrole carbon atoms are named, taken from Ref. [20].

e_g (d_{xz} , d_{yz}) and b_{2g} (d_{xy}), as depicted in Fig. 1.2.

The energetic order of the orbitals is reliant on the strength and the type of the distortion and on the hybridization effects of the metal $3d$ orbitals with the ligand orbitals. The electronic and magnetic properties of the phthalocyanines are determined by the valence and spin state of the transition metal ion in the center, but also by the ligand.

For the divalent Co(II) in CoPc, which has a spin of $S=1/2$, density functional theory calculations have been performed that find different electronic configurations. There are two different ground states, which have been predicted: $b_{1g}^0 a_{1g}^1 e_g^4 b_{2g}^2$ ($d_{x^2-y^2}^0 d_{z^2}^1 [d_{xz}d_{yz}]^4 d_{xy}^2$) and $b_{1g}^0 a_{1g}^2 e_g^3 b_{2g}^2$ ($d_{x^2-y^2}^0 d_{z^2}^1 [d_{xz}d_{yz}]^3 d_{xy}^2$). From previous X-ray absorption and X-ray photoemission studies the ground state configuration of $b_{1g}^0 a_{1g}^1 e_g^4 b_{2g}^2$ dominates [24].

In the case of MnPc, Mn(II) has a d^5 configuration with a spin state of $S=3/2$. From other studies two configurations are possible: $b_{1g}^0 a_{1g}^1 e_g^3 b_{2g}^1$ ($d_{x^2-y^2}^0 d_{z^2}^1 [d_{xz}d_{yz}]^3 d_{xy}^1$) and $b_{1g}^0 a_{1g}^1 e_g^2 b_{2g}^2$ ($d_{x^2-y^2}^0 d_{z^2}^1 [d_{xz}d_{yz}]^2 d_{xy}^2$) [24].

FePc has a spin of $S=1$ and 4 holes because of the d^6 configuration. There are 4 possibilities of expected ground state configurations due to the spin of $S=1$. It is claimed that the configuration with E_g orbital symmetry ($b_{1g}^0 a_{1g}^1 e_g^3 b_{2g}^2$) ($d_{x^2-y^2}^0 d_{z^2}^1 [d_{xz}d_{yz}]^3 d_{xy}^2$) is most likely possible [24].

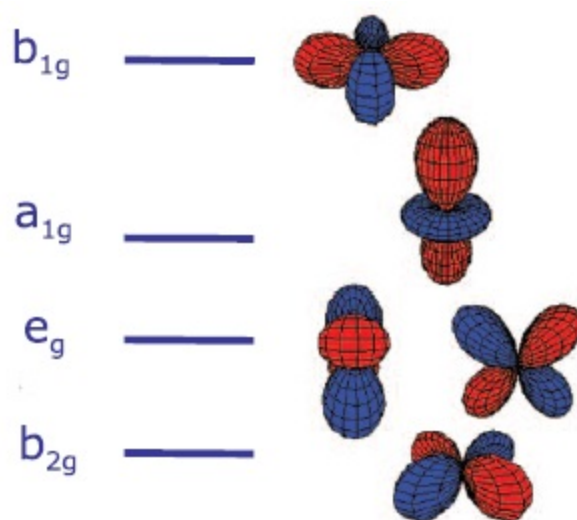


Figure 1.2.: Sketch of the energy splitting as it is present for many transition metal phthalocyanine molecules, together with the corresponding orbitals. The x- and y-axis are oriented along the shortest transition metal-nitrogen bonds, taken from Ref. [24]. Note: The e_g state consists of d_{xz} and d_{yz} orbital.

1.3 Morphology and crystal structure

Transition metal phthalocyanine molecules pertain to the family of planar organic semiconductor in which the nature of bonding is fundamentally dissimilar from inorganic semiconductors. Organic molecular crystals are comprised of weak intermolecular bonding (e.g. van der Waals and $\pi - \pi$ interactions) as compared to covalently bonded semiconductors like silicon (Si) or gallium arsenide (GaAs). In the bulk and in thin films, phthalocyanine molecules form linear chains by columnar stacking. The molecules are tilted by an angle with respect to the chain axis [25]. The angle at the parallel adjacent chain is opposite, thereby producing a herringbone arrangement. The different angles and relative positions of the chains give rise to different polymorphic types, the α - and β -forms of transition metal phthalocyanines are shown in the Fig. 1.3. The main difference between the α - and β -forms is the smaller tilt angle of the molecules relative to the b -axis of the the crystal [25].

In the case of MnPc, the crystal growth by vacuum sublimation leads to crystals in the β -form. Thereby long and thick plates of the crystals can be generated [27]. The magnetic properties depend on the stacking of the planar molecular π system. The stacking angle is defined as the angle between the b -axis and the surface normal of the molecule. β -MnPc crystals with a stacking angle of 45° are ferromagnetic and α -MnPc thin films are antiferromagnetic [28]. The crystals of the β -polymorphic form are monoclinic, with

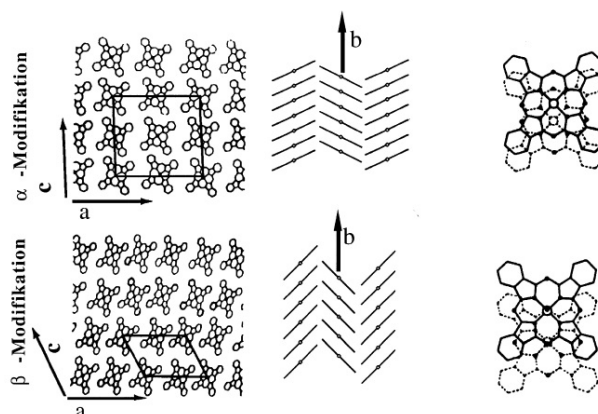


Figure 1.3.: The crystal structures of α - and β - transition metal phthalocyanines, taken from Ref. [26].

following parameters: $a = 14.6 \text{ \AA}$, $b = 4.7 \text{ \AA}$, $c = 19.3 \text{ \AA}$ and $\beta = 121.1^\circ$ [29, 30].

CoPc layers, which were produced by vacuum sublimation, lie flat on a gold crystal substrate until 5 nm [31]. For higher layer thicknesses the typical herringbone structure is generated depending on the substrate temperature, pressure and the evaporation rate [32]. At room temperature the α -type is formed when the substrate is unheated. Due to the increasing of the substrate temperature (over 300°C) a transition in the β -form occurs, where the molecules stand straighter (stacking angle $\gamma = 46^\circ$) [33].

FePc is also found in the α - and β -polymorphs. The α -form is metastable and obtained either as a poly-crystalline powder or as a thin film produced by vacuum deposition onto a cold substrate [34, 35]. The β -form is the most stable one and can be obtained either from the sublimation technique to grow a single crystal or from heating the α -polymorphic sample up to 350 for a few hours [34, 36]. The bulk lattice parameters are $a = 25.5 \text{ \AA}$, $b = 3.8 \text{ \AA}$, $c = 25.5 \text{ \AA}$, $\beta = 90.0^\circ$ for orthorhombic α -FePc and $a = 14.6 \text{ \AA}$, $b = 4.8 \text{ \AA}$, $c = 19.4 \text{ \AA}$ and $\beta = 120.8^\circ$ for monoclinic β -FePc [36]. In α -FePc the molecules are stacked parallel to each other along the b -axis at intervals of 3.78 \AA , and the molecular planes are inclined to the ac -plane at an angle of 26.5° , in a herringbone structure [37]. FePc thin films deposited on single crystals Au(100) [31] and Ag(111) [135] substrates were found to lie parallel to the substrate and well ordered.

2

ELECTRONIC PROPERTIES OF ORGANIC/METAL AND ORGANIC/ORGANIC INTERFACES

2.1 Electronic structure of metals

To explain changes at the metal surface the jellium model is introduced [38–40]. The ground state electron density profile using the jellium model for two choices of positive background densities ($\rho_1 > \rho_2$) is shown in Fig. 2.1.

The discrete ion cores are replaced by a uniform, positive background charge. The density variation perpendicular to the surface reveals two features, which are characteristic of all surface problems. One feature is that the electrons spill out into the vacuum region and thereby an electrostatic dipole layer at the surface is created. There is no sharp edge to the electron distribution. Second, the electron density oscillates as it approaches an asymptotic value that compensates the uniform positive background charge. These are Friedel oscillations. They arise because the electrons try to screen out the positive background charge distribution which has a potential step at $z = 0$ [40].

The formation of a surface dipole D means that the electrostatic potential far into the

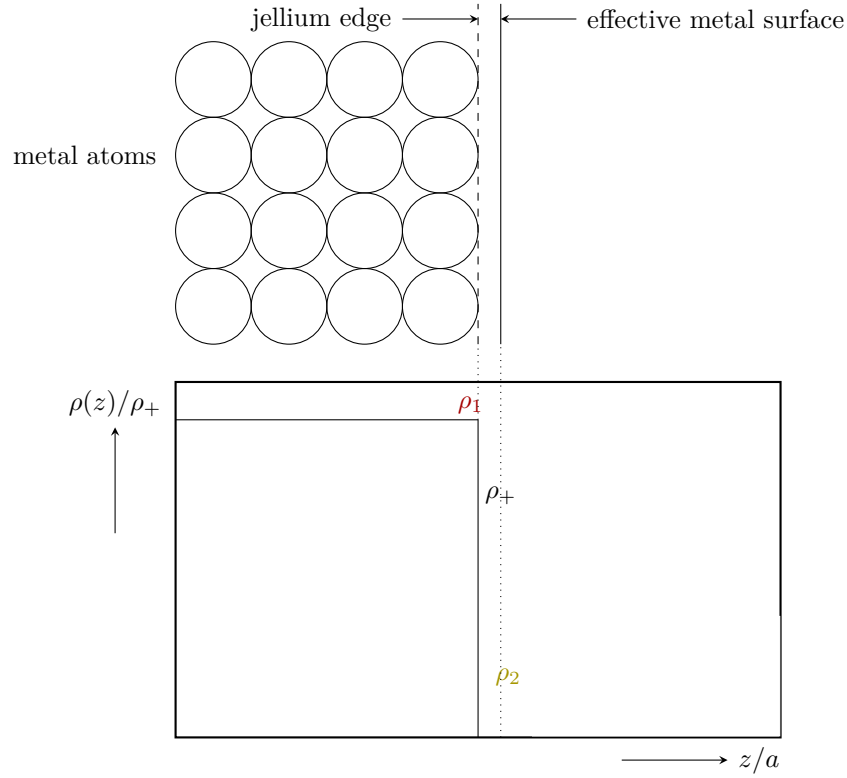


Figure 2.1.: Jellium modell. Die upper panel shows a cut through the metal surface. The lower panel depicts the electron density profile at a jellium surface for two choices ($\rho_1 > \rho_2$) of positive background (ρ_+), after Ref. [39].

vacuum is greater than the mean electrostatic potential deep in the crystal [40, 41],

$$D = v(\infty) - v(-\infty). \quad (2.1)$$

The work function Φ determines the energy, which is necessary for removing an electron from the bulk to a point outside the surface. The work function is directly associated with surface dipole,

$$\begin{aligned} \Phi &= v(\infty) + E_{N-1} - E_N \\ &= v(\infty) - \mu \\ &= D - E_F. \end{aligned} \quad (2.2)$$

The surface dipole moment is a characteristic property of surfaces and it changes depending on the surface. For the same metal, the closely packed faces have generally a greater dipole moment than the loosely packed ones [40, 42]. This can be due to the reconstruction or the charge density smoothing at the metal surface. The electrons spill

out as before, but additionally they confront the sharp steps on a rough surface. As a result, an electrostatic dipole oriented oppositely to the spill out dipole is created, thereby reducing the net dipole moment relative to the flat surface value and with this also the work function. This is known as Smoluchowki Effect [43, 44]. Hence, the work function is changed for different crystal orientations: A good example is copper with its different faces [42]: $\Phi_{Cu(111)} = 4.88$ eV, $\Phi_{Cu(100)} = 4.63$ eV and $\Phi_{Cu(110)} = 4.48$ eV.

2.2 Electronic structure of organic semiconductors

Organic semiconductors contain mainly carbon which can be associated with oxygen, hydrogen or nitrogen. The electronic configuration of carbon is in the ground state $1s^2 2s^2 2p^2$. The electrons of the p orbital are distributed among the $2p_x$, $2p_y$ and $2p_z$ orbitals. A double bond between 2 carbon atoms can be formed due to the sp^2 -hybridization, as shown in Fig. 2.2a. This hybridization effect describes the deformation of the atomic orbitals by

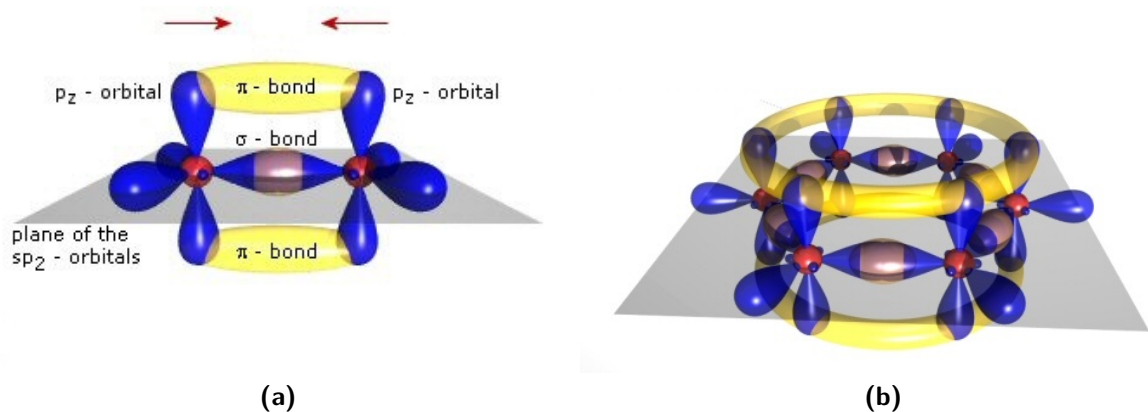


Figure 2.2.: Scheme of (a) the orbitals and bonds for 2 sp^2 -hybridized carbon atoms, and for (b) a benzene ring with delocalized π system, taken from Ref.[45].

the interaction between the atoms of the molecule. Three orbitals are formed out of 2 s and 2 p orbitals, which are coplanar and oriented at 120° relative to one another. Due to the formation of an orbital overlap of 2 sp^2 -orbitals the covalent σ bonds are generated. The remaining orbital, p_z , can overlap with the corresponding p_z orbitals of an adjacent carbon, which leads to an additional bond, the π bond. The π bonds induce states, which can be delocalized over the molecule, as shown in Fig. 2.2b. The semiconducting properties of the organic materials are generated by the extended π electron system, created by the orbital overlap.

The π bonds between carbon atoms in organic molecules form the highest occupied molecular orbital (HOMO) and the lowest unoccupied molecular orbital (LUMO). The

effective potential well of an electron in a polyatomic molecule is generated by the atomic nuclei and other electrons. The inner atomic orbitals are localized in the atomic potential well. They are called core level states. The upper atomic orbitals interact to form delocalized molecular orbitals. The vacuum level E_{vac} is defined as the outermost horizontal part of the well, above which the electron can move away from the molecule.

When molecules form an organic solid, the electronic structure develops as it is presented in Fig. 2.3.

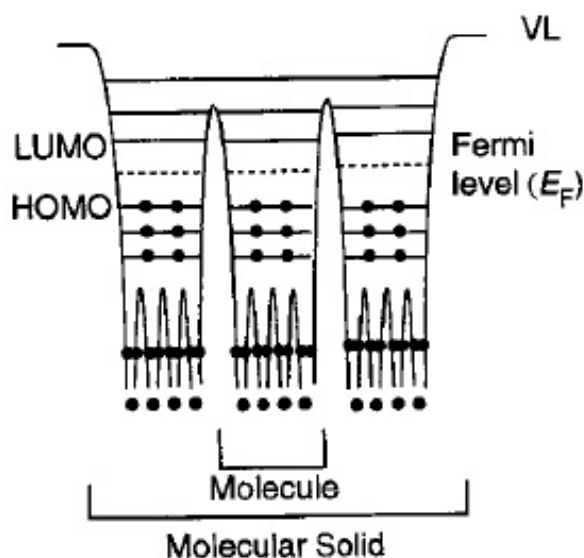


Figure 2.3.: Electronic structure represented with potential wells for an organic solid, taken from Ref. [46].

Then the molecules of an organic solid interact only by weak van der Waals forces, resulting in narrow intermolecular bandwidths and the HOMO and LUMO are completely localized on each molecule [41, 46]. Thus the electronic structure of an organic solid preserves that of the containing molecules.

The electronic structure in Fig. 2.3 is often simplified to the picture of the electronic structure of an organic solid as shown in Fig. 2.4. The Fermi energy E_F is also indicated, which is located in the energy gap of the HOMO and LUMO. The ionization potential I_P is defined as the energy separation of the HOMO from the E_{vac} . The energetic distance between the E_F and E_{vac} is called work function Φ .

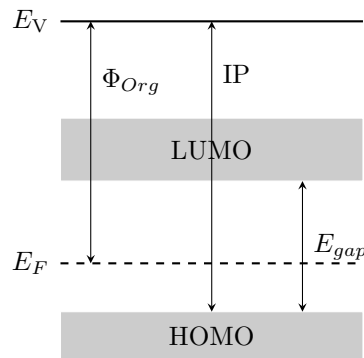


Figure 2.4.: Energy level alignment of an organic solid.

2.3 Organic/metal interfaces

In the performance of molecule-based electronics such an organic/metal interface, which can be a contact between a thin molecular film and a metal electrode, can play an crucial function. An interface between two solid materials can be either formed by a contact of two solids or the deposition of one material on the solid surface of the other. In this scientific work the data of the formation of an interface between various phthalocyanines (CoPc, F₁₆CoPc and FePc) and noble metals (Au and Ag) are analyzed.

The phthalocyanine/metal interface can be described by an organic/metal contact. When an metal and an organic material are far away from each other, the position of the Fermi energy in both solids is normally different. When the solids come into contact, forming an interface, the electronic structure of this interface can be described in the ideal Schottky barrier formation, which is shown schematically in Fig. 2.5. In this case the vacuum level at the semiconductor/metal interface is aligned. As the thermal equilibrium is reached, the Fermi level of both materials are aligned via charge transfer across the interface (see Fig. 2.5).

In general the picture of an ideal Schottky barrier formation does not explain the real behaviour of a semiconductor/metal interface. In Fig. 2.5 a realistic picture of the interface formation is depicted. In this picture an interface dipole Δ exists between the metal and the semiconductor. This interface dipole is established to reach the thermal equilibrium between the two materials and causes an abrupt shift of potentials across the dipole layer. It should be noted, that this interface dipole forms an additional dipole layer, when there is already a dipole layer at free metal surfaces as described in section 2.1. The origin of the interface dipole is discussed in detail in section 2.4.

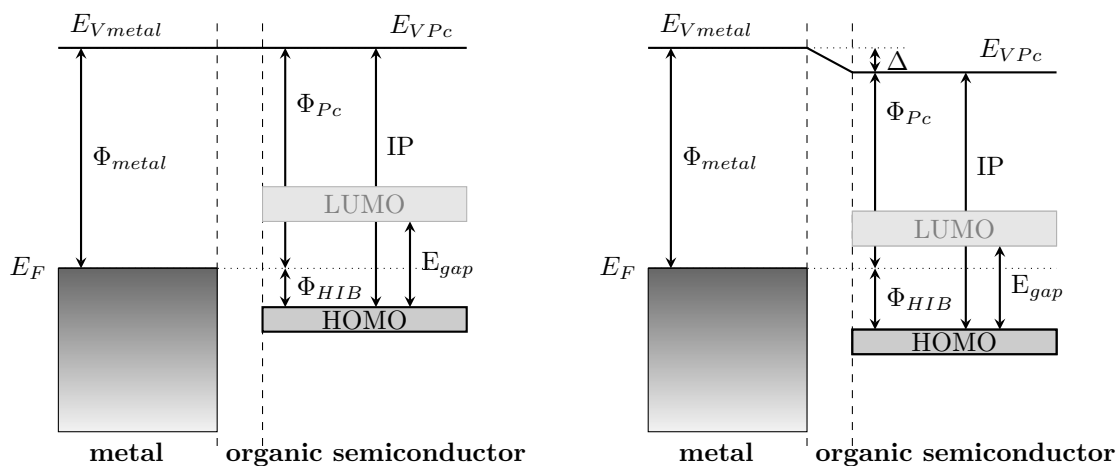


Figure 2.5.: Energy level alignment of an organic/metal interface. With (left) and without (right) formation of an interface dipole .

2.4 Origin of the interface dipole

The origin of the interface dipole is still under discussion. The interface dipole can be caused by more than one factor. There are different effects which can explain the origin of the interface dipole [46]:

- Reduction of the work function of the substrate
- Interface charge transfer
- Induced density of interface states model (IDIS)

2.4.1 Reduce metal work function (Pillow effect)

As described in the section 2.1, the work function of a metal depends on the bulk chemical potential and the surface dipole. The bulk chemical potential will not be affected by adsorption of molecules but the surface dipole depends sensitively on the surface structure. This surface dipole is created by the tailing part of electrons spilling out from the metal surface into the vacuum. This surface dipole contribution is modified by the presence of adsorbed molecules. The repulsion between the electrons of the adsorbate and the metal surface pushes the electronic tail towards the surface, which reduces the metal surface dipole potential energy, thereby decreasing the work function. This charge rearrangement is called pillow effect [47](Fig. 2.6a). The effect of physisorption in the absence of charge transfer and resultant lowering of the metal work function has been concluded by a number of experimental and theoretical studies using closed-shell atoms like Xe [40] and organic

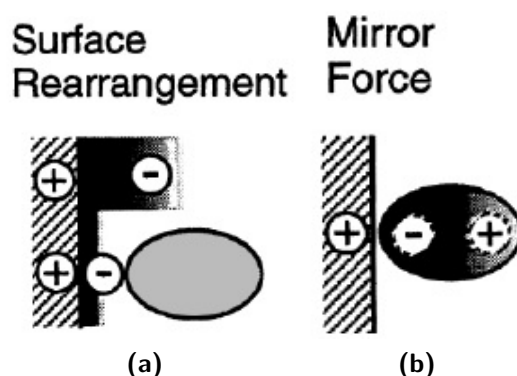


Figure 2.6.: Models for the interface dipole layer formation: (a) pushing back of the electron cloud tail out of the metal surface and (b) image potential induced polarization of the organic material, taken from Ref.[46]

semiconductors [48] on various metal substrates. The variation of the metal work function depends upon the metal surface dipole. Fig. 2.7 presents the work function changes for one xenon monolayer coverage adsorbed on different metal surfaces.

One can clearly see that the metals, which have a large work function, lead to a large interface dipole. Hence, these metal substrates undergo the larger work function changes upon xenon adsorption than the metals with low work function upon physisorption. The pillow effect occurs also at interfaces with stronger interaction, but it is very difficult to differentiate it, among various contributions to the interface dipole formation.

Another factor, which can explain the modification of surface dipole at the interface is known as the image charge effect. The results of another study of xenon on metals attributed the changes in the work function of metal to the polarization of electrons [40]. This image charge screening leads to a deficiency of electrons in the vacuum side, as depicted in the Fig. 2.6b.

2.4.2 Interface charge transfer

The second factor is the electron transfer between the metal and the organic molecule, where the charge remains localized at the interface [41, 46, 50]. If the electronic charge is transferred to the metal substrate, a downshift of the vacuum level will be induced. This is expected for a combination of (strong acceptor)-(low work function metal), as depicted in Fig. 2.8(left panel). If the electronic charge is transferred to the organic molecule by introducing a dipole-induced potential step, an upward shift of the vacuum level will occur. For the combination of (strong donor)-(high work function metal) such case is anticipated. In Fig. 2.8(right panel) the charge transfer with this anion formation is shown.

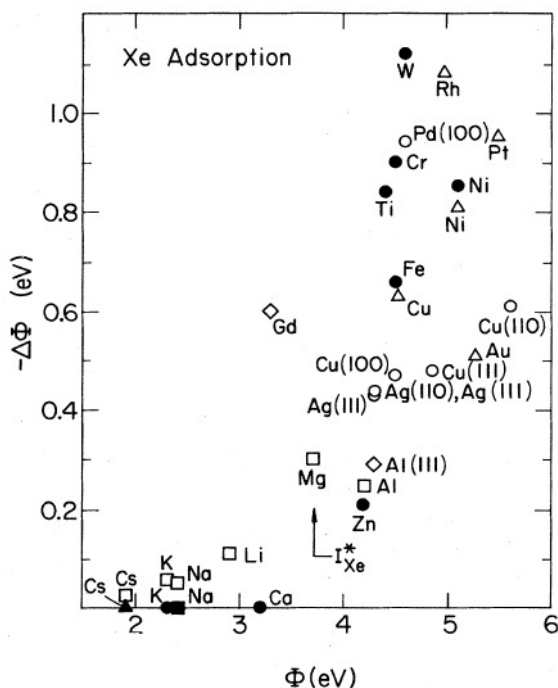


Figure 2.7.: Experimental work function change for monolayer xenon adsorption on several metal surfaces, taken from Ref. [49].

This mechanism is also applicable to organic/organic interfaces for the combination of strong donor and acceptor [46].

2.4.3 Induced density of states model (IDIS)

The Induced density of interfacial states (IDIS) is a model describing interfaces characterized by a (weak) hybridization of the electronic states of the π -conjugated molecules in contact with metal substrates [41, 47]. When the molecules adsorb onto the clean metal surface, the interaction of these two materials give rise to a shift and broadening of the molecular levels, leading to hybridization of the HOMO and LUMO with metal states. The broadening of each state has a Lorentzian shape. Due to this interaction the initial (discrete) distribution of the molecular levels transforms into a continuum density of states (DOS) leading to finite DOS on the former energy gap. The charge-neutrality level (CNL) position of the organic molecule is obtained by filling this induced DOS by the number of electrons of the isolated and neutral molecule [47],

$$N = \int_{-\infty}^{CNL} \rho_{IDIS} dE. \quad (2.3)$$

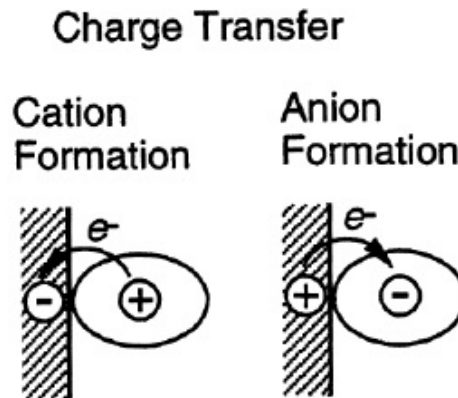


Figure 2.8.: Models for the interface dipole layer formation: Charge transfer across the interface via cation and anion formation, taken from Ref.[46].

A schematic figure of molecular-orbital energies and the Lorentzian-broadened DOS is shown in Fig. 2.9 The direction and size of the charge transfer at the interface between

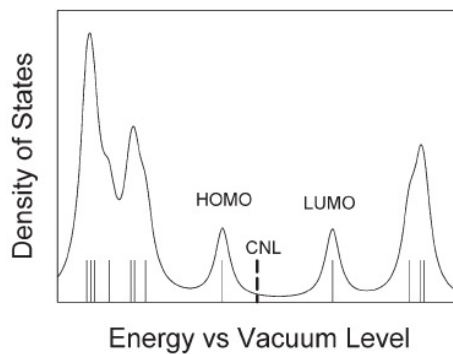


Figure 2.9.: Scheme of the calculated molecular-orbital energies for the isolated (bars) and the Lorentzian-broadened DOS (curve). The CNL is depicted as a dashed line, taken from Ref.[41].

the molecules and the metal substrate is determined by the relative position of the semiconductor CNL and the substrate Fermi level. If the organic CNL is higher than the metal work function, electronic charge is transferred from the organic molecule to the metal substrate. This leads to the formation of an electrostatic dipole at the interface aligning the relative positions of both materials. This induced dipole Δ can be calculated by the difference of the metal work function (Φ_M) and the organic charge-neutrality level (CNL), which is reduced by the interface slope parameter S , which represents the strength of the interaction:

$$\Delta = (1 - S)(\Phi_M - CNL). \quad (2.4)$$

2.5 Organic/organic interfaces

The energy level alignment between two different organic films is important to improve the efficiency of organic light-emitting diodes (OLEDs) and organic photovoltaic devices. The organic/organic interfaces have some features in common with the organic/metal interfaces, but they also have their own characteristics. The interface dipole in organic/organic interfaces is much less common as in metal/organic ones, due to the fact that there exists less itinerant charge carriers. The main contribution to the interface dipole is from the alignment of the permanent dipole of the organic molecule [50]. The model of IDIS can also be used to explain the interface dipole at organic/organic heterojunctions, as explained in section 2.4. In the case of these heterojunctions the same assumptions can be made. However, the formula of interface dipole is changed [51]:

$$\Delta_{OO} = (1 - S_{OO})(CNL_1 - CNL_2)_{initial}. \quad (2.5)$$

Hence, the difference between the CNL levels at the heterojunction (difference at equilibrium) is related to the difference between the CNL levels of the two organic molecules modified by the now called slope parameter S_{OO} . This parameter represents the ability of the molecular materials at the interface to screen the electrostatic-potential difference. The hybridization of the molecular orbitals leads to a continuous density of states in the former HOMO-LUMO gap. Thereby charge can be transferred from the higher lying CNL into the empty states of the lower lying CNL until the equilibrium is reached, as depicted in Fig. 2.10.

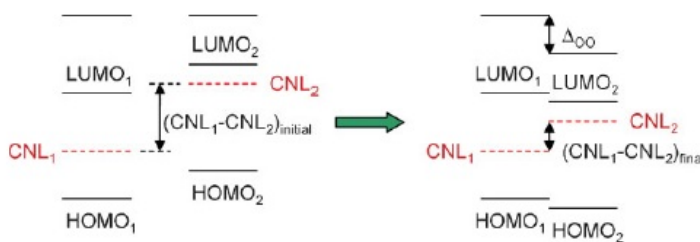


Figure 2.10.: Evolution of the energy-level alignment when two π -conjugated organic semiconductors are brought into contact, as predicted in the IDIS model, taken from Ref.[41].

However, many other features are observed, depending on the investigated system. For more details see the review articles of Braun et al., Gao et al. and Hinderhofer et al. [41, 50, 52].

3

PHOTOELECTRON SPECTROSCOPY

Photoelectron spectroscopy is a popular method to investigate the chemical and the electronic properties of atoms, molecules, solids as well as of surfaces and interfaces. This type of spectroscopy is an important tool in the research field of organic semiconductors, because it is a non-destructive procedure to study their surfaces and interfaces.

In comparison to other particles like photons, atoms or ions, electrons have a lot of advantages [53]. For example electrons can be easily focused and they can be easily detected and counted. An advantage which makes this method attractive in this research area is that the energy of the electrons and their angle can be analyzed using electrostatic fields.

In this chapter we introduce briefly the topic of photoelectron spectroscopy. A short introduction is given in the basic principles of this technique. Furthermore we explain the experimental details, which gives an overview of the used spectrometer system. At the end of the chapter the analysis of the received x-ray (XPS) and ultra-violet photoelectron spectroscopy (UPS) data is described to gain information about the electronic as well as the chemical properties.

3.1 Basic principles

3.1.1 Photoelectric effect

For the first time Hertz detected the phenomenon of photoemission in 1887 [54]. However he was not able to explain this process. In 1905 Einstein could explain this so called photoelectric effect by invoking the quantum nature of light [55]. The condition for the photoelectric effect is that a solid surface is irradiated by mono-energetic photons and the emitted electrons are analyzed with respect to their kinetic energy E_{kin} and momentum \vec{p} (wave vector $\vec{k}^{ex} = \vec{p}/\hbar$). Knowing the energy of the light and the work function Φ of the material (surface), one can determine the binding energy E_B of the corresponding electronic state of the sample:

$$E_{kin} = h\nu - \Phi - E_B. \tag{3.1}$$

The magnitude of the wave vector \vec{k}^{ex} is determined by the kinetic energy of the emitted electron:

$$k^{ex} = (2mE_{kin}/\hbar^2)^{1/2} \tag{3.2}$$

The direction of the emission is expressed by the angles θ and β . These parameters are shown in Fig. 3.1.

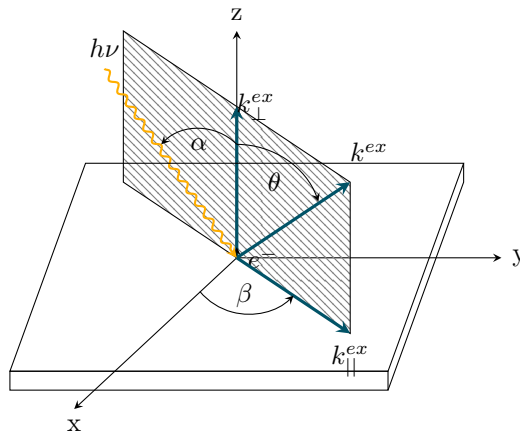


Figure 3.1.: Scheme of the photoemission process: Definition of the angles and the wave vectors of the photon ($h\nu$) and the emitted electron e^- , cf. [56]

3.1.2 Three-step model

A detailed theoretical approach to the process of photoemission necessitates a full quantum-mechanical treatment of the complete coherent process. The simpler and more instructive approach is the three-step model [57], which is less accurate but is useful. In Fig. 3.2 the photoemission process as a three-step model is shown.

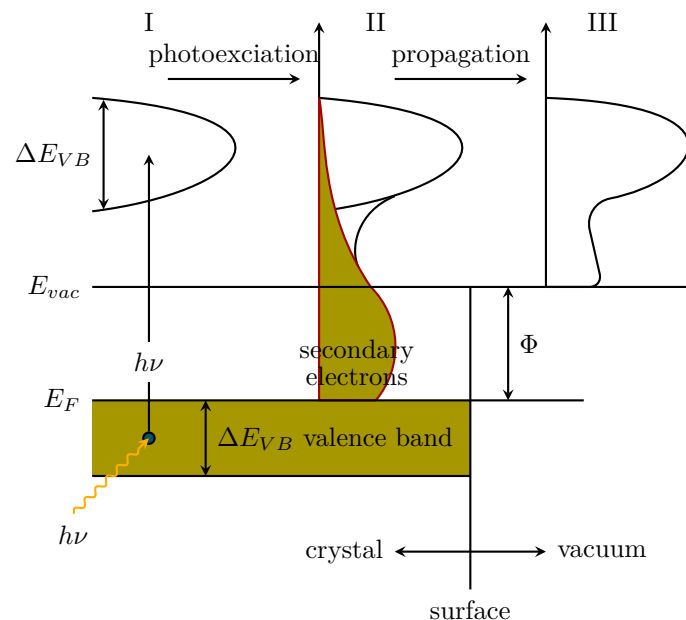


Figure 3.2.: Three-step model:(I) photoexcitation of the electrons; (II) propagation of the excited electron to the surface; (III) penetration through the surface [53]

In this model the photoemission experiment is artificially separated into three independent processes.

- (I) Photoexcitation of an electron from an initial into a final state.
- (II) Propagation the excited electron to the surface.
- (III) Electron escapes through the surface into the vacuum.

In the first step the optical excitation of an electron is simply described by the transition

probability W_{fi} for optical excitations (Fermi's Golden rule):

$$W_{fi} = \frac{2\pi}{\hbar} |\langle f, \vec{k} | \mathcal{H} | i, \vec{k} \rangle|^2 \delta(E_f(\vec{k}) - E_i(\vec{k}) - \hbar\omega) \quad (3.3)$$

In the first approximation direct transitions with nearly unchanged \vec{k} are taken into account between the initial and the final Bloch states $|i, \vec{k}\rangle$ and $\langle f, \vec{k}|$. The perturbation operator \mathcal{H} is given by the momentum operator \vec{p} and the vector potential \vec{A} of the incident electromagnetic wave (dipole approximation):

$$\mathcal{H} = \frac{e}{mc} \vec{A} \cdot \vec{p} \quad (3.4)$$

In Eq. 3.3 the δ -function describes the energy conservation in the excitation of an electron from initial state $E_i(\vec{k})$ into the final state $E_f(\vec{k})$ of the electronic band structure. On the vacuum side (outside of the solid) one can only detect electrons whose energy E is above the vacuum energy E_{vac} and whose vector \vec{k} in the final state is directed outwards the surface, i.e. $|\vec{k}_\perp| > 0$.

The second step describes the movement of the electron through the sample to the surface (propagation). A lot of electrons take part in inelastic scattering processes. They lose energy by electron-phonon or electron-plasmon scattering. Such electrons contribute to the background of the photoemission spectra, which is called secondary background. Due to the loss of kinetic energy the electrons lose also information about the initial state E_i . The probability that an electron will reach the surface without scattering processes is given by the mean free path λ . The value of λ is typically between 5 and 20 Å, which makes the photoemission spectroscopy a surface sensitive technique.

The third step, the transmission of the photoexcited electron through the surface into the vacuum requires conservation of its wave-vector component parallel to the surface:

$$\vec{k}_\parallel^{ex} = \vec{k} + \vec{G}_\parallel \quad (3.5)$$

The component normal to the surface of the wave vector of the electron inside the crystal is not conserved during the transmission through the surface because of the inner microscopic surface potential V_0 . On the vacuum side the dispersion relation for free electrons is effective:

$$E_{kin} = \frac{\hbar^2 k^{ex2}}{2m} \quad (3.6)$$

The wave-vector component parallel to the surface outside the solid (k_\parallel^{ex}) is determined

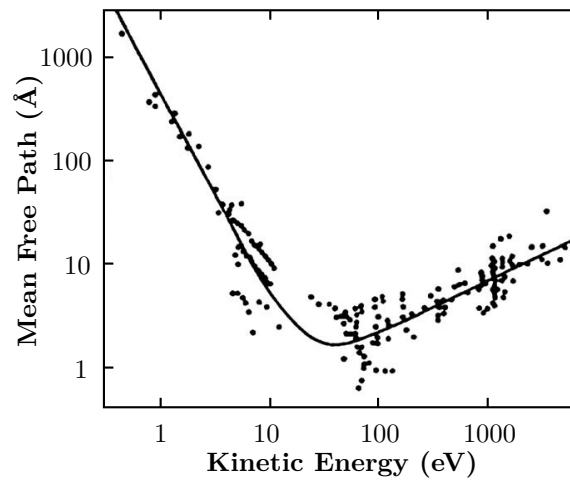


Figure 3.3.: Mean-free path of the electrons in solids as a function of their energy, cf. [56]

from experimental parameters:

$$k_{\parallel}^{ex} = \sqrt{\frac{2m}{\hbar^2} E_{kin} \sin\theta} \quad (3.7)$$

The wave-vector component of the electron inside the solid (k_{\perp}) is changed upon transmission. The outside component is determined by the energy conservation as

$$k_{\perp}^{ex} = \sqrt{\frac{2m}{\hbar^2} E_{kin} \cos\theta}. \quad (3.8)$$

For the interested reader we refer to other publications [53, 56, 58], to get more detailed information about the fascinating topic.

3.1.3 Surface sensitivity and UHV-condition

One of the peculiarity of the photoelectron spectroscopy is demonstrated by the high surface sensitivity. For this two facts are responsible:

- the low mean free path λ of the electrons in the solid
- the susceptibility of the solid surface to gas adsorbates.

As it was mentioned above, excited electrons travel to the surface and may take part in many inelastic scattering processes. They lose energy by electron-phonon, electron-electron and electron-plasmon scattering. The probability that an electron will arrive at the surface without inelastic scattering is given by the mean free path λ .

In Fig. 3.3 the electron mean free path λ as a function of the electron kinetic energy for selected metals is shown, which is also called universal curve. One can see that λ is only a few Å in the kinetic energy range of interest (10 to 2000 eV). The quasi-universal dependence for a lot of different materials is due to the fact that the dominant interaction mechanism between the electrons and the solid is the excitation of plasmon waves, whose energy is determined by electron density in the crystal.

Under ambient pressure conditions the surface of a solid contains a layer of adsorbed contaminants, which consists of air components like water, hydrogen, oxygen and carbon monoxide. The actual coverage depends on the sticking coefficient S , which gives the probability that an atom or molecule remains absorbed. On consideration of $S = 1$ and a vacuum pressure of $p = 1.3 \cdot 10^{-6}$ mbar, in one second a coverage of one monolayer will be obtained at the surface. In order to keep the surface clean over a time period which is in the typical order of the measurement (1h), it is necessary to have a pressure lower than 10^{-9} mbar. Therefore, at ultrahigh vacuum (UHV) condition it is possible to have atomic clean surfaces during the measurements.

3.1.4 Definition of the binding energy

Electrons, which are excited, leave the solid. Therefore, one can detect their kinetic energy. The obtained spectrum of the energy distribution is a picture of the Density Of States (DOS). How the energy-level diagram and the energy distribution of photoemitted electrons relate to each other is shown in Fig. 3.4.

In Eq. 3.1 the labeled energy E_{kin} is the kinetic energy of the photoelectron of the surface. The spectrometer system is detecting the kinetic energy E'_{kin} . These two energies are different due to the different work function of the spectrometer analyzer Φ_{spec} and of the sample Φ_{sample} (see Fig. 3.5).

During the experiment, sample and spectrometer are connected in a conducting way to avoid charging effects. The sample and the spectrometer are in thermodynamic equilibrium and therefore the Fermi energies are at the same level. As a consequence on the way to the surface the emitted photoelectron is affected by a potential difference $\Phi_{spec} - \Phi_{sample}$. The kinetic energy of the electron is outside of the sample

$$E_{kin} = h\nu - \Phi_{sample} - E_B^F \quad (3.9)$$

However, the spectrometer detects the kinetic energy E'_{kin} , which is described by the equation

$$E'_{kin} = h\nu - \Phi_{spec} - E_B^F \quad (3.10)$$

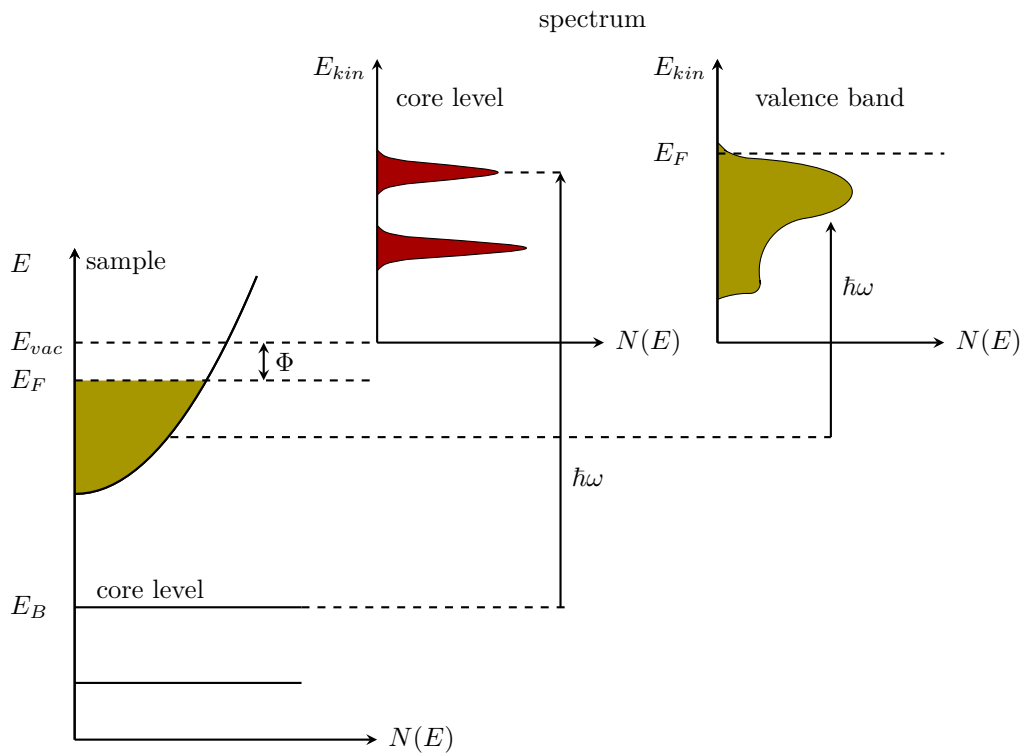


Figure 3.4.: Relation between the energy levels in a solid and the electron distribution produced by photons of energy $\hbar\omega$, cf. [53]

From Eqs. 3.9 and 3.10 one can extract the following relation

$$E_{kin} + \Phi_{sample} = E'_{kin} + \Phi_{spec}. \quad (3.11)$$

Setting Eq. 3.9 in Eq. 3.11, one can eliminate the work function of the sample and one receives

$$E'_{kin} = h\nu - \Phi_{spec} - E_B^F. \quad (3.12)$$

A Fermi energy of 0 eV binding energy is related to metals. The work function of the spectrometer is independent of the used sample. Thereby, one can calibrate the energy scale by determining the position of the Fermi-edge or the known binding energies of the core level peaks of clean metal reference samples like gold, silver or copper, according to Tab. 3.1

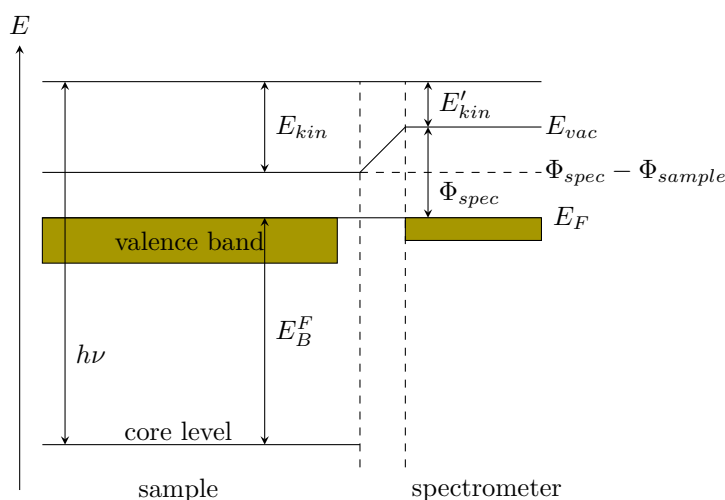


Figure 3.5.: Scheme of the relevant energies of a sample in direct contact with the spectrometer, cf. [59]

Table 3.1.: Binding energies for the energy calibration [60]

Reference signal	Binding energy [eV]
Au $4f_{7/2}$	84.00 ± 0.02
Ag $3d_{5/2}$	368.27 ± 0.02
Cu $2p_{3/2}$	932.66 ± 0.02

3.1.5 Light sources

For measuring the core levels of the molecules by means of x-ray photoelectron spectroscopy (XPS) very high excitation energies (100-1500 eV) are necessary. To realize this energy range, the use of standard x-ray sources is preferred. The characteristic emission of these sources is determined by the anode material. Typical anode materials are aluminium and magnesium [56]. Conventional sources are x-ray tubes, whose anodes are water cooled in order to improve the maximum emission intensity. Without using a monochromator it is difficult to study the fine-structure of a signal or to analyze the chemical shift due to the linewidths of the x-ray emission line, which are several hundred meV. Therefore the x-ray sources are used in combination with an x-ray monochromator which contains a crystalline mirror as a dispersive element.

The ultra-violet photoelectron spectroscopy (UPS) uses excitation energies in the range of 5-100 eV. He discharge is the most important source, but Ne and Ar are also used. A gas discharge lamp is flanged to the UHV chamber through a differentially pumped capillary. The discharge burns in a water-cooled compartment. In a He gas discharge lamp excited He atoms in a generated plasma emit photons with the characteristic energy of 21.21 eV,

which corresponds to a transition of He $2p$ to the He $1s$ states (He I spectral line). Usually, this line is used without a monochromator. The He II line at 40.82 eV, originated from excited He⁺ ions in the discharge, can also be employed without a dispersive element. The relative intensity of the latter depends on the pressure and the discharge current conditions [56].

3.1.6 Electron energy analyzer

The excited electrons, which left the sample with a certain kinetic energy, have to be detected. Electrons that enter the analyzer have different kinetic energies, so that it is necessary to sort electrons. In the following part the detector, an electrostatic hemispherical analyser (HSA), used in the experiments is explained [53, 61].

At the first step an electrostatic lens array decelerates and focuses the electrons on the entrance slit. The electrons are decelerate to a defined kinetic energy, which is called pass energy E_{pass} . The width of the entrance slit limits the electron emission angles that can pass into the hemispheres and therefore define the acceptance angle of the analyzer. The slit width can be modified, which influences the energy resolution and intensity of the photoemission. Electrons that passed the entrance slit are deflected in the electric field between the two hemispheres, which have different potentials and hence form a capacitor. The electrons travels along the mean radius r_0 to refocus at the exit slit [61]. The higher energetic electrons are forced towards the outer sphere whereas the slower electrons are deflected towards the inner sphere. The relative resolution is given by the following equation [61]:

$$\frac{\Delta E}{E_{pass}} = \frac{w + r_0\alpha^2}{2r_0} \quad (3.13)$$

This resolution is dependent on the slit width w and the angular spread α of the beam. Finally, the sorted electrons are passing the exit slit and hit the so called multi-channel-plate where an electron generates a photon that is multiplied and then detected by a CCD camera.

3.2 Experimental details

3.2.1 The spectrometer system

The x-ray photoelectron spectroscopy experiments have been carried out using an ultra-high vacuum system, which is equipped with an electron-energy analyzer PHOIBOS-150 (SPECS). A scheme of this spectrometer system is shown in the Fig. 3.6.

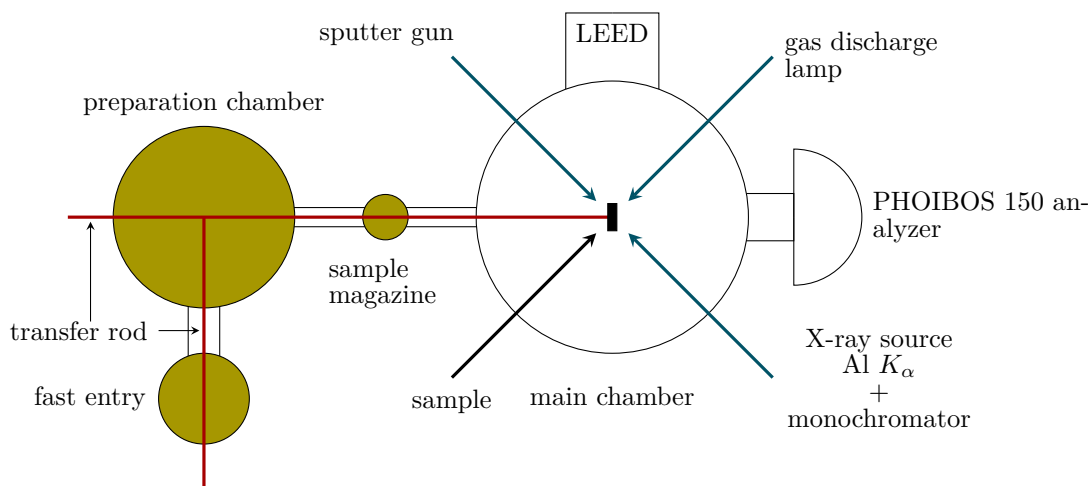


Figure 3.6.: Scheme of the spectrometer SPECS

The spectrometer consists of two UHV chambers, the preparation chamber and the main chamber, which are separated by a gate valve. The basic UHV pressure is lower than $2 \cdot 10^{-10}$ mbar to avoid surface contamination. At first, a sample is placed in the fast entry (third chamber), which is then evacuated with a turbo molecular pump. After reaching a pressure of $1 \cdot 10^{-7}$ mbar in the fast entry, the sample is transferred into the preparation chamber. The preparation chamber contains a sample manipulator with temperature control system which can heat the sample up to 1000°C , Knudsen-type evaporators for the sublimation of organic materials and a quartz microbalance in order to monitor the deposition rate. Without breaking the ultra-high vacuum the sample can be transferred into the main chamber by opening the gate valve. In the main chamber a monochromatized $\text{Al}K_{\alpha}$ source provides photons with an energy of 1486.6 eV for x-ray photoelectron spectroscopy (XPS). The method of XPS is used to measure core level excitations. Photons with an energy of 21.21 eV from a He discharge lamp were used to perform valence band measurements. The total energy resolution of the spectrometer was about 0.35 eV (XPS) and 0.15 eV (UPS). The main chamber is also equipped with a hemispherical energy analyzer, a sputter gun, operated with argon ions (Ar^{+}) and an additional low energy electron diffraction (LEED) system.

3.2.2 Sample preparation

Single crystal preparation

As substrates we used the (100) surface of a gold single crystal (Fig. 3.7a) as well as the (111) surface of silver. Following the standard recipes these surfaces were prepared by repeated Ar^+ sputtering and annealing cycles, after which a typical 5×20 surface reconstruction for gold and a hexagonal structure for silver were observed using low energy electron diffraction, while no remaining contamination was detected in core level photoemission spectra.

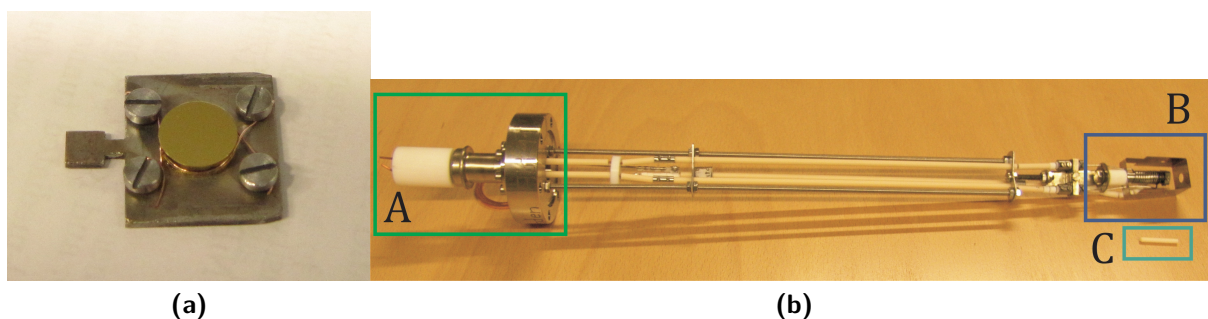


Figure 3.7.: a) Au single crystal fixed on a sample holder , b) Typical evaporator for organic material used at IFW Dresden: A-circuit points for temperature controller, B-crucible with heating wire, C- Al_2O_3 tube filled with organic material

Deposition of the organic layers

The used organic material have been deposited by an *in situ* thermal evaporation. The evaporator typically is shown in Fig. 3.7b.

The single phthalocyanine films (CoPc, F_{16}CoPc and FePc) with a thickness of about 3 nm were prepared by an *in situ* thermal evaporation and with a deposition rate of $1 \text{ \AA}/\text{min}$ onto the metal substrate kept at room temperature. From previous studies it is known that phthalocyanine films grown in this manner result in molecules that are arranged parallel to the substrate surface [31, 62–64]. This has been also verified by our own performed X-ray absorption spectroscopy studies (see section 4.1.1

For the heterostructures, at the beginning, a 3 nm thick phthalocyanine film was deposited on the single crystal at room temperature. This initial film was thick enough to avoid contributions of the metal-organic interface to the spectra. Subsequently, the second phthalocyanine material was deposited. From x-ray absorption spectroscopy (XAS) studies it can be shown that phthalocyanine heterostructures grown in this manner result in molecules that are arranged parallel to the substrate surface (see section 4.2.1).

For the blend, MnPc and F₁₆CoPc have been deposited by simultaneous *in-situ* thermal evaporation and with a deposition rate of 0.1 nm/min (each material). By means of this co-evaporation a 6 nm thick film was deposited on the single crystal at room temperature. This mixed film was thick enough to avoid contributions of the metal/organic interface to the spectra.

A monolayer of each material (CoPc, F₁₆CoPc and FePc) was produced via a thermal annealing process. Thereby, thicker films are gently annealed at a certain temperature which results in a desorption of CoPc, F₁₆CoPc or FePc molecules except the first monolayer, since the interaction in the first monolayer to the gold substrate is stronger than the interaction between the molecules going to thicker layers [65]. The C 1s core level photoemission spectra of these monolayers indicate that the molecules are still intact.

The growth of organic molecules can be distinguished in three different growth modes (see Fig.), depending on the strengths of the adsorbate-adsorbate and adsorbate-substrate [50]:

- Frank-Van der Merwe growth (layer-by-layer growth): If the substrate is chemically reactive, the adsorbate-substrate interaction will have a high magnitude. So the organic molecules are bound strongly at the substrate without moving freely at the surface. The nucleation of the next layer begins after the complete coverage of the substrate. For this growth mode a deposition of homogenous films is characteristic.
- Volmer-Weber growth (3D-island growth): If the substrate is chemically inert, the interaction of the adsorbate-substrate is small, so that it does not influence the growth. Therefore, the molecules can move freely at the surface and can form islands.
- Stranski-Krastanov growth (layer+island growth): Is is an intermediate state between Frank-Van der Merwe and Volmer-Weber growth. This growth mode follows two processes: At first, complete films (up to several monolayers) grow in the layer-by-layer mode. Beyond a critical layer thickness, the Volmer-Weber growth continues. In the Stranski-Krastanov mode, the adsorbate-substrate interaction is neither strong nor weak.

To estimate the thickness of the organic films, we monitored the attenuation of the intensity of the Au 4f_{7/2} and Ag 3d_{5/2} substrate peaks due to the organic film. This is described by the Beer-Lambert law:

$$\frac{I_d}{I_0} = \exp \left[-\frac{d}{\lambda \cdot \cos \theta} \right], \quad (3.14)$$

where I_d is the intensity of the substrate peak after the deposition of the organic material, I_0 stands for the intensity of the clean substrate peak, λ is the electron mean free path, θ is the emission angle relative to the surface normal inside the crystal and d is the thickness of the organic film. For the calculation of the electron mean free path of the organic material, one follows the procedure of Seah and Dench [66]:

$$\lambda[nm] = \frac{49 \cdot E_{kin}^{-2}[eV] + 0.11 \cdot E_{kin}^{1/2}[eV]}{\rho[g/cm^3]} \quad (3.15)$$

In this Eq. 3.15 E_{kin} stands for the kinetic energy of the emitted electrons and ρ is the density of the organic material. This equation is only true for a layer-by-layer growth. In the case of our thin layers it allows a very good estimation of the layer thicknesses.

3.3 Analysis of the electronic and chemical properties

3.3.1 Analysis of UPS data

In ultraviolet photoelectron spectroscopy (UPS) the radiations, which are often used, are the HeI (21.21 eV) and HeII (40.8 eV) radiation. With these photon energies one can map the valence electronic structure of the samples. The obtained spectra can provide information about the electronic structure and about the work function ϕ and the change of the work function Δ . In Fig. 3.8 the UPS spectra of a clean gold single crystal before and after the deposition of a thick layer of a transition metal phthalocyanine (CuPc) are shown. The spectrum of the pure gold crystal shows the Fermi level ($E_F = 0$) of the Au surface, which is used as a reference for the binding energy scale. The width of the spectrum is the difference between the Fermi energy (E_F) and the high binding energy cutoff (HBEC). The HBEC is defined as the energy, where the electrons are able to eject from the surface. This feature is predominantly composed of the electrons which are scattered inelastically. The HBEC is determined by performing a linear fit of the highest binding energy part of the spectrum.

The work function Φ is an important parameter that determines the energy, which is necessary for removing an electron from the sample. When the energy of the radiation is known the work function can be obtained from the HBEC:

$$\Phi = h\nu - HBEC \quad (3.16)$$

The vacuum levels of the substrate and the organic layer are not aligned at the interface. This shift of the vacuum level is shown as an interface dipole Δ . This leads to different

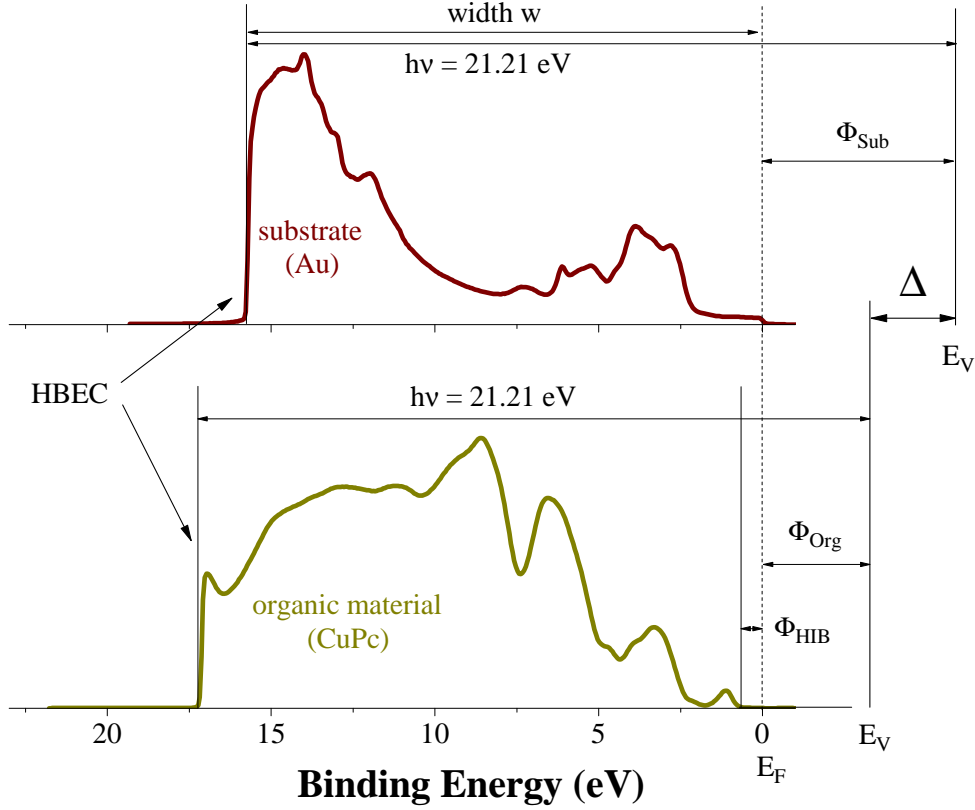


Figure 3.8.: Valence band spectrum of Au(100) (upper part) and CuPc deposited on gold surface (lower part) with a photon energy of 21.21 eV. The measurement allows to calculate the interface parameters like work function (Φ), the interface dipole (Δ), the ionization potential (IP) and the hole injection barrier (HIB).

HBEC positions of the two materials which can be written as:

$$\Delta = \Phi_{sub} - \Phi_{org} = HBEC_{org} - HBEC_{sub} \quad (3.17)$$

For organic semiconductors the valence feature that is used to determine the ionization potential (IP) is the highest occupied molecular orbital (HOMO). The HOMO position is referred to its low binding energy onset. This HOMO onset is determined by linearly extrapolating the low binding energy edge of the spectrum and finding its intersection with the background signal. Therefore, the hole injection barrier Φ_{HIB} can be calculated from the difference in the Fermi energy and the HOMO onset position:

$$\Phi_{HIB} = E_F - E_{HOMO} \quad (3.18)$$

The ionization potential (IP) can be calculated by the sum of the hole injection barrier

Φ_{HIB} and the work function of the organic layer Φ_{org} :

$$\Delta = \Phi_{HIB} + \Phi_{org} \quad (3.19)$$

3.3.2 Analysis of XPS

Chemical shift

The change of the core level binding energy between different chemical forms of the same atoms is called chemical shift. To explain this effect we choose lithium 1s core levels in lithium metal and in lithium oxide, which are depicted in Fig. 3.9.

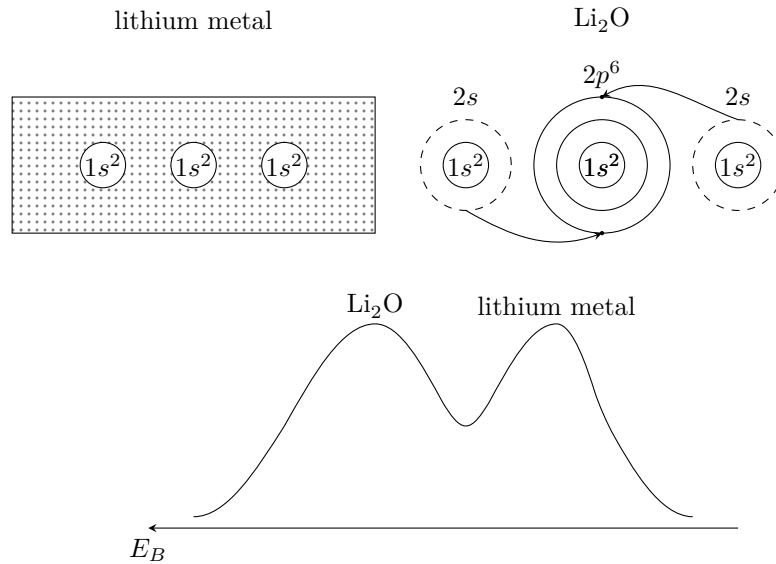


Figure 3.9.: Scheme of the electron configuration of Li metal and Li_2O and the corresponding (schematic) Li 1s core level spectrum [53]

In the pure metal the 2s electrons form a conduction band. The lithium nucleus is screened from the 1s shell through the 2s valence electrons. In lithium oxide every lithium atom donates the 2s electrons into the 2p shell of the oxygen. Thereby an closed $2p^6$ configuration for oxygen is obtained. In lithium oxide the 1s (core electrons) electrons feel a stronger Coulomb interaction than in lithium metal, which reduces the kinetic energy of the corresponding photo-excited electrons. Therefore, the core level feature of the lithium oxide is observed at a higher binding energy than that of the metal.

From the chemical point of view the detected binding energies are also related to the electronegativity of the surrounding covalently bounded atoms. If the electronegativity is very high, the electronic charge of the atom is reduced and core levels of the atoms can thereby observed at higher binding energies. This is illustrated in Fig. 3.10 where the C 1s

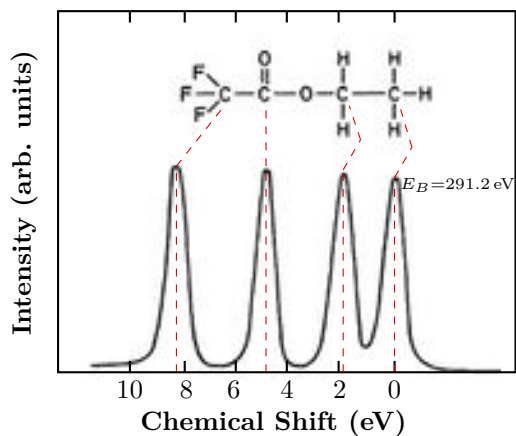


Figure 3.10.: Chemical shifts of C 1s core level in ethyl trifluoroacetate. The chemical shift can be related to the difference in the electronegativity [53]

core level signal of ethyl trifluoroacetate is shown. This compound consists of 4 chemically different carbon atoms. The highest chemical shift is detected for the carbon atom that is bounded to 3 fluorines, which is the element with the highest electronegativity. Consequently, the electron charge density is shifted to the fluorine site and this results in an increasing effective atomic number for the 1s carbon electrons.

Final state effects

The most elementary final state effect in photoelectron spectroscopy is observed in the binding energy. In a simple way, the binding energy is the total energy difference between the final state E_f^{N-1} of the $(N - 1)$ electron system and the initial state E_i^N with N electrons and therefore given by

$$E_B = E_f^{N-1} - E_i^N \quad (3.20)$$

One method to approximate the ground state for the determination of the binding energies is the Koopmans approximation. To obtain the right energy of the final $(N - 1)$ electron states, one begins from the energies of the ground state and try to correct them by the relaxation energies. The binding energy difference can be calculated from Hartree-Fock wave functions for the state with N and $(N - 1)$ electrons. With this the observed binding energy is the negative one electron energy of that orbital from which the photoelectron has been ejected:

$$E_B(k) \simeq -\epsilon_k \quad (3.21)$$

The theory of Koopmans does not consider that after the photoemission process from the orbital k all the other orbitals will regulate this new situation (relaxation). Therefore the correct binding energy is given by

$$E_B(k) = -\epsilon_k - E_R \quad (3.22)$$

where E_R is the (positive) relaxation energy. In a solid this relaxation energy consists of 2 contributions. One is due to the relaxation of the orbitals on the same atom (*intra-atomic relaxation*). The other one results from the charge flow from the solid onto the ion/atom that has the core hole (*extra-atomic relaxation*).

Furthermore, in the XPS spectra one can observe the splitting of the spectral feature in to doublets. The process is the spin-orbit splitting. The electrons move around the core and can be seen as moving charge which induce a magnetic field. The velocity and the orbit of these electrons can be described by the quantum number l . This so called angular quantum number can receive values from $l = 1, 2, 3, \dots$. The electrons have a spin, which is described by the spin quantum number s . Possible values for this quantum number are only $s = \pm 1/2$. One can observe a dipole interaction because the electron spin is linked with the magnetic field and the spin momentum. Such an interaction is called spin-orbit splitting. The combination of the 2 quantum numbers is the total angular momentum quantum number j , which is defined as

$$j = | l + s | \quad (3.23)$$

In Tab. 3.2 the spin-orbit splitting parameter are shown for the different XPS lines. One

Table 3.2.: Spin-orbit splitting parameter [60]

orbital	l	s	j	intensity ratio
s	0	$1/2$	$1/2$	-
p	1	$1/2$	$1/2, 3/2$	1:2
d	2	$1/2$	$3/2, 5/2$	2:3
f	3	$1/2$	$5/2, 7/2$	3:5

can clearly see that in the case of electrons, which are emitted from the s shell, no spin-orbit splitting is detectable. The reason is that the electrons possess a angular quantum number of $l = 0$ and the same total angular momentum quantum number $j = 1/2$ which is spin independent. For all the other orbitals there are 2 different states of the total angular momentum quantum number and therewith a multiplet-splitting is observable.

Satellites

After the photoionisation there is a finite probability that an ion will be left in an excited energy state a few eV above the ground state through excitation of the ion by the outgoing photoelectron. The kinetic energy of this emitted photoelectron is reduced and this is observed as a shake-up line at a higher binding energy than the main spectral feature.

If an electron is excited into an unbound continuum state thereby leaving an ion with vacancies both in a core level and in the valence level, the spectral feature is called shake-off satellite. Other possible satellites are plasmon satellites which are defined as the collective oscillations of electrons with respect to the positively charged ion core.

Secondary electron background

For the subtraction of the background in the following we will introduce the Shirley algorithm [67, 68] which is used in this thesis. The background intensity of each spectrum is caused by the inelastic scattering of the electrons. This intensity of the background is proportional to the intensity of the peak area above the background and to higher binding energies. The method is an iterative one, where the calculation converges after 4 to 5 steps. Starting from a constant background $S_{S,0}(E')$ the correct formula for the Shirley background is given by

$$S_{S,i}(E) = k \int_E^{+\infty} dE' (j(E') - S_{S,i-1}(E')). \quad (3.24)$$

Here the S stands for Shirley-related quantities, k denotes the constant related to the inelastic energy loss cross section and $j(E')$ is the measured intensity at the binding energy E' [68].

4

RESULTS AND DISCUSSION

This chapter of the thesis represents its heart. It presents the results in the field of charge transfer at phthalocyanine interfaces and is divided into two parts:

At first this chapter addresses to the charge transfer at phthalocyanine interfaces to noble metals. The focus lies on the interesting properties of the fluorinated cobalt phthalocyanine. Other phthalocyanines like CoPc, FePc and CuPc are also considered in the studies.

The second section of this chapter contains charge transfer at phthalocyanine hetero-interfaces. In this part of the thesis the heterojunction made of F₁₆CoPc and MnPc dominates, which has been intensively studied. The physical explanation of our experimental data was possible due to the valuable results of the density functional theory calculations, which have been initiated on the basis of our experimental results and which were performed by Rico Friedrich, Torsten Hahn and Jens Jortus, members of the Institute of Theoretical Physics at the TU Bergakademie Freiberg. In the end of this section we extend to other phthalocyanine heterojunctions like CoPc/MnPc and FePc/MnPc.

4.1 Charge transfer at phthalocyanine interfaces to noble metals

The formation of interfaces between molecular materials and metals is an important subject both from the viewpoint of basic science as well as in regard of application aspects. In particular, the understanding of various phenomena and processes that can occur at interfaces between organic films and metals is crucial for the performance of organic based devices. In general, research on organic semiconductors has been carried out in recent years because of their application in advanced optical and electronic devices. Metal phthalocyanines represent a family of organic semiconductors that is characterized by molecules which are rather stable against e.g. heat, light, moisture or oxygen, and metal phthalocyanines have been used already in organic light-emitting diodes (OLEDs) [13], organic photovoltaic cells [13–15], organic field-effect transistors (OFETs) [17, 69] and organic spintronic devices [16, 18], which all contain functional interfaces to metals.

Although the electronic properties of phthalocyanine films have been intensively investigated, the explanation of the interaction at some interfaces is still under discussion. It has been shown previously, that charge transfer can be achieved by the formation of some well ordered phthalocyanine or porphyrine monolayers on noble metal surfaces (Au, Ag). Often, the charge is transferred from the metal substrate to a particular part of the corresponding molecules, the transition metal center. Consequently, the formation of the respective monolayer is connected to valence changes of these transition metal centers, and for many investigated molecules, the transition metal in the center is Co [19, 62, 70–80]. This valence change then must be directly related to a change of the magnetic moment of the corresponding molecule, which represents an important aspect in view of the application of magnetic molecules in molecular or organic spintronic devices or the appearance of the Kondo effect in adsorbed molecules on surfaces [19]. It could also be shown that this ion-substrate bond has often a covalent character [80]. A comparison of theoretical and experimental data of CoPc deposited on metal surfaces indicated that this charge transfer is due to the formation of a molecule-metal hybrid state, most likely a local bond between the $\text{Co } 3d_{z^2}$ and metal states [74, 81].

In contrast to cobalt phthalocyanine, copper phthalocyanine shows no evidence of charge transfer on Au [136]. In this case copper as central atom is unaffected by the noble metal substrate.

In order to gain further information in regard of the interaction of transition metal phthalocyanines to noble metals we focus on iron phthalocyanine (FePc), where the electronic configuration of the iron central ion is d^6 . Moreover, phthalocyanines offer the possibility to change the energy position of the (ligand) molecular orbitals via fluorination, i.e. the

replacement of hydrogen atoms by fluorine. It has been demonstrated that complete fluorination of CuPc and ZnPc to F_{16} CuPc and F_{16} ZnPc results in a shift of the ionization potentials by about 1 eV [83–87] while the energy gap as revealed by optical absorption [85] or a combination of photoemission and inverse photoemission spectroscopy [88] is kept almost the same. In other words, fluorination can be used to engineer the molecular levels in energy, which for instance has allowed the preparation of air stable, n-type OFETs [69]. In the context of charge transfer at interfaces to metals as discussed here, this enables the interesting possibility to investigate the impact of the energy shift of the ligand orbitals (induced by fluorination) on the charge transfer to the transition metal centers of the phthalocyanine molecules.

4.1.1 F_{16} CoPc and CoPc on Au(100)

In this part of the chapter we study the interface between cobalt phthalocyanine (CoPc) and its fluorinated relative (F_{16} CoPc), and a gold single crystal substrate [89]. Our results clearly demonstrate that fluorination, i.e. the different energy position of the ligand molecular orbitals does not influence the charge transfer to the Co molecular center in the first monolayer, which is in good agreement to the picture of a local hybrid state without contribution of the phthalocyanine ligands.

We start the presentation of our results with the valence band photoemission spectra of 3 nm thick CoPc and F_{16} CoPc films as shown in Fig. 4.1. The right panel of Fig. 4.1 shows the spectral profiles near the Fermi energy, which corresponds to a binding energy (BE) of 0 eV. Both spectra are characterized by three maxima in the depicted energy range. The data for CoPc are in very good agreement to previously reported data taken with similar photon energies [76, 90]. The spectral feature, labeled A, at lowest binding energy (about 1.4 eV) represents photoelectron emission from the ligand-derived highest occupied molecular orbital (HOMO) of CoPc. Its shape and energy position is also rather similar to what has been reported previously for other transition metal phthalocyanines [20]. Going to higher BE a second structure (B) is observed at about 2.5 eV. This feature has been attributed to emission from a hybrid molecular orbital of ligand and cobalt $3d$ states [91]. The broader maximum around 3.5 eV cannot be associated with a particular molecular orbital but is related to several states in this energy range. Going to F_{16} CoPc, the maximum of the lowest energy feature is shifted by about 0.1 eV to higher BE, and it is somewhat broader in energy. A shift to higher energies is also observed for the further two peaks the general spectral shape however is very similar to that of CoPc.

In the left panel of Fig. 4.1, we show the high binding energy cutoff, which represents

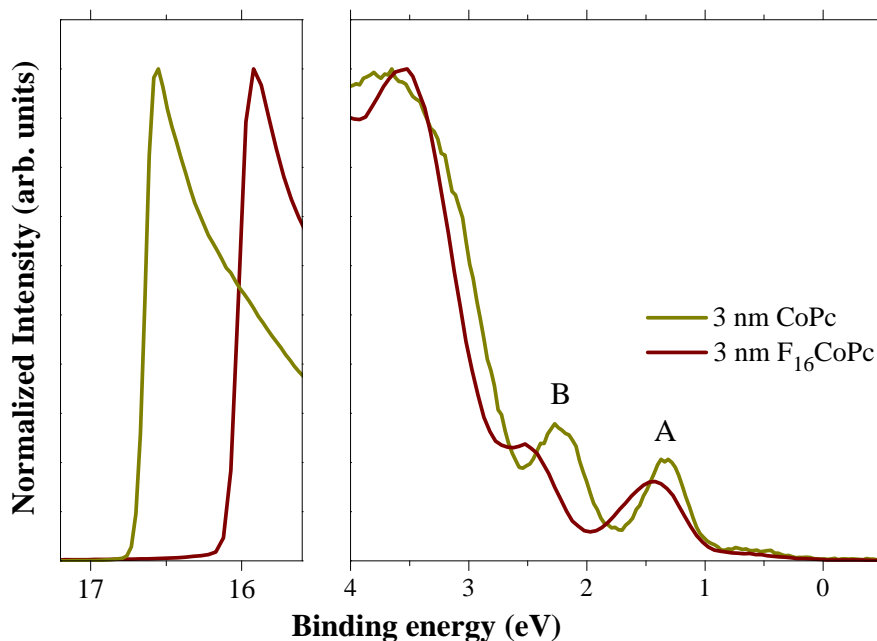


Figure 4.1.: Valence band photoemission spectra of the thick films of CoPc and F_{16} CoPc taken with a photon energy of 21.21 eV up to 4 eV BE, in the left panel the high binding energy cutoff is shown.

the variation in the vacuum level position going from CoPc to F_{16} CoPc. We observe a clear shift by 0.6 eV. Fluorination of phthalocyanines has been studied in the past also for CuPc [84, 85, 137] and ZnPc [83, 86, 87] and there it has been shown that the substitution of all hydrogens by fluorine results in an increase of the molecular ionization potential by about 1 eV, while the energy gap only changes slightly. This is a result of the larger electron affinity of fluorine as compared to hydrogen. An equivalent behavior is also seen for CoPc. The energy shift of the high binding energy cutoff and the valence band features signal a significant increase of the ionization potential of the ligand molecular orbitals by about 0.6 - 0.7 eV upon fluorination.

The photoemission profiles drastically change going to a monolayer of CoPc or F_{16} CoPc on Au(100). In Fig. 4.2 we depict the corresponding valence band photoemission data. Note that the spectral features of the two phthalocyanines sit on a background due to photoemission from the Au substrate (dashed line). The inset of Fig. 4.2 shows the photoemission data of the two monolayers after this Au spectral contribution has been subtracted. In the BE range near the Fermi level the two monolayer spectra are very similar. Both show a first maximum at 0.5 eV (labeled II) followed by a further structure at about 1.3 eV (I). Previous studies of CoPc [76] and related molecules (Co-porphyrines) [73] on noble metal surfaces have revealed that in the first monolayer there is a charge transfer from the metal substrate to the Co center of the molecules resulting in Co(I) ions.

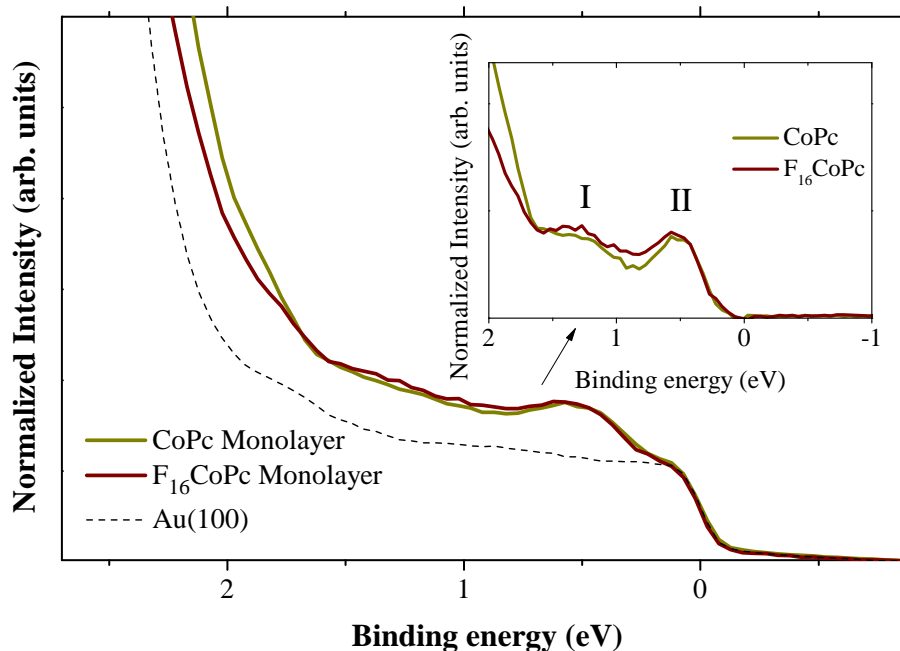


Figure 4.2.: Valence band photoemission spectra of the monolayers of CoPc and F_{16} CoPc taken with a photon energy of 21.21 eV up to 2.7 eV BE. Note: The dashed line is the spectrum of gold and in the inset we show the result of the subtraction of this Au related background (see text).

It has been concluded by these studies that this charge transfer is very local, and does hardly affect the ligand orbital. The spectral feature (II) at lowest binding energy in the photoemission spectra as shown in Fig. 4.2 then is related to an electronic state that is caused by a local hybrid interaction between the Co $3d_{z^2}$ orbital and metal states. From the very close similarity of the two spectra of CoPc and F_{16} CoPc as presented in Fig. 4.2 we conclude that also for F_{16} CoPc in contact to gold there is a local interaction between the Co center and metal states, the formation of a hybrid state and the related charge transfer resulting in a Co(I) center. At this point we note that for higher photon energies (110 eV) an additional feature arises at lower BE than the HOMO level in the valence band of a thick CoPc film on Au(100) due to the higher cross section of the half filled d_{z^2} orbital [91]. This can be associated with the monolayer charge transfer peak observed here even at 21.2 eV photon energy, since the hybrid character increases the cross section, too.

The conclusion above now can be substantiated by the consideration of the corresponding Co $2p$ core level excitation spectra (Fig. 4.3). The upper panel (Fig. 4.3a) depicts the spectra for a CoPc monolayer and a 3 nm thick film on Au(100). Again, the two spectra are drastically different. For the thicker film we observe a main photoemission feature at about 780.3 eV followed by a shoulder at 780.9 eV and a further less intense maximum at

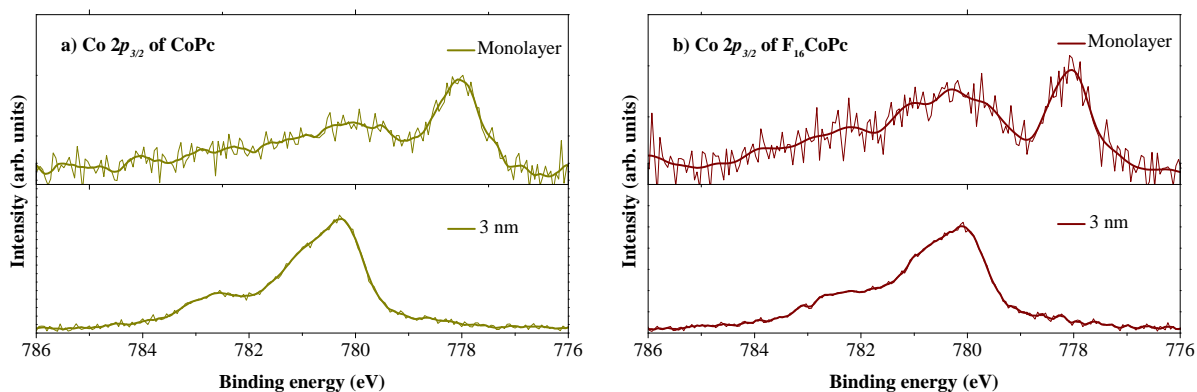


Figure 4.3.: Co $2p$ core level spectra of a monolayer and a thick film of a) CoPc and b) F_{16} CoPc

782.6 eV. These data are in very good agreement to previously published core level spectra of CoPc, and the corresponding spectra represent the divalent Co(II) centers in CoPc [76, 92]. The satellite structures in this case are attributed to the open-shell character of the Co(II) ion with its $3d^7$ electron configuration [70]. Going to the CoPc monolayer on Au(100) the Co $2p$ spectrum clearly changes. There is a core level feature at 778 eV BE followed by a broad maximum around 780 eV. The variation of the Co $2p$ core level spectra going from the 3 nm thick CoPc film to the monolayer is caused by the charge transfer to the Co atom due to the interaction at the metal surface and the related formation of a local hybrid state [74, 81].

Exactly the same behavior is also observed for the fluorinated phthalocyanine F_{16} CoPc (Fig. 4.3b). Both spectra for a 3 nm thick film and the monolayer cannot be distinguished from those of CoPc. This clearly demonstrates that the valence of the Co center and the corresponding changes when the molecules are in contact to a Au(100) surface are practically identical. Thus, also in the case of F_{16} CoPc the Co centers are reduced to Co(I) in the monolayer.

Our results demonstrate that this very close similarity regarding the Co orbital occupation and the interaction on gold between CoPc and F_{16} CoPc is independent of the fact, that fluorination significantly changes the position of the phthalocyanine orbitals with respect to the vacuum level. In other words, the ligand orbitals practically do not play a role in the related interaction at the gold surface which confirms the conclusions that there is a local hybrid formed by Co $3d_{z^2}$ and metal states. Such a local interaction is also in good agreement to the fact that the Co $3d_{z^2}$ orbital with a_{1g} symmetry does not hybridize with any of the ligand π states. Moreover, a ligand independent interaction between Co and the metal surface has also been observed for cobalt tetraphenylporphyrin (CoTPP)

and cobalt octaethylporphyrin (CoOEB) [70, 73, 80]. These organic materials are flat molecules which have Co centers similarly bounded as the case of the phthalocyanines. Finally, in the case of CuPc or ZnPc such an interaction on gold single crystal surfaces is not observed due to the fact that the $3d_{z^2}$ orbital of Cu and Zn is fully occupied and much deeper in energy as a result of the larger potential due to the nuclear charge [87, 137](see also section 4.1.3).

To summarize, the photoemission studies of the phthalocyanine systems CoPc and F₁₆CoPc have shown that for the monolayers on a Au(100) single crystal a charge transfer occurs from the substrate to the Co central ion, which causes a reduction of this ion to Co(I). Our data demonstrate that this charge transfer is fluorination and ligand independent. Most likely a hybrid state between Co $3d_{z^2}$ and metal orbitals is responsible for this behavior. Such a charge transfer also changes the magnetic properties of the molecules since Co(I) most likely is diamagnetic ($S = 0$).

4.1.2 FePc on Ag(111)

Another candidate for charge transfer processes is FePc with its open shell character (d^6). In analogy to the previous studies of cobalt containing phthalocyanines on Au(100), we studied also the system FePc/Au(100), but in this case no interaction was observable. Hence we decided to focus on a different substrate, which is an other noble metal single crystal and therefore comparable to Au(100). We decided to study the interface between iron phthalocyanine (FePc) and a silver single crystal substrate Ag(111), which is focused in this part of the thesis. Here we detect a charge transfer right at the interface.

In Fig. 4.4 the Fe $2p$ core level excitations are depicted. The upper panel shows the spectra for FePc for a monolayer and the lower one shows the spectra for a thick layer of the organic material. Again, we can observe two different line shapes of the core levels. For the thick film a main photoemission feature is observable at 708.4 eV with a shoulder at 709.5 eV. This fits to the typical oxidation state of +2 and is in very good agreement to other photoemission spectra published elsewhere [93]. The asymmetric and broad line shape of the Fe $2p_{3/2}$ can be attributed to the multiplet structures which are caused due to the coupling of the core hole to the open valence shell of the Fe atom [94]. Going to the monolayer of FePc on Ag(111), in the Fe $2p$ spectrum a new peak appears. This new feature is located at 707.7 eV. Analogous what is observed for a CoPc monolayer (see section 4.1.1). The shift to lower binding energies of this new peak indicates a partial reduction of the Fe atoms. Again these data are in good agreement to other published studies of FePc on Ag(111) [95, 96]. The spectra of the Fe $2p$ core level remind to the

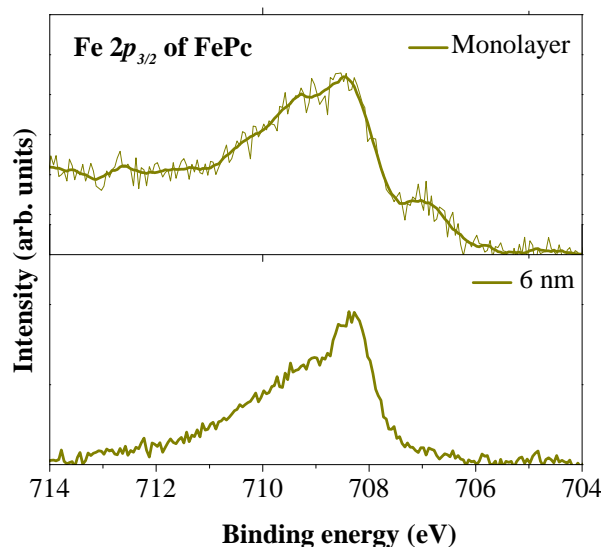


Figure 4.4.: Fe $2p$ core level spectra of a monolayer and a thick film of FePc.

above discussed system CoPc or F_{16} CoPc on gold, where the the variation of the transition metal core level going from a thick layer to a monolayer is caused by a charge transfer to the Co atom due to the interaction at the metal surface and the related formation of a local hybrid state (see section 4.1.1). To substantiate this interface reaction for FePc we also show the corresponding valence band photoemission spectra of the thick FePc film and the monolayer in Fig. 4.5. In the left panel of Fig. 4.5, we show the high binding energy cutoff, which represents the variation in the vacuum level position going from a monolayer to a thick layer of FePc. There is an abrupt shift to higher binding energies due to the deposition of the monolayer, while no significant change is observable going from the monolayer to the thick FePc layer. The shift of the HBEC and therewith a decreasing of the workfunction is due to the formation of an interface dipole in order to achieve thermodynamic equilibrium. The right panel of Fig. 4.5 depicts the spectral profiles near the Fermi energy of the monolayer and the thick film of FePc. The spectrum of the thick FePc layer is characterized by one maximum in the depicted energy range. This feature at 1.5 eV, labeled A, represents the photoelectron emission from the ligand derived highest occupied molecular orbital (HOMO) of FePc [91, 96]. For the monolayer of FePc an additional small peak appears at 0.3 eV, named A_0 . This new spectral feature is a clear evidence for the formation of a new state due to an interaction at the interface. From DFT studies it is proposed that the origin of this interface reaction of FePc on Ag(100) is the strong hybridization of the Fe $3d$ states with the silver ones [97]. The a_{1g} molecular orbitals of FePc are the strongest hybridized states, as expected because of

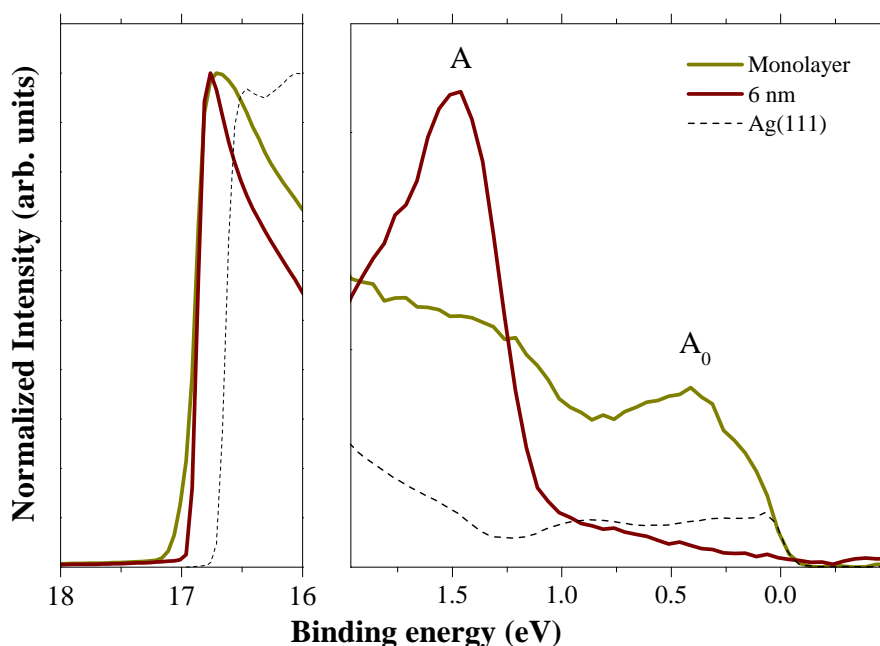


Figure 4.5.: Valence band photoemission spectrum of the thick film of FePc and the corresponding monolayer taken with a photon energy of 21.21 eV up to 4 eV BE, in the left panel the high binding energy cutoff is shown. Note: The dashed line is the spectrum of silver.

their dominant d_{z^2} character. The iron d_{z^2} electrons hybridize with the sp_z states of silver, confirming this direct transition metal- substrate interaction. For the interface reaction on Ag(111), we expect an equivalent hybridization leading to different line shapes in the core level spectra, as well to an additional state near the Fermi energy. Also in the case of FePc on Ag the ligand orbitals do not play a role in this interface interaction, confirming that the charge transfer is local. Again this is in good correspondence to the fact, that the Fe d_{z^2} orbital with a_{1g} symmetry does not hybridize with any of the ligand π states.

To summarize, the photoemission study of the system FePc has shown that for a monolayer on a Ag(111) single crystal a charge transfer occurs from the substrate to the Fe central ion, which causes a reduction of this ion to Fe(I). Most likely a hybrid state between Fe d_{z^2} and metal orbitals is responsible for this behavior.

4.1.3 The complex nature of phthalocyanine/gold interfaces

This section is intended as a summary for the first part of the thesis. The complex nature of phthalocyanine/gold interfaces is discussed, giving the reader an overview of this interesting research field [98]. Here we consider the interface between copper phthalocyanine (CuPc), iron phthalocyanine (FePc), cobalt phthalocyanine (CoPc) and its fluorinated relative (F_{16} CoPc), and a gold single crystal substrate (Au(100)) on the basis of photoemission spectroscopy (XPS, UPS) results, respectively. Our data demonstrate that the interface formation for these phthalocyanine systems is determined by two independent and opposite charge transfer processes which involve either the phthalocyanine ligand or the central Co ion.

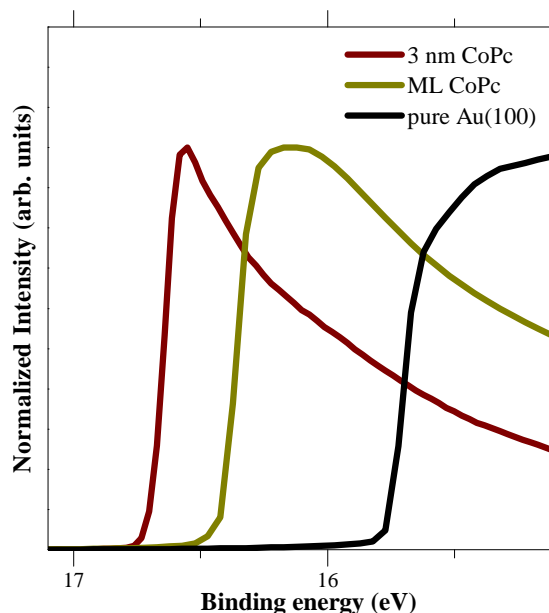


Figure 4.6.: High binding energy cutoff for 3nm CoPc, a monolayer (ML) of CoPc and Au(100).

In general, a large number interfaces between organic semiconductors and metals are characterized by the occurrence of a short range interface dipole, i.e. a change of the electrostatic potential when crossing the interface [46, 50, 99, 100]. Moreover, it has been pointed out that the rationalization of these interface dipoles requires the inclusion of several mechanisms such as a reduction of the metal work function, a (partial or integer) charge transfer between metal and π -electronic system of the organic material depending upon the strength of the interaction at the interface, screening effects, and the contribution of molecular dipoles. Using photoemission spectroscopy, the presence of an interface dipole is signaled by an energy shift of the so-called secondary electron cutoff (for details see

Refs. [50, 100]). In Fig. 4.6 we show the evolution of this cutoff for the interface between CoPc and Au(100) as a function of CoPc coverage. From this figure it becomes clear that this interface also supports a rather large interface dipole. Analogous data of the interface between CuPc and Au(100) [101] show a very similar behavior.

In Fig. 4.7 and Tab. 4.1 we summarize the results of such measurements for the investigated interfaces CuPc/Au(100), FePc/Au(100), CoPc/Au(100) and F₁₆CoPc/Au(100).

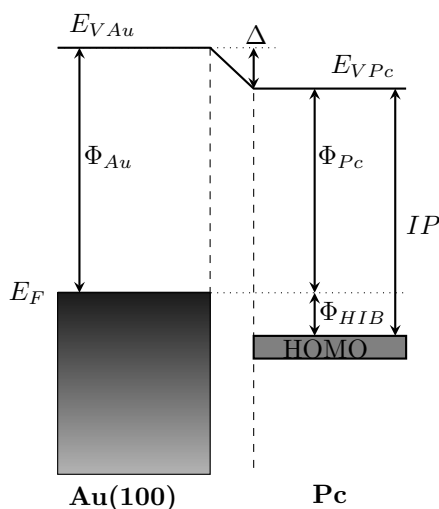


Figure 4.7.: Schematic energy level alignment for an organic semiconductor heterojunction with charge transfer. An important condition for charge transfer is fulfilled when the ionisation energy (IP) of molecule 1 approaches the electron affinity (E_A) of molecule 2. HOMO means highest occupied molecular orbital, whereas lowest occupied molecular orbital is abbreviated LUMO.

Table 4.1.: Interface parameter taken from the photoemission experiments for CuPc, FePc, CoPc and F₁₆CoPc on Au(100). The values of CuPc are taken from Ref.[137]. Note: All parameters are given in eV.

	Φ_{Au}	Φ_{Pc}	IP	Φ_{HIB}	Δ
CuPc	5.3	4.1	5.0	0.9	-1.2
FePc	5.4	4.4	5.3	0.9	-1.0
CoPc	5.4	4.5	5.5	1.0	-0.9
F ₁₆ CoPc	5.4	5.3	6.1	0.8	-0.1

For the unfluorinated systems, the resulting interface parameters are very similar. CoPc, which is a p-type semiconductor, has an ionization potential (IP) of 5.5 eV, somewhat larger than that of CuPc and FePc, and the determined hole injection barriers (Φ_{HIB}) for the three phthalocyanines are nearly the same (about 1 eV). Importantly, the observed interfacial dipole (Δ) of -0.9 eV for CoPc, -1.0 eV for FePc and -1.2 eV for CuPc indicates a charge transfer of electrons from the π - states of the organic semiconductor to

the Au substrate, in other words a positive charging of the organic semiconductor. The high IP (6.1 eV) of F₁₆CoPc can be understood in terms of the replacement of hydrogen by fluorine, causing an energetic lowering of the electronic states while the relative energy level alignment stays the same.

We note that the reduction of the metal work function at these interfaces most likely cannot explain the entire dipoles as observed, which underlines the necessity of a charge transfer in order to understand the complete dipole formation [47].

Furthermore, there is a wealth of information on the CuPc/Au and FePc/Au interfaces, and there is plenty of evidence that the interaction at these interfaces is rather weak, i.e. apart from the above mentioned charge redistribution to achieve the thermodynamic equilibrium, there is no further hybridization between metal and phthalocyanine orbitals (i.e. no chemical interaction). For CuPc/Au such a behavior can be well described within the induced density of interface states (IDIS) model [47, 102]. Due to the decreased atomic number of Fe compared to Co, the energetic position of the Fe 3*d* orbitals is changed in the case of FePc and with this also the formation of the HOMO and LUMO. As a result of the changed energy level alignment in the case of FePc, a charge transfer from gold to FePc can be not energetically preferred. The very similar interface parameters for CoPc/Au suggest that the formation of the interface to gold is independent of the transition metal ion in the three phthalocyanine centers. Moreover, we demonstrate that the dipole formation to a large extent occurs in the first monolayer, which then should also harbor most of the positive charge resulting from the charge transfer or redistribution.

Surprisingly, the transition metal core level photoemission data tell a completely different story. Whereas, there is absolutely no evidence that the electronic levels of Cu [101] and FePc on Au(100) are affected by the interface formation, the Co 2*p* core level excitation spectra (Fig. 4.8) are drastically different between the first monolayer of CoPc on Au(100) and thicker layers (cf. section 4.1.1). Fig. 4.8 again summarizes the spectra for a CoPc monolayer and a 3 nm thick film on Au(100). For the thicker film we observe a main photoemission feature at about 780.3 eV followed by a shoulder at 780.9 eV and a further less intense maximum at 782.6 eV. Going to the CoPc monolayer on Au(100) the Co 2*p* spectrum substantially changes. Now, there is a core level feature at 778 eV BE followed by a broad maximum around 780 eV. This variation of the Co 2*p* core level spectra going from the 3 nm thick CoPc film to the monolayer is caused by a charge transfer to the Co atom due to the interaction at the metal surface and the related formation of a local hybrid state [74, 81]. Importantly, this hybrid state is formed by Co 3*d*_{2,2} and metal states and therefore does hardly affect the phthalocyanine ligand.

We are thus left with the intriguing scenario that at the CoPc/Au interface two opposite

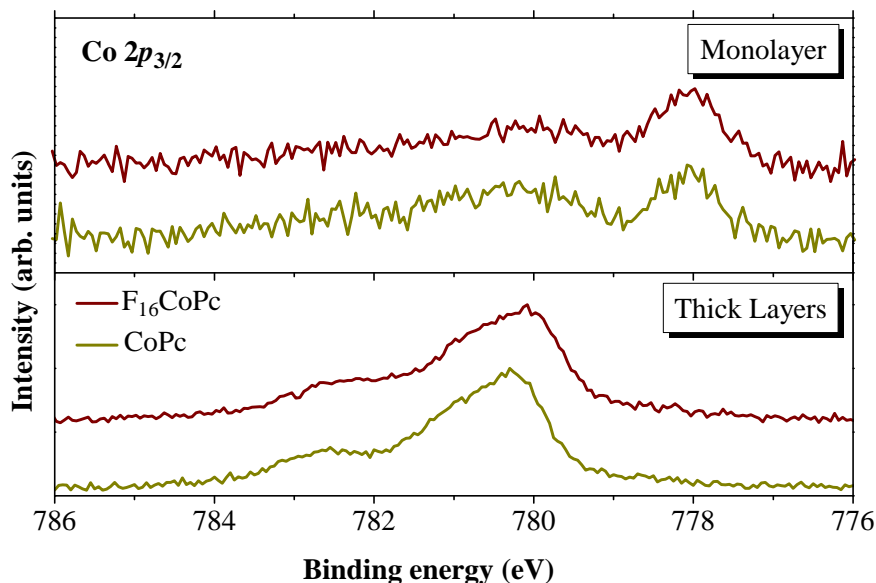


Figure 4.8.: Co $2p$ core level spectra of a monolayer and a thick film of CoPc and F_{16} CoPc on Au(100) to illustrate the close similarity.

charge transfer channels are open. While the organic ligand is responsible for thermodynamic equilibrium and energy level alignment at the interface, which is managed by a (partial) charge redistribution as described within the IDIS model, there is an additional but independent local interaction of gold and the central Co ion, which as a result is oppositely charged. To further demonstrate the local character of this Co-Au hybrid, we show in Fig. 4.8 the corresponding Co $2p$ core level excitation spectra also for fluorinated F_{16} CoPc deposited onto Au(100) (cf. section 4.1.1). For both materials, CoPc and its fluorinated relative F_{16} CoPc, the valence of the Co center and the corresponding changes when the molecules are in contact to a Au(100) surface are practically identical.

To summarize, the photoemission studies of the phthalocyanine systems CoPc and F_{16} CoPc have shown that for the monolayers on a Au(100) single crystal a charge transfer occurs from the substrate to the Co central ion, which causes a reduction of this ion to Co(I). Importantly, this charge transfer is local and independent of the phthalocyanine ligand. The energy level alignment at the interface however is not governed by this local interaction but by the ligand of the Pc molecules in close analogy to CuPc and FePc. Consequently, interfaces between CoPc materials and gold exhibit two types of independent and opposite charge transfer resulting in a final charge distribution in the molecules close to the gold surface as depicted schematically in Fig. 4.9.

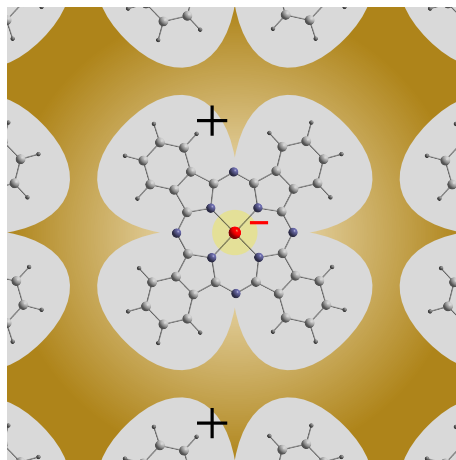


Figure 4.9.: Scheme of the two types of charge transfer at the CoPc/Au interface: From the interaction of the ligand and gold a "positive" charge occurs. A "negative" charge of the center originates from a local interaction between the Co and Au.

4.2 Charge transfer at phthalocyanine hetero-interfaces

The concept of charge transfer in purely organic materials has played a very important role in fundamental as well as applied sciences. Prominent examples are organic conductors and superconductors [1–4]. Entire classes of so-called charge transfer salts have been synthesized and demonstrated interesting and often unexpected physical properties ranging from metallicity and superconductivity over complex phase diagrams including charge density and spin density wave phases to highly correlated materials (Mott insulators) [2, 4]. Recently, the formation of a two-dimensional metallic layer has been reported as a consequence of charge transfer between the two insulating organic crystals (TTF and TCNQ) [5, 6]. In view of more applied aspects, charge transfer has also been investigated and exploited in order to improve or engineer the performance of organic electronic devices. For instance, it has been shown that the inclusion of organic dopants in organic semiconductors can significantly enhance charge carrier injection from electrodes [10], and the modification of electrode surfaces with particular organic layers accompanied by charge transfer allows tuning of hole injection barriers at such junctions [9].

4.2.1 Heterojunction: MnPc/F₁₆CoPc

In this section, we present a heterojunction made of two structurally very similar transition metal phthalocyanines (TMPc's), MnPc and F₁₆CoPc, where photoelectron spectroscopy studies and calculations based upon density functional theory (DFT) clearly demonstrate the occurrence of hybridization and charge transfer [103]. Moreover, our results strongly indicate that this charge transfer is very local and essentially affects the transition metal centers only, which presents a unique property of this corresponding interface.

We start the presentation and discussion of our results with the evolution of the C 1s core level photoemission signal when F₁₆CoPc is gradually deposited on a 3 nm thick MnPc film on Au(100) as shown in Fig. 4.10. As a consequence of the high surface sensitivity

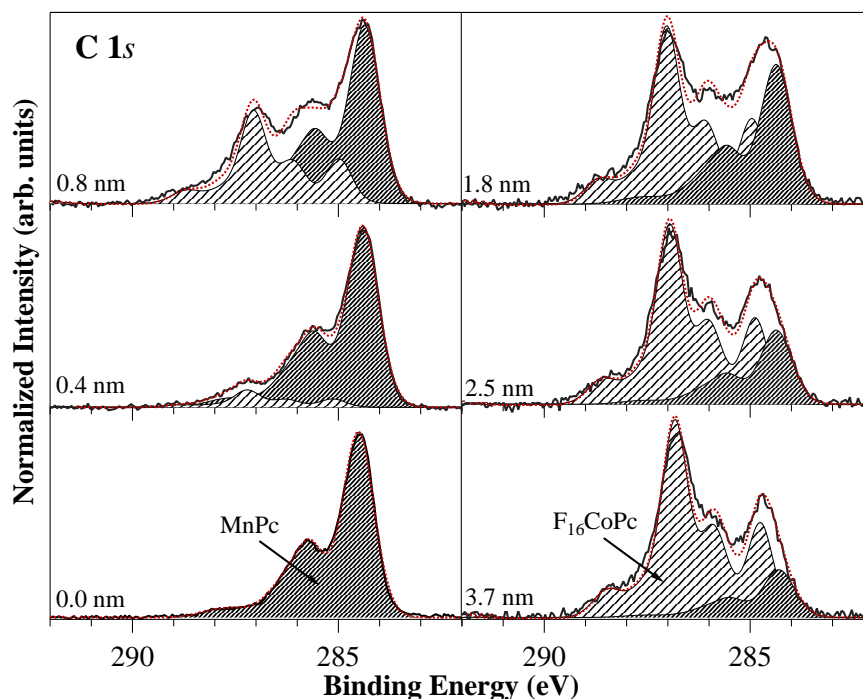


Figure 4.10.: Evolution of the C 1s core level photoemission profile upon deposition of F₁₆CoPc on a 3 nm thick layer of MnPc. We additionally show the results of a modelling of the data using an appropriately weighted sum (dashed line) of otherwise unchanged photoemission profile of the two individual phthalocyanines (filled areas).

of such measurements we observe an increasing contribution of the signal from F₁₆CoPc with respect to that of MnPc. Fortunately, the two C 1s emission spectra can be well distinguished due to the presence of fluorine in F₁₆CoPc and the resulting spectral shape with an additional maximum at about 287 eV binding energy in this case [20, 63]. Fig. 4.10 also shows the results of a modelling of our data with a simple superposition of the C 1s core level spectra of the two materials with appropriate weights but without any change

in relative peak heights, positions or widths.

The agreement of the measured data and the modelling in Fig. 4.10 is very good, which clearly shows that the two phthalocyanine ligands are virtually not affected by the neighborhood of the other molecule, respectively, at the heterojunction. In other words, there is no interaction at our $F_{16}CoPc/MnPc$ interface which significantly modifies the Pc ligands, in contrast to e.g. doping of phthalocyanine films with potassium, where the C 1s photoemission profile is characterized by the appearance of an additional core level feature [104, 105]. We note that this conclusion is corroborated by the fact that the variation of the relative C1s binding energies of the two species during data modelling is less than 300 meV. In Fig. 4.11 the evolution of the N1s core level photoemission profile upon de-

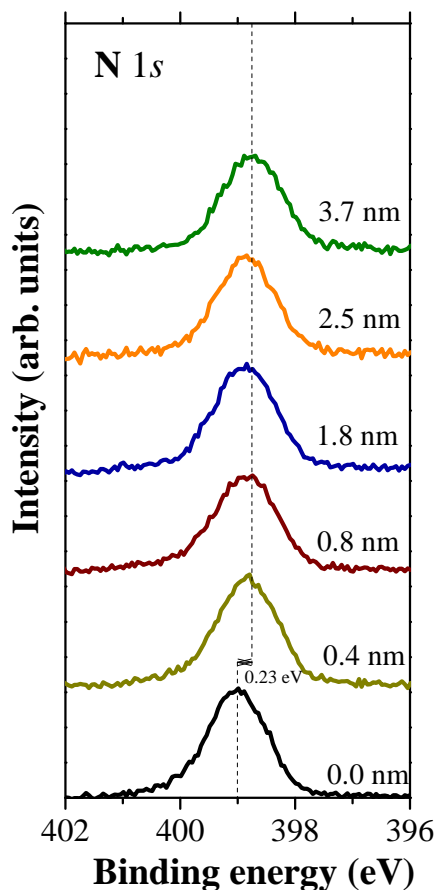


Figure 4.11.: Evolution of the N 1s core level photoemission profile upon deposition of $F_{16}CoPc$ on a 3 nm thick layer of MnPc.

position of $F_{16}CoPc$ on a thick layer of MnPc is shown. After the first deposition the binding energy varies only around 230 meV and then no significant change is observable upon deposition. This fact emphasize the conclusion that the charge transfer only effects

the transition metal center and the ligand is not involved in this process.

Turning to the $\text{Co } 2p_{3/2}$ photoemission spectra at the same interface intriguingly discloses us an opposite behavior. There is a dramatic change in line shape and binding energy when going from a very thin F_{16}CoPc layer on top of MnPc to a thick layer. This is depicted in Fig. 4.12, where we also show the $\text{Co } 2p_{3/2}$ photoemission spectrum of a monolayer of F_{16}CoPc deposited on Au(100) (see section 4.1.1) [89]. The latter data are

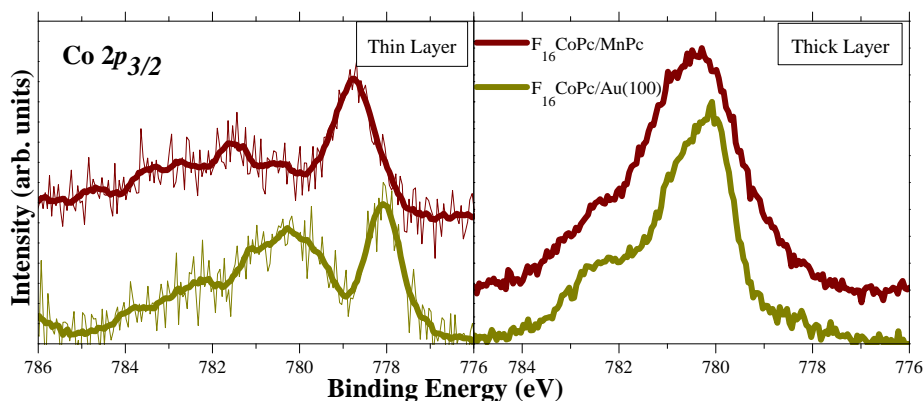


Figure 4.12.: $\text{Co } 2p_{3/2}$ core level photoemission spectra of a thin and thick F_{16}CoPc layer on top of MnPc. Also shown is the corresponding result for a F_{16}CoPc monolayer on Au(100) [89].

in almost perfect agreement to a number of studies in the literature where the interaction of Co-phthalocyanines and Co-porphyrines on various metal surfaces has been reported [72, 76, 89] (see section 4.1.1). There is a general agreement that the data as shown in Fig. 4.12 arise from a rather strong interaction of the Co metal center in the molecules and the metal substrate which results in a reduction of this metal center to (at least) Co(I) [72, 74, 76, 89, 106], while the Co valence in undisturbed CoPc's and Co porphyrins is Co(II), which gives rise to a $\text{Co } 2p_{3/2}$ photoemission line shape and energy as shown in Fig. 4.12 for the thick F_{16}CoPc film on MnPc. Consequently, there is clear evidence that direct at the $\text{F}_{16}\text{CoPc}/\text{MnPc}$ heterojunction the Co center of the F_{16}CoPc is reduced, i.e. there is substantial interaction accompanied by charge transfer at this interface.

Our photoemission data of the equivalent interface but prepared in the opposite manner by depositing MnPc on a 3 nm thick F_{16}CoPc layer complement this surprising result. We note that for this deposition sequence we present data, where in a first step F_{16}CoPc is deposited onto a Ag(111) surface. In this way we avoid the contribution of $\text{Au } 4p_{1/2}$ core level photoemission features, which energetically overlap with that from $\text{Mn } 2p$ and therefore renders a reasonable data analysis impossible.

In Fig. 4.13 we show both the $\text{Co } 2p_{3/2}$ and $\text{Mn } 2p_{3/2}$ core level data as a function of MnPc overlayer thickness on F_{16}CoPc . The $\text{Co } 2p$ core level data of F_{16}CoPc before MnPc

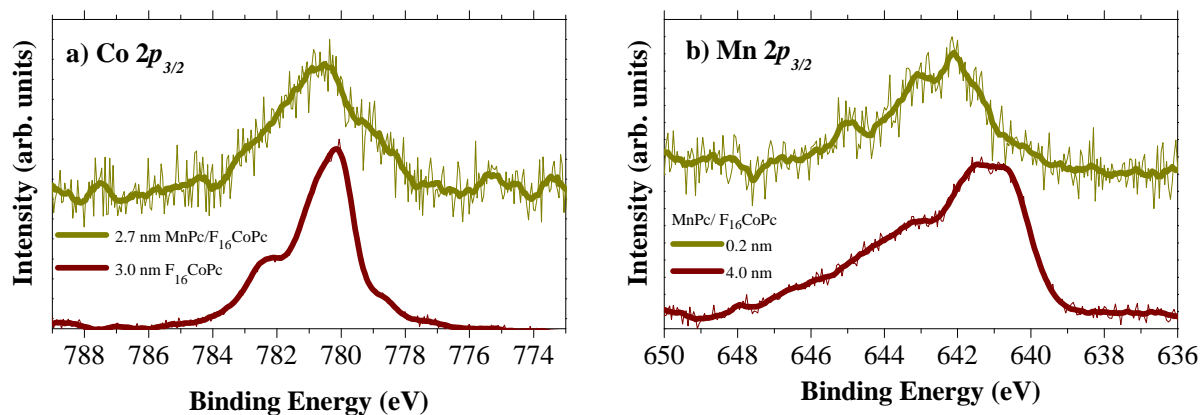


Figure 4.13.: a) $\text{Co } 2p_{3/2}$ and b) $\text{Mn } 2p_{3/2}$ core level photoemission spectra for a $\text{MnPc}/\text{F}_{16}\text{CoPc}$ heterojunction when MnPc is deposited on a 3 nm thick F_{16}CoPc layer.

addition are virtually identical to those measured for thick F_{16}CoPc films on various substrates (see also Fig. 4.12 above) and thus represent undisturbed F_{16}CoPc . Upon addition of MnPc a low energy structure appears, which is a clear evidence for the reduction of cobalt as described above in the context of F_{16}CoPc deposition on MnPc . This arises from the F_{16}CoPc molecules in direct contact to the MnPc layer surface. Note that in this case the $\text{Co } 2p_{3/2}$ core level spectra always represent a superposition of the reacted upper-most layer (interface) and the other undisturbed layers (bulk) below. For this reason the spectra in Fig. 4.12 and Fig. 4.13 a do not have the same line shape. Consequently, the reduction of the central Co atom of F_{16}CoPc in contact to MnPc is independent of the formation sequence of the $\text{F}_{16}\text{CoPc}/\text{MnPc}$ heterostructure.

The question now arises, where does this charge, which is necessary for the reduction of Co atoms, come from? Fig. 4.13 additionally shows the $\text{Mn } 2p_{3/2}$ spectra for a very thin and a thicker MnPc layer on F_{16}CoPc . These two spectra are clearly different. Both the spectral shape and in particular the binding energy change, which signals a variation of the Mn charge state in MnPc , whereas in this case the Mn atoms are oxidized, as seen by the upshift in binding energy.

To summarize the experimental observations, we have presented clear evidence for the formation of a $\text{MnPc}^{\delta+}/\text{F}_{16}\text{CoPc}^{\delta-}$ heterojunction, with particular involvement of the two transition metal centers. Calculations of a dimer made from these two phthalocyanines now give detailed insight into the nature of the interaction at the hetero-interface.

Within the theoretical treatment¹, which was initiated by our experimental results,

¹The theoretical treatments were performed by Rico Friedrich, Torsten Hahn and Jens Kortus, members of the Institute of Theoretical Physics; TU BA Freiberg. For more details on the computational aspects see appendix (A.1).

we first studied the systems $F_{16}\text{CoPc}$ and MnPc individually. For $F_{16}\text{CoPc}$ one finds that all energy levels as well as the Fermi level is pulled down in energy compared to hydrogenated CoPc due to the strong electronegativity of fluorine, which is depicted in Fig. 4.14. Consequently the electron affinity of $F_{16}\text{CoPc}$ is increased by 0.8 eV compared

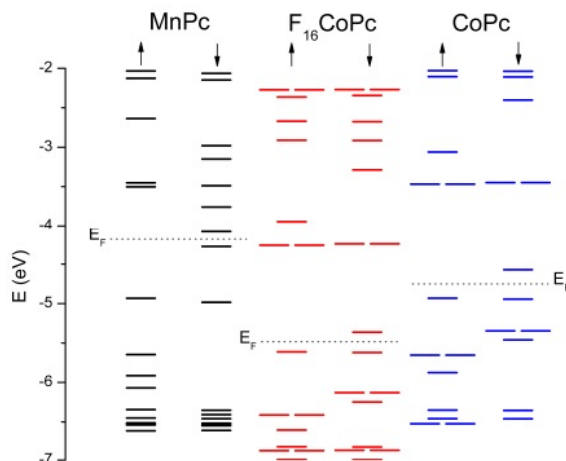


Figure 4.14.: Comparison of the energy levels of MnPc , $F_{16}\text{CoPc}$, CoPc aligned at the vacuum energy, taken from Ref. [107].

to CoPc (from 2.9 eV to 3.7 eV), which is in good agreement to the data showed in Tab. 4.1 (cf. section 4.1.3). Note that these absolute values are for individual free molecules and shielding effects in the bulk will change this quantity. However the energy ordering of the molecular levels near the Fermi level stays the same and also the spin of the system ($S = 1/2$) is preserved. The HOMO is a purely ligand-derived π state whereas the LUMO is a $\text{Co } 3d_{z^2}$ state.

For MnPc the orbital alignment around the Fermi-level has already been published recently [108]. There the energy levels around the Fermi-level are of $\text{Mn } 3d_{xz}$ and $\text{Mn } 3d_{yz}$ nature. It is also pointed out that MnPc has an ionization potential of 4.5 eV, which is considerably smaller than the values for all other transition metal phthalocyanines due to the additional levels at the Fermi-level. The spin of MnPc is found to be $S = 3/2$.

Because the experimentally revealed charge transfer indicated a strong confinement to the phthalocyanine interface, calculations of a $\text{MnPc}-F_{16}\text{CoPc}$ dimer system were performed. The results of the DFT calculation show that the level ordering for the molecules is preserved and that the states of the two systems combine to form a new energy level diagram. The crucial finding is that the $\text{Mn } 3d_{xz}$ (respectively $\text{Mn } 3d_{yz}$) and the $\text{Co } 3d_{z^2}$ state hybridize and form a two-level system as shown qualitatively in Fig. 4.15. As those two orbitals couple to each other, they form one bonding state lowered in energy and one

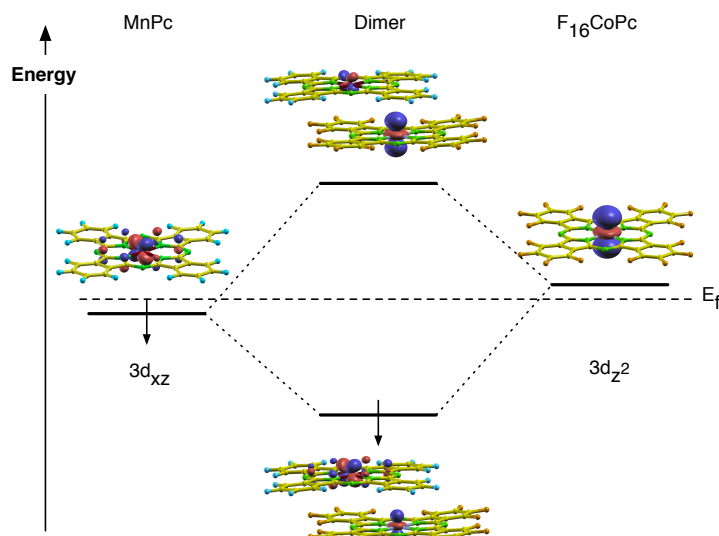


Figure 4.15.: Interaction of the MnPc and $F_{16}\text{CoPc}$ states in the MnPc- $F_{16}\text{CoPc}$ dimer close to the Fermi-level. The Mn $3d_{xz}$ (respectively Mn $3d_{yz}$) and the Co $3d_{z^2}$ orbitals hybridize to form a two-level system.

anti-bonding state increased in energy as it is the case within the formation of a chemical bond. Since the Mn $3d_{xz}$ (respectively Mn $3d_{yz}$) state is the HOMO of MnPc and the Co $3d_{z^2}$ state is the LUMO of $F_{16}\text{CoPc}$ only the lower one of the two hybrid states is occupied forming the HOMO of the dimer system. As this hybrid state is delocalized over both molecules with the largest contributions at the metal centres also the charge within this orbital is spread out to the dimer system. Hence a charge of approximately 0.2 electrons is transferred from MnPc to $F_{16}\text{CoPc}$. The value of this charge transfer is very sensitive to the actual distance of the molecules at the interface. In addition the systematic underestimation of the band gap within GGA-DFT which is well known for metal Pc's [109] further complicates an accurate estimation of the transferred charge. However the formation of the hybrid state corresponds quite nicely to the observed experimental data and the charge transfer stated before ². The finding can be rationalized by both the low ionization potential of MnPc and the enhanced electron affinity of $F_{16}\text{CoPc}$. As the states of $F_{16}\text{CoPc}$ are lowered in energy the LUMO approaches the Mn $3d_{xz}$ HOMO allowing us to observe the fundamental interaction behind. Hence one can attribute the synthesized phthalocyanine heterojunction as a route to a rational design of interface induced charge transfer systems based on well known molecules. Further, based on the theoretical results the studied dimer has a net spin of $S = 2$, which also might make this arrangement attractive for spintronic applications since spin filter effects could be

²The formation of the hybrid state at the interface was also preserved within DFT calculations including van der Waals interaction.

observable.

To show the high degree of order of the produced phthalocyanine heterojunctions and to substantiate the charge transfer we performed **X-ray absorption spectroscopy (XAS)**³ on films growing in an equivalent manner. XAS is a helpful method to obtain information to the molecular orientation or unoccupied electronic structure which monitors transitions from a core level into unoccupied orbitals.

We begin the presentation of our XAS results in Fig. 4.16, which shows the N 1s absorption spectra of different layer thicknesses of the heterojunction F₁₆CoPc/MnPc and also of the individual phthalocyanine materials deposited on a gold single crystal (Au(100)). These spectra were recorded at different angles of beam incidence, whereas the angle $\theta = 0^\circ$ ($\vec{E} \perp z$) corresponds to normal and $\theta = 70^\circ$ ($\vec{E} \parallel z$) to grazing incidence of the horizontal linearly polarized synchrotron light. The angle θ gives the angle between the incident light and the surface normal (z -axis).

At first, we discuss the spectra of pure MnPc (Fig. 4.16 a) and F₁₆CoPc (Fig. 4.16 e) as grown on the metal substrate. It is well established that for planar π -conjugated systems, as is the case for F₁₆CoPc and MnPc molecules, the $1s-\pi^*$ and $1s-\sigma^*$ transitions take place for a light polarization vector perpendicular and parallel to the molecular planes, respectively [110]. Furthermore, previous investigations have shown that the rather sharp N 1s XAS peaks in the energy region between 398 and 405 eV can be assigned to transitions from the N 1s core-level into the unoccupied π orbitals with N 2p orbital contributions, which are oriented perpendicular to the molecular plane. The high-energy structures above 405 eV, are related to N 1s - σ^* transitions. The corresponding XAS features are quite broad if compared to the π^* peaks which is due to a shorter lifetime and a larger energy bandwidth of the σ^* states.

Our results for the N 1s absorption spectra of MnPc and F₁₆CoPc reveal a very strong polarization dependence. In particular, the absorption features related to transitions into π^* states are strongest for grazing incidence, while the opposite is observed for the transitions into σ^* molecular orbitals. This represents clear evidence that in both cases the phthalocyanine molecules are arranged parallel to the substrate surface with a very high precision. In comparison to previous studies [92, 111] our data signals an average misorientation with respect to exactly parallel molecules in the entire film of about 5%.

This very high degree of order with the phthalocyanine molecules lying parallel to the substrate surface now can be transferred to the F₁₆CoPc/MnPc phthalocyanine heterojunction as studied in this contribution. This is demonstrated in Fig. 4.16 b, c and d, where we show F₁₆CoPc layers of different thickness as grown on a MnPc layer. It is

³For more details on the method and the experiment see appendix (A.2).

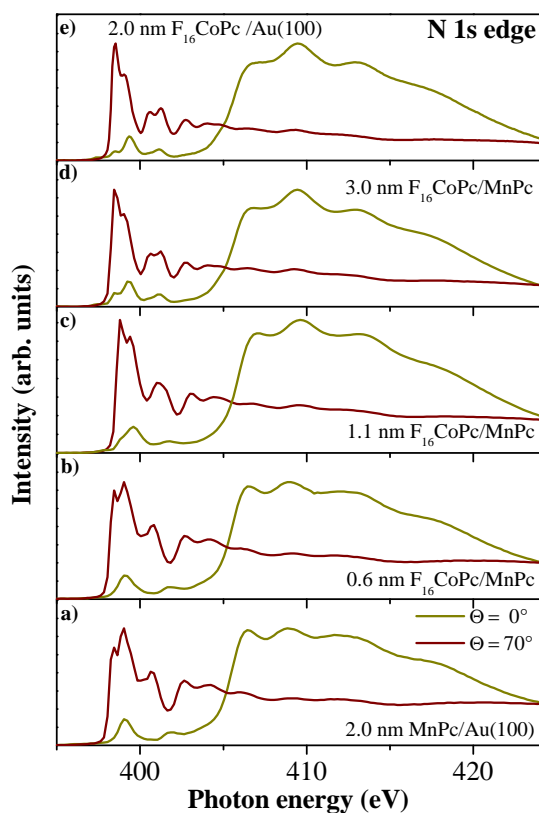


Figure 4.16.: N $1s$ excitation spectra for a) 2.0 nm MnPc on Au(100) b) 0.6 nm F_{16} CoPc on MnPc c) 1.1 nm F_{16} CoPc on MnPc d) 3.0 nm F_{16} CoPc on MnPc and e) 2.0 nm F_{16} CoPc on Au(100). The spectra were recorded with different angles of beam incidence. θ gives the angle between the surface normal and the direction of the incident beam. ($\theta = 0^\circ$ corresponds to normal and $\theta = 70^\circ$ to grazing incidence.)

evident that the strong polarization of the spectra does not change in comparison to the films out of one phthalocyanine molecule only.

The high degree of molecular order allows additional insight into the anisotropy of the excitations into Co derived $3d$ levels in F_{16} CoPc close and far from the interface to MnPc. In Fig. 4.17 we show the corresponding Co L_3 edge absorption spectra. Again, these spectra were recorded at two different angles of beam incidence (see Fig. 4.17).

In Fig. 4.17c, the Co L_3 edge absorption spectrum of a 2 nm thick F_{16} CoPc layer on Au(100) is depicted. In contrast to cobalt phthalocyanine (CoPc), such XAS data of F_{16} CoPc have not been reported yet. Also in this case the absorption data show a very clear anisotropy when taken at different polarization directions of the incident synchrotron light, corroborating the high degree of molecular order. At grazing incidence, the absorption feature at about 778 eV (labelled A) dominates the spectrum, while for normal incidence we observe maximal absorption for feature B_1 and B_2 at about 780 - 782 eV.

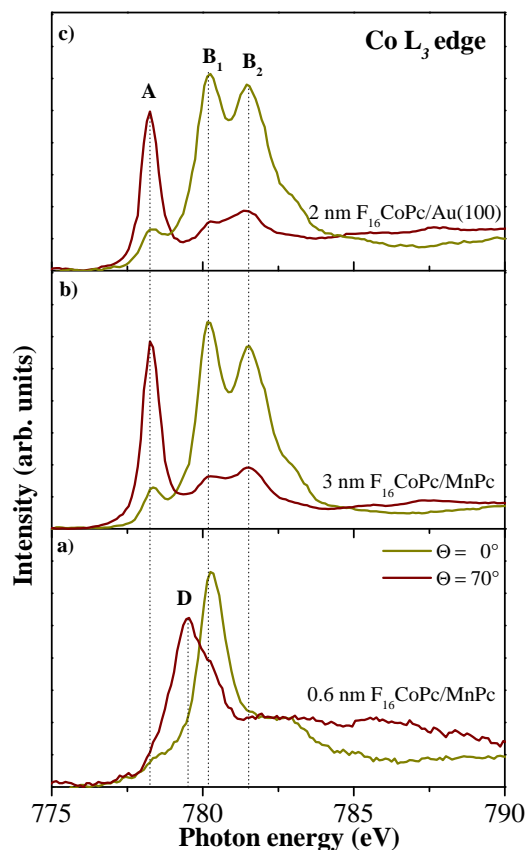


Figure 4.17.: Co L_3 edge absorption spectra for a) 0.6 nm $F_{16}\text{CoPc}$ on MnPc b) 1.1 nm $F_{16}\text{CoPc}$ on MnPc c) 3.0 nm $F_{16}\text{CoPc}$ on MnPc and d) 2.0 nm $F_{16}\text{CoPc}$ on Au(100). The spectra were recorded with different angles of beam incidence. θ gives the angle between the surface normal and the direction of the incident beam. ($\theta = 0^\circ$ corresponds to normal and $\theta = 70^\circ$ to grazing incidence.)

These spectra and their polarization dependence are very similar to the corresponding absorption spectra of CoPc [24, 77, 92]. We take this as evidence that fluorination of CoPc to $F_{16}\text{CoPc}$ has little impact on the electronic $3d$ states of the central Co atom and their occupancy. This is in good agreement to calculations which predicted a rigid-like energy shift of the molecular orbitals upon fluorination of CoPc but essentially no other changes [112]. Consequently, we assign the absorption feature A, which is maximal for a light polarisation perpendicular to the $F_{16}\text{CoPc}$ molecules to transitions from the Co $2p$ into unoccupied $3d_{z^2}$ states. Analogously, features B_1 and B_2 arise from an excitation multiplet related to the excitations into the Co $3d_{x^2-y^2}$ orbital [24, 77, 92].

The evolution of the Co L_3 edge absorption spectra upon formation of the $F_{16}\text{CoPc}/\text{MnPc}$ heterojunction are shown in Fig. 4.17a and b. While for thicker $F_{16}\text{CoPc}$ layers on top of MnPc the absorption spectra closely resemble those of the pure $F_{16}\text{CoPc}$ film, they radically change for a thin layer of $F_{16}\text{CoPc}$ deposited on MnPc, i.e. for $F_{16}\text{CoPc}$ molecules in contact to MnPc. The absorption features that are representative for $F_{16}\text{CoPc}$ essen-

tially disappear, while two new absorption maxima are observed around 780 eV, still with a visible anisotropy with respect to the light polarization. Following the recent observation of an interaction between the transition metal centers of $F_{16}\text{CoPc}$ and MnPc with a charge transfer from $\text{Mn } 3d$ to $\text{Co } 3d$ levels, we associate the clear spectral changes to the formation of $F_{16}\text{CoPc}/\text{MnPc}$ dimers and this charge transfer. The disappearance of feature A supports the results from photoemission spectroscopy that a hybrid state is formed between the two types of phthalocyanines, which causes a (partial) filling of the $\text{Co } 3d_{22}$ orbital of $F_{16}\text{CoPc}$, i.e. a reduction of the Co center in this phthalocyanine [103]. This interpretation is also in good agreement with the evolution of the $\text{Co } L_3$ edge absorption spectra of CoPc when intercalated with K [113], which is depicted in Fig. 4.18. For lower intercalation levels, potassium addition results in an initial charge transfer to

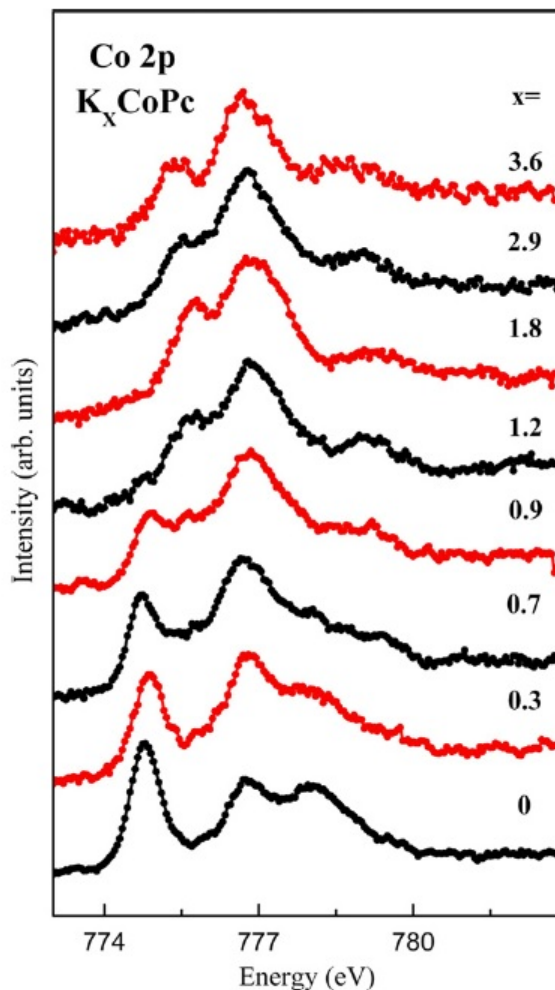


Figure 4.18.: $\text{Co } 2p_{2/3}$ x-ray absorption edges of K_xCoPc films, taken from Ref. [113].

the Co center of CoPc and the change of the $\text{Co } L_3$ edge absorption spectra is very similar to what is observed in our data.

To conclude, the CoL_3 edge absorption spectra for the F_{16}CoPc can be understood in terms of the formation of the hybrid state between Co and Mn 3d levels as well as the associated charge transfer. While the absorption feature D then is related to the excitation into the Co $3d_{z^2}$ contribution to the hybrid state, the vanishing multiplet splitting of feature B seen for a light polarization parallel to the molecular planes is a result of the charge transfer to the Co 3d states. Within the atomic multiplet theory in total 16 transitions would be allowed for $3d^7 \rightarrow 2p^5 3d^8$ (i.e. F_{16}CoPc), only 4 transitions would be expected after Co is reduced: $3d^8 \rightarrow 2p^5 3d^9$, which is connected to a loss of the wide and prominent multiplet as seen for pure F_{16}CoPc and a light polarization parallel to the molecular plane (for detailed information see de Groot et. al [114]). For instance, in the case of Ni in NiPc ($3d^8$) the $2p_{2/3}$ absorption spectrum consists basically of a single intense feature for in-plane polarized light [24, 115].

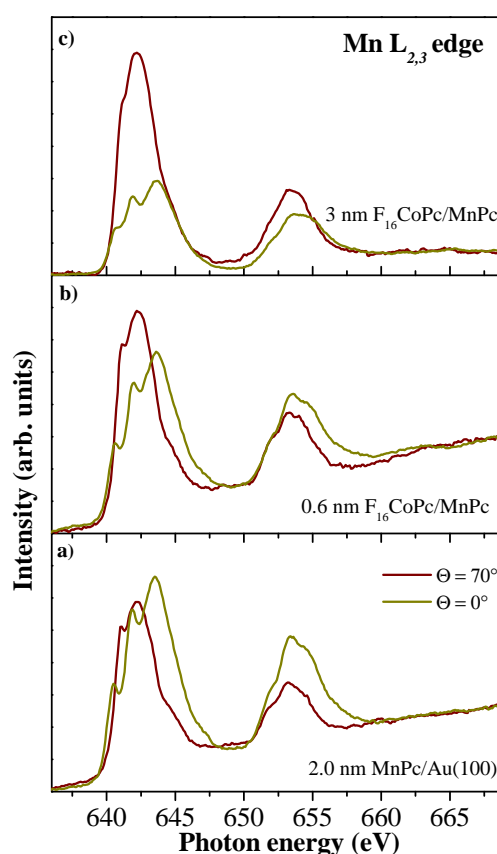


Figure 4.19.: $\text{MnL}_{2,3}$ edge absorption spectra for a) 2.0 nm MnPc on Au(100) b) 0.6 nm F_{16}CoPc on MnPc c) 3 nm F_{16}CoPc on MnPc. The spectra were recorded with different angles of beam incidence. θ gives the angle between the surface normal and the direction of the incident beam. ($\theta = 0^\circ$ corresponds to normal and $\theta = 70^\circ$ to grazing incidence.)

The question remains, of whether the above identified reaction and charge transfer can also be observed in the Mn absorption spectra? Fig. 4.19 a,b,c additionally depict

the evolution of the Mn-related $L_{2,3}$ x-ray absorption spectra upon formation of the $F_{16}CoPc/MnPc$ heterojunction. The data are normalized at energies of 670 eV, where the corresponding absorption edges should be polarization independent. The spectrum of a thick layer of MnPc on Au(100) is in very good agreement to previously published spectra [24, 116]. This is true for the spectral shape as a function of light polarization as well as for the intensity ratios for $E \parallel z$ and $E \parallel x, y$ ($R^{exp} = I_{x,y}/I_z$). We obtain a value of $R^{exp} = 1.5$ as in Ref. [24]. Going to the data for the heterojunction with little (0.6 nm) $F_{16}CoPc$ deposited onto MnPc these characteristics slightly change. The spectral features become blurred or broadened and the intensity ratio R^{exp} changes visibly with a relative intensity increase for the data taken at grazing incidence. These changes clearly signal that the addition of $F_{16}CoPc$ indeed impacts the electronic states of the Mn atoms close to. The effect can be enhanced by the consideration of a thick $F_{16}CoPc$ layer on MnPc. Due to the applied total electron yield method, the information depth of the spectra depends on the electron mean free path in the material. This is relatively small and in turn means that with increasing $F_{16}CoPc$ overlayer we become more and more sensitive to the MnPc molecules adjacent to this overlayer. Obviously, the Mn absorption spectrum of 3 nm $F_{16}CoPc$ on MnPc, measured in grazing incidence, shows a dramatic intensity change ($R^{exp} = 0.7$). With the light polarization perpendicular to the phthalocyanine molecules we are sensitive to electronic core excitations into Mn $3d$ orbitals with z -character. In case of the hybrid state as discussed above, the Mn $3d_{xz,yz}$ orbitals interact with the Co $3d_{z^2}$ orbital leading to a two-level system. Also, there is charge transfer from Mn to Co $3d$ states. Due to the charge transfer more z -derived states ($d_{xz,yz}$) of Mn can be reached as compared to in-plane polarized excitations leading to a modification of the intensity ratio as observed.

To summarize, we have demonstrated that the $MnPc/F_{16}CoPc$ organic hetero-interface is characterized by an interface reaction that causes the formation of hybrid states and charge transfer between the two types of molecules right at the interface. The interaction is due to a local hybrid where the Co $3d_{z^2}$ orbital of $F_{16}CoPc$ and the Mn $3d_{xz}$ orbital of MnPc are involved forming a two-level system.

In addition, we have demonstrated epitaxial growth of well ordered phthalocyanine heterojunctions out of MnPc and $F_{16}CoPc$. Additionally, we demonstrate the filling of the Co $3d_{z^2}$ orbital due to the charge transfer, which occurs at this interface, resulting in charged $MnPc^{\delta+}$ and $F_{16}CoPc^{\delta-}$ species. This fact supports the results of the performed DFT calculations, revealing a hybrid state.

These results are of importance for the application of such interfaces in organic electronic devices since charge transfer considerably affects the energy level alignment and

the transport behavior of the respective heterojunction. Moreover, MnPc and F₁₆CoPc may also be able to form a (bulk) charge transfer salt, purely made from phthalocyanines with potentially novel and unexpected physical properties. Since the transfer of charge is also connected to a transfer of spin and the hybrid system has a net spin of $S = 2$, such compounds could also be termed *spintransfer materials* with future applications in the area of spintronics. Finally, since it is reasonable to assume similar interaction for other flat transition metal complexes, the molecule pair studied in this contribution might be an initial representative of a fascinating incipient material class.

4.2.2 A phthalocyanine blend: MnPc/F₁₆CoPc

In this section, it is shown that also a bulk material can be formed by simple co-evaporation, which is characterized by the charge and spin transfer between the two molecules MnPc and F₁₆CoPc [117]. Moreover, the charge transfer interaction also affects the optical properties significantly, a new low energy electronic excitation has been identified, whereby the origin of it is clarified using density functional theory (DFT) investigations.

At first we want to focus on the the composition of the produced phthalocyanine blend. In order to obtain "pure" Co 2*p* spectra which represent reduced F₁₆CoPc molecules only (analogous to very thin F₁₆CoPc layers on top of MnPc) we have chosen a MnPc/F₁₆CoPc ratio of about 3:1. In Fig. 4.20 the C 1*s* core level photoemission profile for such produced coevaporated blend of MnPc and F₁₆CoPc is shown. Due to the different chemical envi-

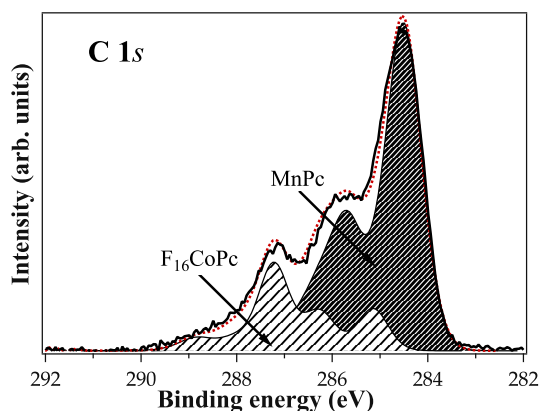


Figure 4.20.: C 1*s* core level photoemission profile for a coevaporated blend of MnPc and F₁₆CoPc. We additionally show the result of a modelling of the data using an appropriately weighted sum (dashed line) of otherwise unchanged photoemission profile of the two individual phthalocyanines (filled areas).

ronments of carbon in two phthalocyanines as described before, the C 1*s* photoemission

profiles can be well distinguished. Getting the ratio of our blend we also make simple superposition of the different carbon signals. The ratio MnPc:F₁₆CoPc was calculated to be 3:1. In Fig. 4.20 it is clearly observable that MnPc dominates the C 1s photoemission signal of the blend.

We continue the presentation and discussion of our results with the Co 2p_{3/2} core level photoemission spectra of a co-evaporated blend of MnPc and F₁₆CoPc, as shown in Fig. 4.21. The line shape and also the binding energy of the Co 2p_{3/2} spectra clearly

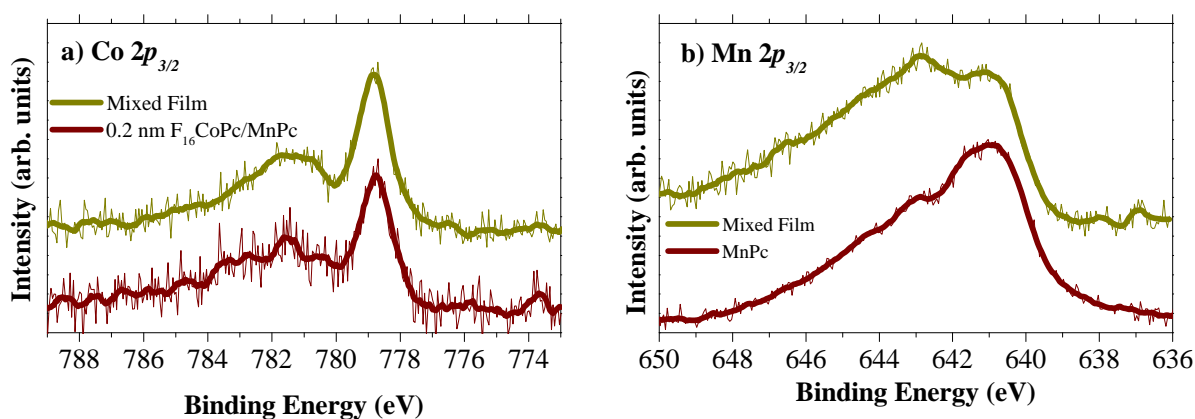


Figure 4.21.: a) Co 2p_{3/2} and b) Mn 2p_{3/2} core level photoemission spectra for a co-evaporated blend of MnPc and F₁₆CoPc. These data are compared to those found at heterojunctions of these two molecules and a thick MnPc film, respectively. Note: In order to obtain "pure" Co 2p spectra which represent reduced F₁₆CoPc molecules only - analogous to very thin F₁₆CoPc layers on top of MnPc - we have chosen a MnPc/F₁₆CoPc ratio of about 3:1.

indicate a reduction of the metal center in F₁₆CoPc to at least Co(I) [74, 76, 89, 106], which is in very good agreement to what is observed for CoPc and similar molecules on metal surfaces [74, 76, 89, 106] (cf. section 4.1.1) and also in direct correspondence to the Co reduction at a MnPc/F₁₆CoPc heterojunction [103] (cf. section 4.2.1). This reveals that the theoretically introduced dimer model [103] (see also below) is also able to provide an understanding of mixed films, where the two molecules need to find each other during the co-evaporation process to interact in a similar way as in case of the layered samples. This finding also holds great promise that a mixed crystal of the dimer system can be obtained. As discussed above DFT calculations showed that a hybrid state is formed between the two phthalocyanines [103] which is rendered possible by the relatively low ionization potential of MnPc and the high electron affinity of F₁₆CoPc. The hybrid state is made of the Mn 3d_{xz} (HOMO of MnPc) and the Co 3d_{z2} (LUMO of F₁₆CoPc) orbitals. As only the lower of the two hybrid states is occupied, charge is directly transferred to the Co 3d_{z2} orbital. To emphasize this we also show the Mn 2p_{3/2} photoemission spectra of the phthalocyanine blend and a thick MnPc film in Fig. 4.21b. For the comparison to the

heterojunction, we refer to the Mn $2p_{3/2}$ photoemission spectra of 0.2 nm MnPc deposited on F₁₆CoPc, which is published in [103]. The spectra shown here in Fig. 4.10b look really different. The line shape and binding energy for the thick MnPc film reveal the oxidation state of +2 for manganese, which is in good agreement with Mn $2p$ core level spectra of MnPc published elsewhere [116]. In contrast, an additional feature for the phthalocyanine blend arises at higher binding energy, which is well consistent with the mentioned charge transfer and the concomitant oxidation of the Mn centers. This higher binding energy feature is also observed for MnPc molecules that have been deposited onto a F₁₆CoPc layer, where the MnPc molecules are in direct contact to F₁₆CoPc and reduced [103].

Furthermore, we present the electronic excitation spectra of the mixed phthalocyanine film in Fig. 4.22 in comparison to those of the pure phthalocyanine films. These data were

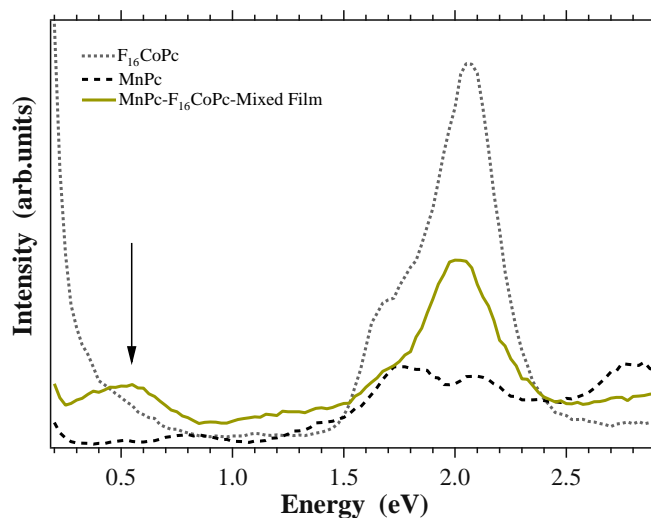


Figure 4.22.: Electronic excitation spectra of the phthalocyanine blend in comparison to the pure materials measured with EELS at a momentum transfer q of 0.1 \AA^{-1} .

taken using **electron energy-loss spectroscopy (EELS)**⁴ with a momentum transfer of 0.1 \AA^{-1} , which is close to the optical limit [118, 119]. All spectra are characterized by an excitation feature around 1.8-2 eV which is typical for all phthalocyanines, which represents HOMO-LUMO transitions and frequently labelled as Q-band [20, 25, 120, 121]. The interesting fact in this figure is the new spectral feature which appears at 0.6 eV for the MnPc/F₁₆CoPc blend and which cannot be understood as a pure sum of the two individual components, but is qualitatively different from the spectra of isolated MnPc and F₁₆CoPc. We attribute the new spectral feature to the interaction of the two phthalocyanine species in the blend leading to the hybridization of the respective transition metal states. This higher binding energy feature is also observed for MnPc

⁴For more details on the method and the experiment see appendix (A.3).

molecules that have been deposited onto a $F_{16}CoPc$ layer, where the $MnPc$ molecules are in direct contact to $F_{16}CoPc$ and reduced [103].

Finally, we complete the description of our results with the comparison of measured and calculated electronic excitation data⁵, which are shown in Fig. 4.23. In general, these two

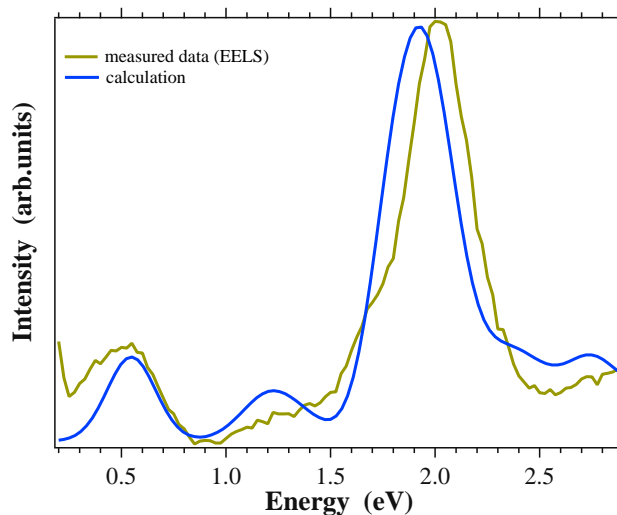


Figure 4.23.: Electronic excitation spectrum of the phthalocyanine blend in comparison to the theoretical calculation.

spectra are in very good agreement as the theoretical spectrum incorporates all qualitative features of the experimental spectrum and furthermore even well reproduces the relative intensities compared to the Q-band region. Most importantly the theoretical spectrum does show the qualitatively new signal at 0.6 eV. We note that the experimental data are measured using EELS, i.e. they represent the loss function $\text{Im}(-1/\epsilon)$, while the calculations are proportional to $\text{Im}(\epsilon)$. However, these two response functions are directly comparable for small momentum transfer [118] which was especially pointed out for phthalocyanines in Ref. [121].

In addition a consideration of the underlying states of this transition can now help to clarify the origin of this excitation. For this purpose the spectral region below 1.5 eV is depicted in Fig. 4.24 with the corresponding initial and final dimer states directly on top of the specific signal as obtained by the calculations.

Obviously the strong new peak at 0.6 eV originates from a transition between the bonding state $Mn 3d_{xz} + Co 3d_{z^2}$ and the antibonding state $Mn 3d_{xz} - Co 3d_{z^2}$ of the two-level system that represents the charge transfer interaction. Hence this signal is unambiguously

⁵The theoretical treatments were performed by Rico Friedrich, Torsten Hahn and Jens Kortus, members of the Institute of Theoretical Physics; TU BA Freiberg. For more details on the computational aspects see appendix (A.4).

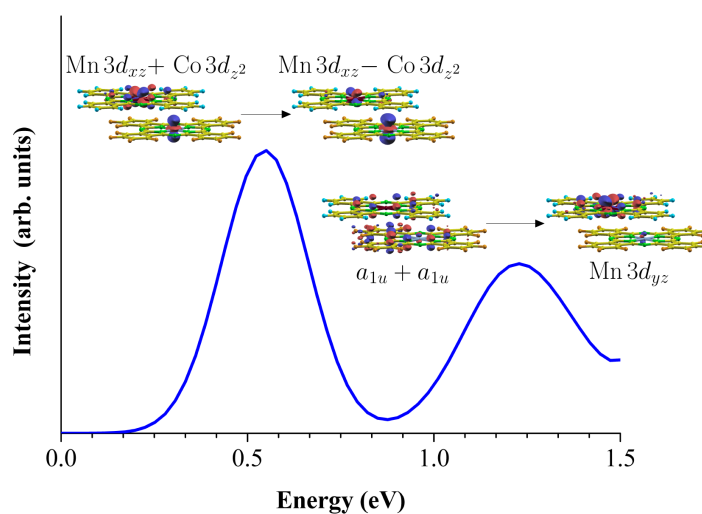


Figure 4.24.: Transitions in the spectral region below 1.5 eV. The corresponding initial and final dimer states are drawn directly above the signals they belong to. The new signal at 0.6 eV is related to an intense transition between the states of the two-level system. Note: The upper molecule within the dimer represents MnPc whereas the lower one corresponds to F₁₆CoPc.

connected to the interaction of the two molecular species and the observation of this signal can be taken as a direct proof for the formation of the charge transfer hybrid states in the blend in close analogy to the heterojunction studies previously. Moreover, it is not a surprise that this transition between the states of the two-level system is very strong. In such two-level systems excitations are always very efficient as the transition between a bonding and antibonding state is always optically allowed due to the formation of a bonding and antibonding linear combination.

The second peak at 1.2 eV is due to a transition between a ligand derived π state of a_{1u} symmetry at both molecules into the Mn $3d_{yz}$ state at MnPc. This is mainly an internal transition inside MnPc and is also a typical excitation for the free MnPc molecule [122]. Furthermore, all transitions of the considered energy range correspond to excitations of minority spin (spin down) electrons. This is caused by the fact that the hybridization near the Fermi level is dominated by spin down states and also for the isolated molecules spin down states are abundant near the Fermi energy. Furthermore, we note that the Q-band region is still dominated by the typical transitions between ligand states of the individual molecules for which a detailed explanation can be found in [122].

As a *final* remark, one should not be confused about a transition from an initial $3d$ state to a final $3d$ state as one would of course expect them to be disallowed for the isolated species because of symmetry selection rules. The labelling of the states is only made in accordance to the levels of the isolated molecules which does not mean that they really characterize the symmetry of the overall state. The real symmetry of the dimer

structure is C_1 to which only the totally symmetric representation a belongs. Hence all states and also the space operator will belong to this representation and the specific dipole matrix element will always be different from zero indicating optically allowed transitions. However we labeled the states in accordance to the states of the individual molecules which have higher symmetry. In this way the formation of the hybrid state is directly encoded in the labeling. Otherwise we would lose the information of the formation of the two-level system within the nomenclature.

To summarize, we have demonstrated that the $\text{MnPc}^{\delta+}/\text{F}_{16}\text{CoPc}^{\delta-}$ organic dimer can directly be formed via co-evaporation leading to a phthalocyanine blend. This blend is characterized by a molecular interface reaction that causes a charge transfer from the Mn to the Co center of the two molecules. Furthermore, we studied the electronic properties of this system using energy-loss spectroscopy revealing the existence of a new electronic excitation at 0.6 eV, which was confirmed by DFT calculations. The calculations show that the new signal is caused by a dipole allowed transition between the hybrid interface states of the resulting two level system. These results indicate that the interaction between the two molecule dimer species is strong enough to show the electronic characteristics of the interaction even in a co-evaporated film. Finally, the low energy excitation suggests that such mixed films might be applicable as small band gap organic semiconductors.

4.2.3 Other phthalocyanine heterojunctions

In this part of the chapter, we present two further heterojunctions made of unfluorinated phthalocyanines which differ only in the transition metal center. We focus on the CoPc/MnPc and on the FePc/MnPc heterojunction.

We start the presentation and discussion of our results with the CoPc/MnPc heterojunction. Therefore we show the evolution of the ligand core level spectra. In Fig. 4.25 the C 1s and N 1s core level photoemission profiles when CoPc is gradually deposited on a 3 nm thick MnPc layer on Au(100) are depicted. Due to the same chemical environment of the carbon atoms in the two phthalocyanines, the C 1s emission spectra can not be distinguished in the case of the heterojunction $\text{F}_{16}\text{CoPc}/\text{MnPc}$ (cf. section 4.2.1). After the first deposition the binding energy changes only around 140 meV and afterwards no significant modification of the spectra is observable. The data however show that the both phthalocyanine ligands are less affected by the surrounded organic molecules. This means, that the interaction at the CoPc/MnPc interface does not modify the ligand in contrast to the doping of phthalocyanine layers, where the C 1s core level photoemission spectrum is characterized by an additional core level feature [104, 105]. The picture of

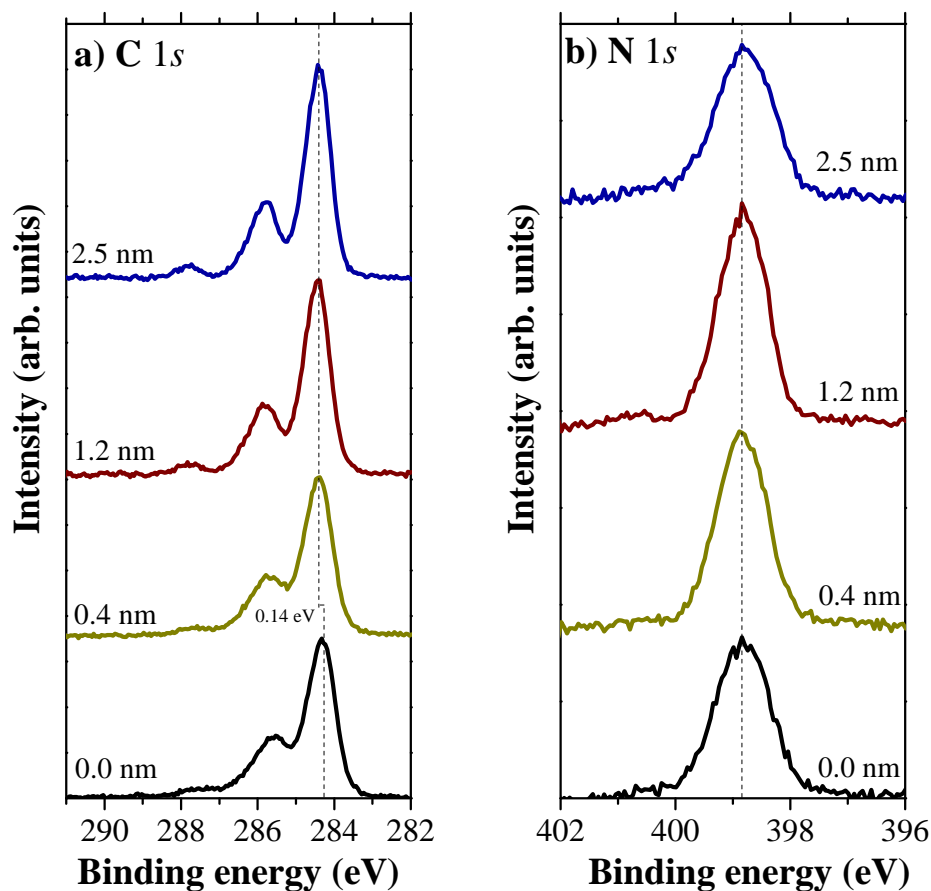


Figure 4.25.: Evolution of the a) C 1s and the b) N 1s core level photoemission profile upon deposition of CoPc on a 3 nm thick layer of MnPc.

the unaffected ligand is also corroborated in the corresponding evolution of the N 1s core level spectra, which is displayed in Fig. 4.25 b. In these spectra no significant changes are observable, which emphasize the conclusion that the charge transfer only effects the transition metal center and the ligand is not involved the process.

Turning to the Co $2p_{3/2}$ photoemission spectra at this interface a clear difference of the line shapes is detected when going from a thin layer of CoPc on top of MnPc to a thick film. This is depicted in Fig. 4.26, where the Co $2p_{3/2}$ core level photoemission spectrum for a 0.4 nm F_{16} CoPc film deposited on a 3 nm thick MnPc layer is also shown. For the thick layer of CoPc on top of a thick MnPc layer the typical line shape of Co(II) is shown. For the detailed discussion of this spectra see the section about the F_{16} CoPc/MnPc heterojunction. A reduction of the cobalt center in the direction of Co(I) gives rise to the observed shoulder at lower binding energies of the Co $2p_{3/2}$ core level photoemission spectrum of the thin layer CoPc on MnPc. The results of DFT calculations reveal a similar

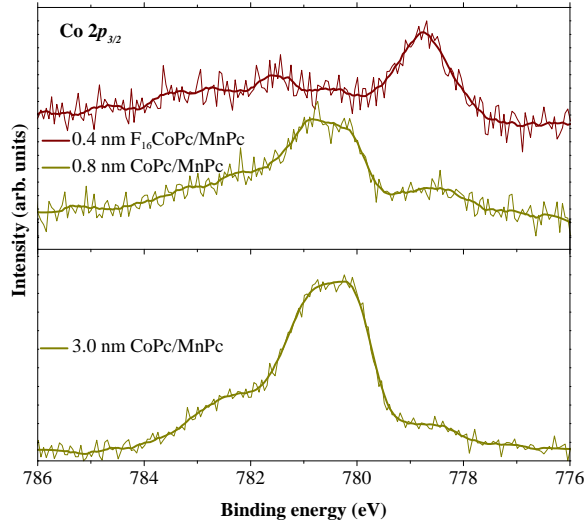


Figure 4.26.: $\text{Co } 2p_{3/2}$ core level photoemission spectra for a CoPc/MnPc heterojunction when CoPc is deposited on a 3 nm thick MnPc layer. Note: For the comparison to the $\text{F}_{16}\text{CoPc/MnPc}$ heterojunction the $\text{Co } 2p_{3/2}$ core level photoemission spectrum for a 0.4 nm F_{16}CoPc film deposited on a 3 nm thick MnPc layer is also shown.

coupling scheme for CoPc/MnPc as in the case of $\text{F}_{16}\text{CoPc/MnPc}$ [107]. Hence a dimer system is formed again and a hybridization of the $\text{Co } 3d_{z^2}$ orbital of CoPc and the $\text{Mn } 3d_{xz}$ orbital of MnPc is predicted. As this hybrid state is delocalized over both molecules with the largest contributions at the metal centres also the charge within this orbital is spread out to the dimer system. Hence a charge of only approximately 0.1 electrons is transferred from MnPc to CoPc [107], which is lower than the charge transfer from MnPc to F_{16}CoPc . When we compare this $\text{Co } 2p_{3/2}$ core level photoemission spectrum of the thin layer CoPc on MnPc with the corresponding spectrum of the $\text{F}_{16}\text{CoPc/MnPc}$ heterojunction (see Fig. 4.26), it seems that the charge transfer process is not so strong for the CoPc/MnPc heterojunction. Why is the interaction of CoPc/MnPc weaker than in the case of the $\text{F}_{16}\text{CoPc/MnPc}$ heterojunction? For comparison, the energy levels of MnPc , F_{16}CoPc and CoPc all aligned at the vacuum energy $E_{vac} = 0$ are depicted in Fig. 4.14 (see section 4.1.1).

One can clearly see that Fermi energy of the F_{16}CoPc is lower than the MnPc one. This is caused due to the high electron affinity of F_{16}CoPc and the high ionization potential of MnPc . Therefore a charge transfer from MnPc to F_{16}CoPc is favorable because this leads to an energy gain of about 1 eV. If we compare the Fermi energy position of MnPc and CoPc , the Fermi energies are much closer to each other and hence the energy gain would be much less than the energy gain of the other heterojunction, which results in a weaker

charge transfer interaction.

Finally, we present the heterojunction, FePc/MnPc. Due to the data of the pure FePc on noble metals, which shows only a weak charge transfer process in the case of Ag(111) as substrate, it is not surprising in the case of this studied heterojunction, that no charge transfer is expected. We show the Fe $2p$ core level photoemission spectra for a FePc/MnPc heterojunction when FePc is deposited on a 3 nm thick MnPc layer in Fig. 4.27. The line

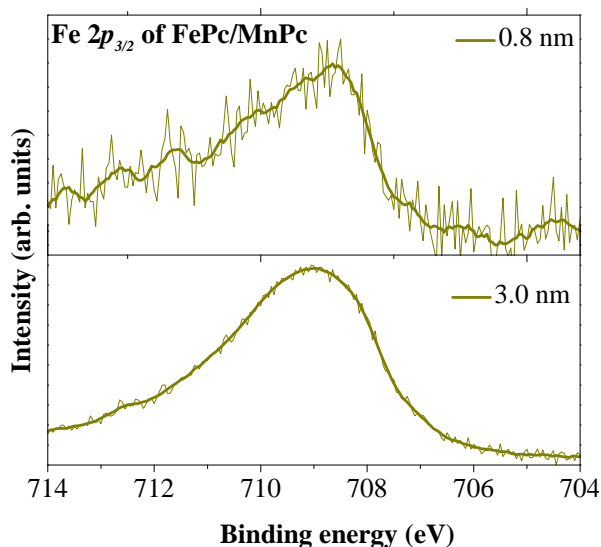


Figure 4.27.: Fe $2p$ core level photoemission spectra for a FePc/MnPc heterojunction when FePc is deposited on a 3 nm thick MnPc layer.

shape and the binding energy do not change upon deposition of FePc on top of a thick MnPc layer. There is no evidence for the reduction of the iron center. But in general this is no surprise, when we compare the ionization potential of the two phthalocyanines. MnPc has the lowest ionization potential of all phthalocyanines (IP = 4.5 eV). In the case of FePc the ionization potential is higher (IP = 5.3 eV), but it is lower than the ionization potential of CoPc, where the charge transfer is already weak. It is not enough to take only the ionization potential into account. It needs also suitable empty d -states, which should be available at the acceptor side. In the case of FePc a b_{2g} -LUMO exists, which corresponds to a metal center $3d_{xy}$ state. This orbital has no z -component, which is necessary for the interaction. But nonetheless the LUMO+1 of FePc is an a_{1g} state, which is the same state that interacts in the case of F₁₆CoPc. However this state is clear above the Fermi energy and therefore the energy gain is less pronounced [107]. Hence the appearance of no charge transfer at the FePc/MnPc heterojunction can be understood on the basis of the molecular orbital energies.

To summarize, we studied different heterojunctions made of two structurally similar phthalocyanine, which differ only in the transition metal center. We have demonstrated that the CoPc/MnPc organic hetero-interface is characterized by a weaker charge transfer process compared to the corresponding heterojunction of F₁₆CoPc/MnPc. This can be understood based on the comparison of the energy levels of the three different phthalocyanines (F₁₆CoPc, CoPc and MnPc), where the F₁₆CoPc/MnPc heterojunction achieves a higher energy gain than the one of CoPc/MnPc and hence results in a stronger charge transfer interaction. The interface reaction causes also the formation of hybrid states, where Co $3d_{z^2}$ orbital of CoPc and the Mn $3d_{xz}$ orbital of MnPc are involved forming a two-level system. The other studied FePc/MnPc heterojunction shows neither an interface reaction nor an charge transfer between the two molecules right at the interface. Here the energy gain is expected to be less pronounced and so a FePc/MnPc interaction is energetically not preferred.

4.3 Outlook

In section 4.2.1 we showed that an interaction between $F_{16}CoPc$ and $MnPc$ takes place. This interaction is characterized by an interface reaction causing the formation of hybrid states and charge transfer between the two organic molecules direct at the interface. The charge transfer process is possible due to the low ionization potential of $MnPc$ and the high electron affinity of $F_{16}CoPc$ which is caused by the surrounding fluorines. In the case of $CoPc$, it is well known that the replacement of hydrogen by fluorine offers the possibility to shift down the electronic states energetically while the energy level alignment stays the same.

For further experiments it would be interesting to find other suitable candidates for the phthalocyanine/ $MnPc$ heterojunction. One can also think about the fluorination of $FePc$. With the full fluorination of $FePc$ we can achieve that the energy levels might be pulled down enough to reach a favorable energy gain. Unfortunately, $F_{16}FePc$ is not commercially available, but the chlorine related compound, $Cl_{16}FePc$, is purchasable. To investigate the electronic properties of this organic molecule, we started photoelectron spectroscopy studies. The experiments failed because of the required evaporation of the material. $Cl_{16}FePc$ is not stable during the evaporation process. If $F_{16}FePc$ can be produced, it will be of crucial importance to study the $F_{16}FePc/MnPc$ heterojunction. It would also be of special interest because the spin of the iron centered molecule is $S = 1$ and therefore higher compared to $CoPc$.

Another way to engineer the Fermi level for manufacturing other promising heterojunctions is the replacement of the $MnPc$. So a reverse effect of the fluorination has to be realized by a chemical substitution. The substituent should be able to push the electron density into the ring system of the phthalocyanine and to increase the repulsion. In this way all electronic levels can be lifted energetically and therefore the ionization potential is reduced. A possible candidate for the substitution is the methoxy function ($-OCH_3$) which offers the delocalization of the free electron pair at the oxygen into the ring system [123]. DFT calculations on the $F_{16}CoPc/(CH_3O)_8CoPc$ heterojunction demonstrate promising results regarding the charge transfer process [123].

One can clearly see that this thesis is not the end of this fascinating incipient material class. The heterojunction $F_{16}CoPc/MnPc$ can be seen as an initial representative, but other molecule pairs have to be studied further. The question arises how can we find other possible combinations? The theoretical physics shows a way, but we need also the chemistry to produce well defined pure materials. Hence this research topic is an interdisciplinary one, whose questions are not already answered.

A

APPENDIX

A.1 Computational aspects for the phthalocaynine heterojunction

The all electron DFT calculations were carried out using the NRLMOL program package [124]. To include exchange and correlation effects the generalised gradient functional developed by Perdew, Burke and Ernzerhof was applied [125]. First we relaxed the structures of the individual MnPc and F₁₆CoPc molecule by performing a geometry optimization. In order to reproduce the relations of the molecules at the interface, the distance and relative shift of the molecules in a dimer consisting of MnPc and F₁₆CoPc was deduced from crystallographic data on the β -MnPc phase obtained from CSD. This data clearly shows that neighbouring molecules arrange such that the metal centers are positioned above nitrogen atoms bridging two isoindolic units of a neighbouring molecule. The distance of the nitrogen and the metal is about 3 Å. Using this startup geometry we performed a relaxation of the dimer system.

A.2 XAS: Experimental details

The X-ray absorption spectroscopy (XAS) experiments were performed at the Russian-German beamline of the synchrotron radiation source Bessy II, Berlin. The XAS spectra were recorded in the total-electron yield mode with a resolution of about 30 meV at photon energies of 410 eV and 785 eV. The spectra were normalized to have the same absorption edge step height well above the threshold. In addition, we have used x-ray photoelectron spectroscopy in order to characterize the substrate and the phthalocyanine films. The data have been taken with a photon energy of 1080 eV and an energy resolution of 50 meV. The photon energies were referenced to the Au $4f$ binding energy.

A.3 EELS: Experimental details

For our investigations using electron energy-loss spectroscopy (EELS), free-standing phthalocyanine films were prepared under ultrahigh vacuum (UHV) conditions by equivalent thermal evaporation onto a KBr (100) substrate kept at room temperature. In this case the deposition rate was about 0.5 nm/min as measured using a quartz microbalance and the resulting film thicknesses were about 100 nm. For the mixed film, we kept the deposition rates for the two molecules at the same value. Subsequently, the films were floated off in distilled water, mounted onto standard electron microscopy grids, and transferred into a purpose built spectrometer for EELS [118]. Prior to the EELS measurements the films were characterized *in-situ* using electron diffraction. This revealed that the films were essentially polycrystalline.

The electron energy-loss spectroscopy measurements in transmission were carried out at 20 K using a 172 keV spectrometer described elsewhere [118], and we note that at this high primary beam energy only singlet excitations are possible. The energy and momentum resolution were chosen to be 85 meV and 0.03 \AA^{-1} , respectively. We have measured the loss function $\text{Im}(-1/\epsilon(q, \omega))$ ($\epsilon(q, \omega)$ is the dielectric function) for a small momentum transfer, parallel to the film surface [118]. Further details of the sample preparation procedure and the experimental technique can be found in previous publications [118, 119].

A.4 Computational aspects for the phthalocaynine dimer

The unrestricted density functional calculations were performed with the NRLMOL program package [124, 126–132]. This package uses a specially optimized gaussian basis set [133] to describe the molecular states. Furthermore, the exchange correlation functional of Perdew, Burke and Ernzerhof (PBE) [125] was applied within the calculations. For the model dimer system made up of MnPc and F₁₆CoPc the geometry was based on the (thermodynamically stable) β -phase of MnPc. Hence the molecular planes were placed 3.1 Å apart from one another and the metal centers are positioned below and above a nitrogen atom bridging two isoindolic units of the neighbouring molecule. The presented results are deduced from a single point calculation for this geometry as the preservation of the overall electronic properties during a relaxation has already been presented in [103] and an optimization on PBE level is expected to show the well known underbinding effect. Furthermore an LDA optimization of the system was carried out which often leads to very reasonable geometries compared to experiment [134]. During this relaxation the initial distance of the molecular planes was slightly shortened by about 0.2 Å which further underlines the expected underbinding effect for the PBE relaxation.

The theoretical absorption spectrum was obtained from the Kohn-Sham states by the calculation of the specific dipole matrix elements. Afterwards the transitions were weighted with the square of the dipole matrix element according to Fermi's golden rule. As discussed in [118] these calculated results are directly comparable to the loss function of EELS measurements performed with small momentum transfer. In order to correct for the systematic underestimation of the band gap within DFT the calculated spectra were shifted to 0.5 eV higher energies which allowed to align calculated and measured Q-band. This shift has already been successfully applied earlier and led to good agreement with various experimental results [122].

BIBLIOGRAPHY

- [1] P. Batail. *Chem. Rev.* 104, 4887 (2004).
- [2] L. Ouahab. *Organic conductors, Superconductors and Magnets*. Kluwer Academic (2004).
- [3] O. Gunnarsson. *Alkali-doped Fullerenes*. World Scientific, Singapore (2004).
- [4] N. Toyota, M. Lang, and J. Müller. *Low-Dimensional Molecular Metals*. Springer Berlin (2007).
- [5] H. Alves, A. S. Molinari, H. Xie, and A. F. Morpurgo. *Nat. Mater.* 7, 574 (2008).
- [6] S. Wen, W. Deng, and K. Han. *Chem. Commun.* 46, 5133 (2010).
- [7] R. Mitsuhashi, Y. Suzuki, Y. Yamanari, H. Mitamura, T. Kambe, N. Ikeda, H. Okamoto, A. Fujiwara, M. Yamaji, N. Kawasaki, Y. Maniwa, and Y. Kubozono. *Nat.* 464, 76 (2010).
- [8] M. Xue, T. Cao, D. Wang, Y. Wu, H. Yang, X. Dong, J. He, F. Li, and G. F. Chen. *Sci. Rep.* 2, 389 (2012).
- [9] N. Koch, S. Duhm, J. P. Rabe, A. Vollmer, and R. L. Johnson. *Phys. Rev. Lett.* 95, 237601 (2005).
- [10] K. Walzer, B. Maennig, M. Pfeiffer, and K. Leo. *Chem. Rev.* 107, 1233 (2007).
- [11] S. Sanvito. *Nat. Phys.* 6, 562 (2010).
- [12] S. Sanvito. *Nat. Mater.* 10, 484 (2011).

Bibliography

- [13] N. R. Armstrong, W. Wang, D. M. Alloway, D. Placencia, E. Ratcliff, and M. Brumbach. *Macromol. Rapid Commun.* 30, 717 (2009).
- [14] P. Peumans, and S. R. Forrest. *Appl. Phys. Lett.* 79, 126 (2001).
- [15] B. P. Rand, J. Genoe, P. Heremans, and J. Poortmans. *Prog. Photovolt.* 15, 659 (2007).
- [16] V. Dediu, M. Murgia, F.C. Maticotta, C. Taliani, and S. Barbanera. *Solid State Commun.* 122, 181 (2002).
- [17] M. Ling, and Z. Bao. *Org. Electron.* 7, 568 (2006).
- [18] W. J. M. Naber, S. Faez, and W. G. van der Wiel. *J. Phys. D: Appl. Phys.* 40, (2007).
- [19] A. Zhao, Q. Li, L. Chen, H. Xiang, W. Wang, S. Pan, B. Wang, X. Xiao, J. Yang, J. G. Hou, and Q. Zhu. *Science.* 309, 1542 (2005).
- [20] M. Grobosch, C. Schmidt, R. Kraus, and M. Knupfer. *Org. Electron.* 11, 1483 (2010).
- [21] A.B.P. Lever. "The Phthalocyanines". In: vol. 7. *Adv. Inorg. Chem. Radiochem.* Academic Press, 1965, 27.
- [22] K. A. Nguyen, and R. Pachter. *J. Chem. Phys.* 114, 10757 (2001).
- [23] A. Rosa, G. Ricciardi, E. J. Baerends, and S. J. A van Gisbergen. *J. Phys. Chem. A.* 105, 3311 (2001).
- [24] T. Kroll, R. Kraus, R. Schönfelder, V. Y. Aristov, O. V. Molodtsova, P. Hoffmann, and M. Knupfer. *J. Chem. Phys.* 137, 054306 (2012).
- [25] N.B. McKeown. *Phthalocyanine Materials.* Cambridge University Press (1998).
- [26] R. Hiesgen, M. Rübisch, H. Böttcher, and D. Meissner. *Sol. Energ. Mat. Sol. Cells.* 61, 73 (2000).
- [27] S. Mitra, A. K. Gregson, W. E. Hatfield, and R. R. Weller. *Inorg. Chem.* 22, 1729 (1983).

- [28] W. Wu, A. Kerridge, A. H. Harker, and A. J. Fisher. *Phys. Rev. B.* 77, 184403 (2008).
- [29] R. Mason, G. A. Williams, and P. E. Fielding. *J. Chem. Soc., Dalton Trans.* 4, 676 (1979).
- [30] B. N. Figgis, R. Mason, and G. A. Williams. *Acta Crystallogr. B.* 36, 2963 (1980).
- [31] O. V. Molodtsova, M. Knupfer, Yu. A. Ossipyan, and V. Yu. Aristov. *J. Appl. Phys.* 104, 083704 (2008).
- [32] A. L. C. C. Leznoff. *Phthalocyanines Properties and Applications*. Wiley VCH, New York (1989).
- [33] A. Hoshino, Y. Takenaka, M. Izukashi, H. Yoshida, and H. Miyaji. *Jpn. J. Appl. Phys.* 43, 4344 (2004).
- [34] S. E. Harrison, and K. H. Ludewig. *J. Chem. Phys.* 45, 343 (1966).
- [35] C. Ercolani, C. Neri, and P. Porta. *Inorg. Chim. Acta.* 1, 415 (1967).
- [36] C. W. Miller, A. Sharoni, G. Liu, C. N. Colesniuc, B. Fruhberger, and I. K. Schuller. *Phys. Rev. B.* 72, 104113 (2005).
- [37] M. Evangelisti, J. Bartolomé, L. J. de Jongh, and G. Filoti. *Phys. Rev. B.* 66, 144410 (2002).
- [135] K. Manandhar, K.T. Park, S. Ma, and J. Hrbek. *Surf. Sci.* 603, 636 (2009).
- [38] N. D. Lang, and W. Kohn. *Phys. Rev. B.* 1, 4555 (1970).
- [39] M. Henzler, W. Göpel, and C. Ziegler. *Oberflächenphysik des Festkörpers*. Teubner (1994).
- [40] A. Zangwill. *Physics at surfaces*. Cambridge University Press (2001).
- [41] S. Braun, W. R. Salaneck, and M. Fahlman. *Adv. Mater.* 21, (2009).
- [42] K. Oura. *Surface science / an introduction ; with 16 tables*. Springer (2003).
- [43] R. Smoluchowski. *Phys. Rev.* 60, 661 (1941).

Bibliography

- [44] M. W. Finnis, and V. Heine. *J. Phys. F: Met. Phys.* 4, (1974).
- [45] . www.iapp.org/world/?Basics:What_are_organic_semiconductors. (as from October 27, 2013).
- [46] H. Ishii, K. Sugiyama, E. Ito, and K. Seki. *Adv. Mater.* 11, 605 (1999).
- [47] H. Vázquez, Y. J. Dappe, J. Ortega, and F. Flores. *J. Chem. Phys.* 126, 144703 (2007).
- [48] N. Koch, A. Kahn, J. Ghijsen, J.-J. Pireaux, J. Schwartz, R. L. Johnson, and A. Elschner. *Appl. Phys. Lett.* 82, 70 (2003).
- [49] Y. C. Chen, J. E. Cunningham, and C. P. Flynn. *Phys. Rev. B.* 30, 7317 (1984).
- [50] Y. Gao. *Mat. Sci. Eng. R.* 68, 39 (2010).
- [51] H. Vázquez, F. Flores, and A. Kahn. *Org. Electron.* 8, 241 (2007).
- [52] A. Hinderhofer, and F. Schreiber. *ChemPhysChem.* 13, 628 (2012).
- [53] S. Hüfner. *Photoelectron Spectroscopy*. Springer-Verlag (2003).
- [54] H. Hertz. *Ann. Phys.* 267, 983 (1887).
- [55] A. Einstein. *Ann. Phys.* 14, 164 (2005).
- [56] H. Lüth. *Solid Surfaces, Interfaces and Thin Films*. Springer-Verlag Berlin (2010).
- [57] C. N. Berglund, and W. E. Spicer. *Phys. Rev.* 136, A1030 (1964).
- [58] M. Cardona, and L. Ley. *Photoemission in Solids I*. Springer-Verlag Berlin (1978).
- [59] M. Grobosch. *Experimentelle Bestimmung der elektronischen Eigenschaften anwendungsrelevanter Grenzflächen organischer Halbleiter mittels Photoelektronenspektroskopie*. Thesis. TU Dresden. (2009).
- [60] J. F. Moulder, W. F. Stickle, P. E. Sobol, and K. D. Bomben. *Handbook of X-ray Photoelectron Spectroscopy*. Perkin-Elmer Corporation, Physical Electronics Division (1992).

- [61] D. Briggs, and J. T. Grant. *Surface Analysis by Auger and X-ray Photoelectron Spectroscopy*. IM Publications and SurfaceSpectra Limited (2003).
- [62] T. S. Ellis, K. T. Park, M. D. Ulrich, S. L. Hulbert, and J. E. Rowe. *J. Appl. Phys.* 100, 093515 (2006).
- [63] M. Toader, M. Knupfer, D. R.T. Zahn, and M. Hietschold. *Surf. Sci.* 605, 1510 (2011).
- [64] F. Petraki, H. Peisert, F. Latteyer, U. Aygül, A. Vollmer, and T. Chassé. *J. Phys. Chem. C* 115, 21334 (2011).
- [65] A. J. Maxwell, P. A. Brühwiler, A. Nilsson, N. Mårtensson, and P. Rudolf. *Phys. Rev. B* 49, 10717 (1994).
- [66] M. P. Seah, and W. A. Dench. *Surf. Interface Anal.* 1, 2 (1979).
- [67] D. A. Shirley. *Phys. Rev. B* 5, 4709 (1972).
- [68] J. Végh. *J. Electron. Spectrosc. Relat. Phenom.* 151, 159 (2006).
- [69] Z. Bao, A. J. Lovinger, and A. Dodabalapur. *Appl. Phys. Lett.* 69, 3066 (1996).
- [70] T. Lukasczyk, K. Flechtner, L. R. Merte, N. Jux, F. Maier, J. M. Gottfried, and H. Steinrück. *J. Phys. Chem. C* 111, 3090 (2007).
- [71] J. Xiao, and P. A. Dowben. *J. Phys.: Condens. Matter* 21, (2009).
- [72] Y. Bai, F. Buchner, I. Kellner, M. Schmid, F. Vollnhals, H. Steinrück, H. Marbach, and J. M. Gottfried. *New J. Phys.* 11, (2009).
- [73] Y. Bai, M. Sekita, M. Schmid, T. Bischof, H. Steinrück, and J. M. Gottfried. *Phys. Chem. Chem. Phys.* 12, 4336 (2010).
- [74] Z. Li, B. Li, J. Yang, and J. G. Hou. *Acc. Chem. Res.* 43, 954 (2010).
- [75] P. Gargiani, M. Angelucci, C. Mariani, and M. G. Betti. *Phys. Rev. B* 81, 085412 (2010).
- [76] F. Petraki, H. Peisert, I. Biswas, and T. Chassé. *J. Phys. Chem. C* 114, 17638 (2010).

Bibliography

- [77] F. Petraki, H. Peisert, I. Biswas, U. Aygöl, F. Latteyer, A. Vollmer, and T. Chassé. *J. Phys. Chem. Lett.* 1, 3380 (2010).
- [78] J. D. Baran, J. A. Larsson, R. A. J. Woolley, Y. Cong, P. J. Moriarty, A. A. Cafolla, K. Schulte, and V. R. Dhanak. *Phys. Rev. B.* 81, 075413 (2010).
- [79] M. Toader, T. G. Gopakumar, P. Shukryna, and M. Hietschold. *J. Phys. Chem. C.* 114, 21548 (2010).
- [80] W. Hieringer, K. Flechtner, A. Kretschmann, K. Seufert, W. Auwärter, J. V. Barth, A. Görling, Hans-Peter Steinrück, and J. M. Gottfried. *J. Am. Chem. Soc.* 133, 6206 (2011).
- [81] Z. Hu, L. Chen, A. Zhao, Z. Li, B. Wang, J. Yang, and J. G. Hou. *J. Phys. Chem. C.* 112, 15603 (2008).
- [136] J. M. Auerhammer, M. Knupfer, H. Peisert, and J. Fink. *Surf. Sci.* 506, (2002).
- [83] D. Schlettwein, K. Hesse, N. E. Gruhn, P. A. Lee, K. W. Nebesny, and N. R. Armstrong. *J. Phys. Chem. B.* 105, 4791 (2001).
- [84] H. Peisert, M. Knupfer, T. Schwieger, G. G. Fuentes, D. Olligs, J. Fink, and Th. Schmidt. *J. Appl. Phys.* 93, 9683 (2003).
- [85] H. Peisert, M. Knupfer, and J. Fink. *Appl. Phys. Lett.* 81, 2400 (2002).
- [86] U. Weiler, T. Mayer, W. Jaegermann, C. Kelting, D. Schlettwein, S. Makarov, and D. Wöhrle. *J. Phys. Chem. B.* 108, 19398 (2004).
- [87] H. Peisert, D. Kolacyak, and T. Chassé. *J. Phys. Chem. C.* 113, 19244 (2009).
- [88] D. R.T. Zahn, G. N. Gavrilu, and M. Gorgoi. *Chem. Phys.* 325, 99 (2006).
- [89] S. Lindner, U. Treske, M. Grobosch, and M. Knupfer. *Appl. Phys. A.* 105, 921 (2011).
- [90] L. Scudiero, K. W. Hipps, and D. E. Barlow. *J. Phys. Chem. B.* 107, 2903 (2003).
- [91] M. Grobosch, V. Yu. Aristov, O. V. Molodtsova, C. Schmidt, B. P. Doyle, S. Nannarone, and M. Knupfer. *J. Phys. Chem. C.* 113, 13219 (2009).

- [137] H. Peisert, M. Knupfer, T. Schwieger, J. M. Auerhammer, M. S. Golden, and J. Fink. *J. Appl. Phys.* 91, 4872 (2002).
- [92] T. Kroll, V. Yu. Aristov, O. V. Molodtsova, Yu. A. Ossipyan, D. V. Vyalikh, B. Büchner, and M. Knupfer. *J. Phys. Chem. A.* 113, 8917 (2009).
- [93] J. Åhlund, K. Nilson, J. Schiessling, L. Kjeldgaard, S. Berner, N. Mårtensson, C. Puglia, B. Brena, M. Nyberg, and Y. Luo. *J. Chem. Phys.* 125, 034709 (2006).
- [94] T. Kawai, M. Soma, Y. Matsumoto, T. Onishi, and K. Tamaru. *Chem. Phys. Lett.* 37, 378 (1976).
- [95] Y. Bai, F. Buchner, M. T. Wendahl, I. Kellner, A. Bayer, H. Steinrück, H. Marbach, and J. M. Gottfried. *J. Phys. Chem. C.* 112, 6087 (2008).
- [96] F. Petraki, H. Peisert, U. Aygül, F. Latteyer, J. Uihlein, A. Vollmer, and T. Chassé. *J. Phys. Chem. C.* 116, 11110 (2012).
- [97] A. Mugarza, R. Robles, C. Krull, R. Korytár, N. Lorente, and P. Gambardella. *Phys. Rev. B.* 85, 155437 (2012).
- [98] S. Lindner, U. Treske, and M. Knupfer. *Appl. Surf. Sci.* 267, 62 (2013).
- [99] N. Koch. *ChemPhysChem.* 8, 1438 (2007).
- [100] S. Braun, W. Osikowicz, Y. Wang, and W. R. Salaneck. *Org. Electron.* 8, 14 (2007).
- [101] F. Evangelista, A. Ruocco, R. Gotter, A. Cossaro, L. Floreano, A. Morgante, F. Crispoldi, M. G. Betti, and C. Mariani. *J. Chem. Phys.* 131, 174710 (2009).
- [102] H. Vázquez, W. Gao, F. Flores, and A. Kahn. *Phys. Rev. B.* 71, 041306 (2005).
- [103] S. Lindner, M. Knupfer, R. Friedrich, T. Hahn, and J. Kortus. *Phys. Rev. Lett.* 109, 027601 (2012).
- [104] O. V. Molodtsova, M. Knupfer, V. Yu. Aristov, D. V. Vyalikh, V. M. Zhilin, and Yu. A. Ossipyan. *J. Appl. Phys.* 103, 053711 (2008).
- [105] V. Yu. Aristov, O. V. Molodtsova, V. V. Maslyuk, D. V. Vyalikh, T. Bredow, I. Mertig, A. B. Preobrajenski, and M. Knupfer. *Org. Electron.* 11, 1461 (2010).

Bibliography

- [106] S. Stepanow, P. S. Miedema, A. Mugarza, G. Ceballos, P. Moras, J. C. Cezar, C. Carbone, F. M. F. de Groot, and P. Gambardella. *Phys. Rev. B.* 83, 220401 (2011).
- [107] R. Friedrich. *Density Functional Investigation of a Phthalocyanine Based Spin Transfer Material*. Thesis. TU Bergakademie Freiberg. (2012).
- [108] M. Grobosch, B. Mahns, C. Loose, R. Friedrich, C. Schmidt, J. Kortus, and M. Knupfer. *Chem. Phys. Lett.* 505, 122 (2011).
- [109] X. Shen, L. Sun, Z. Yi, E. Benassi, R. Zhang, Z. Shen, S. Sanvito, and S. Hou. *Phys. Chem. Chem.* 12, 10805 (2010).
- [110] J. Stöhr. *NEXAFS Spectroscopy*. Springer Berlin (1992).
- [111] H. Peisert, I. Biswas, U. Aygül, A. Vollmer, and T. Chassé. *Chemical Physics Letters.* 493, 126 (2010).
- [112] R. Friedrich, S. Lindner, T. Hahn, C. Loose, S. Liebing, M. Knupfer, and J. Kortus. *Phys. Rev. B.* 87, 115423 (2013).
- [113] V.Yu. Aristov, O.V. Molodtsova, and M. Knupfer. *Org. Electron.* 12, 372 (2011).
- [114] F. de Groot. *Coord. Chem. Rev.* 249, 31 (2005).
- [115] S. A. Krasnikov, A. B. Preobrajenski, N. N. Sergeeva, M. M. Brzhezinskaya, M. A. Nesterov, A. A. Cafolla, M. O. Senge, and A. S. Vinogradov. *Chem. Phys.* 332, 318 (2007).
- [116] F. Petraki, H. Peisert, P. Hoffmann, J. Uihlein, M. Knupfer, and T. Chassé. *J. Phys. Chem. C.* 116, 5121 (2012).
- [117] S. Lindner, B. Mahns, A. König, F. Roth, M. Knupfer, R. Friedrich, T. Hahn, and J. Kortus. *J. Chem. Phys.* 138, 024707 (2013).
- [118] J. Fink. *Adv. Electr. Electr. Phys.* 75, (1989).
- [119] M. Knupfer. *Surf. Sci. Rep.* 42, 1 (2001).
- [120] M. Pope, and C. E. Swenberg. *Electronic Processes in Organic Crystals and Polymers*. Oxford University Press (1999).

- [121] R. Kraus, M. Grobosch, and M. Knupfer. *Chem. Phys. Lett.* 469, 121 (2009).
- [122] R. Friedrich, T. Hahn, J. Kortus, M. Fronk, F. Haidu, G. Salvan, D. R. T. Zahn, M. Schlesinger, M. Mehring, F. Roth, B. Mahns, and M. Knupfer. *J. Chem. Phys.* 136, 064704 (2012).
- [123] R. Friedrich, B. Kersting, and J. Kortus. *Phys. Rev. B.* 88, 155327 (2013).
- [124] M.R. Pederson, D.V. Porezag, J. Kortus, and D.C. Patton. *Phys. Stat. Sol. B.* 217, 197 (2000).
- [125] J. P. Perdew, K. Burke, and M. Ernzerhof. *Phys. Rev. Lett.* 77, 3865 (1996).
- [126] M. R. Pederson, and K. A. Jackson. *Phys. Rev. B.* 41, 7453 (1990).
- [127] K. Jackson, and M. R. Pederson. *Phys. Rev. B.* 42, 3276 (1990).
- [128] M. R. Pederson, and K. A. Jackson. *Phys. Rev. B.* 43, 7312 (1991).
- [129] A. A. Quong, M. R. Pederson, and J. L. Feldman. *Solid State Commun.* 87, 535 (1993).
- [130] D. Porezag, and M. R. Pederson. *Phys. Rev. B.* 54, 7830 (1996).
- [131] D. Porezag. *Development of Ab-Initio and Approximate Density Functional Methods and their Application to Complex Fullerene Systems*. Thesis. TU Chemnitz. (1997).
- [132] A. Briley, M. R. Pederson, K. A. Jackson, D. C. Patton, and D. V. Porezag. *Phys. Rev. B.* 58, 1786 (1998).
- [133] D. Porezag, and M. R. Pederson. *Phys. Rev. A.* 60, 2840 (1999).
- [134] W. Kohn. *Rev. Mod. Phys.* 71, 1253 (1999).

LIST OF PUBLICATIONS

- [P1] H. Stöcker, M. Zschornak, J. Seibt, F. Hanzig, Wintz, S., B. Abendroth, J. Kortus, and D. C. Meyer. *Appl. Phys. A.* 100, 437 (2010).
- [P2] J. Hanzig, B. Abendroth, F. Hanzig, H. Stöcker, R. Strohmeyer, D. C. Meyer, Lindner, S., M. Grobosch, M. Knupfer, C. Himcinschi, U. Muhle, and F. Munnik. *J. Appl. Phys.* 110, 064107 (2011).
- [P3] Lindner, S., U. Treske, M. Grobosch, and M. Knupfer. *Appl. Phys. A.* 105, 921 (2011).
- [P4] Lindner, S., M. Knupfer, R. Friedrich, T. Hahn, and J. Kortus. *Phys. Rev. Lett.* 109, 027601 (2012).
- [P5] B. Mahns, F. Roth, M. Grobosch, Lindner, S., M. Knupfer, T. P. I. Saragi, T. Reichert, J. Salbeck, and T. Hahn. *J. Chem. Phys.* 136, 124702 (2012).
- [P6] G. Bepete, Z. N. Tetana, Lindner, S., M. H. Rummeli, Z. Chiguvare, and N. J. Coville. *Carbon.* 52, 316 (2013).
- [P7] Lindner, S., U. Treske, and M. Knupfer. *Appl. Surf. Sci.* 267, 62 (2013).
- [P8] Lindner, S., B. Mahns, A. König, F. Roth, M. Knupfer, R. Friedrich, T. Hahn, and J. Kortus. *J. Chem. Phys.* 138, 024707 (2013).
- [P9] R. Friedrich, Lindner, S., T. Hahn, C. Loose, S. Liebing, M. Knupfer, and J. Kortus. *Phys. Rev. B.* 87, 115423 (2013).
- [P10] C. Bof Bufon, C. Vervacke, D. Thurmer, M. Fronk, G. Salvan, Lindner, S., M. Knupfer, D. Zahn, and O. Schmidt. *J. Phys. Chem. C.* to be published, (2014).

DANKSAGUNG

Folgende Personen haben mich auf dem Weg der Promotion unterstützt und einen wichtigen Beitrag zu dieser Dissertation geleistet.

Ich danke herzlich:

- Prof. Dr. Bernd Büchner für die Möglichkeit, meine Dissertation am IFW Dresden anzufertigen und für die dabei entgegengebrachte Unterstützung
- Prof. Dr. Martin Knupfer für seine jahrelange Unterstützung und Hilfsbereitschaft
- Prof. Dr. Georgeta Salvan für die Übernahme des Zweitgutachtens
- Dr. Andreas König, Dr. Friedrich Roth, Uwe Treske und Benjamin Mahns für die Hilfe bei der Arbeit im Labor
- Rico Friedrich, Dr. Torsten Hahn und Prof. Dr. Jens Kortus für die großartigen DFT Rechnungen
- Dr. Roland Hübel, Stefan Leger und Marco Naumann für technische Unterstützung im Labor
- den Kollegen der Abteilung 11 und meinen C2E.04 Büromitbewohnern für das angenehme Arbeitsklima
- dem IFF Sekretariat für jegliche administrative Leistung
- meinen Eltern, Grit und Jirka Tartsch, für die liebevolle Unterstützung in allen Lebenslagen
- ... meinem Mann, Björn Lindner, und meiner Tochter, Luise Lindner, ohne deren Liebe die Welt und die Physik nur halb so schön wären.

SELBSTSTÄNDIGKEITSERKLÄRUNG

Hiermit versichere ich, dass ich die vorliegende Arbeit ohne unzulässige Hilfe Dritter und ohne Benutzung anderer als der angegebenen Hilfsmittel angefertigt habe; die aus fremden Quellen direkt oder indirekt übernommenen Gedanken sind als solche kenntlich gemacht. Die Arbeit wurde bisher weder im Inland noch im Ausland in gleicher oder ähnlicher Form einer anderen Prüfungsbehörde vorgelegt.

Die vorliegende Dissertation wurde unter der wissenschaftlichen Betreuung von Herrn Prof. Dr. B. BÜCHNER im Institut für Festkörperforschung am Leibniz-Institut für Festkörper- und Werkstoffforschung in Dresden angefertigt.

Bis zum jetzigen Zeitpunkt habe ich keinerlei erfolglose Promotionsverfahren absolviert.

Ich erkenne die Promotionsordnung der Fakultät für Mathematik und Naturwissenschaften der Technischen Universität Dresden an.

Dresden, den 24.03.2014

Susi Lindner